Modelling of Single Phase Diffusive Transport in Porous Environments

by

Elsa du Plessis

Thesis presented in partial fulfilment of the requirements for the degree of Master of Sciences

at

Stellenbosch University

Department of Mathematical Sciences
Applied Mathematics Division
Faculty of Natural Sciences

Supervisor: Ms Sonia Woudberg

Date: March 2010

Declaration

By submitting this thesis electronically, I declare that the entirety of the work contained therein is my own, original work, that I am the owner of the copyright thereof (unless to the extent explicitly otherwise stated) and that I have not previously in its entirety or in part submitted it for obtaining any qualification.

Signature:  Date: 11-02-2010

Abstract

Macroscopic diffusion through porous media is considered in systems where this process does not occur along with or induce bulk convective flow of the diffusing species. The diffusion coefficient present in the governing equations of such macroscopic diffusion is unique to a pair of species in a binary system. This coefficient may be determined experimentally, but such experimentation must be carried out for every different pair of species. Taking this into consideration, a deterministic pore-scale model is proposed to predict the effective diffusivity of homogeneous and unconsolidated porous media which ultimately depends solely on the porosity of the media. The approach taken is to model a porous medium as either a fibre bed or an array of granules through which the diffusive process is assumed to be homogenous and transversally isotropic. The fibre bed and granular models may be viewed as two-dimensional and three-dimensional models respectively, and may also be combined to form a weighted average model which adjusts to differing diffusive behaviour at different porosities. The model is validated through comparison with published analytical and numerical models as well as experimental data available in the literature. A numerical program is implemented to generate further data for various arrangements of homogeneous, anisotropic and transversely isotropic porous media. The numerical results were validated against an analytical model from the literature which proved to be inapplicable to a specific case. The weighted average analytical model is proposed for this case, instead. The results of this study indicate that the weighted average analytical model is in good agreement with the numerical and experimental data and as such may be applied directly to a binary system of which the porosity is known in order to predict the effective diffusivity.

Opsomming

Makroskopiese diffusieprosesse deur poreuse media word oorweeg in sisteme waar geen konveksie van die diffunderende stof plaasvind of geïnduseer word nie. Die wiskundige beskrywing van hierdie prossese bevat die sogenaamde diffusiekoëffisïent, 'n konstante wat uniek is tot 'n tweeledige sisteem. Dié konstante kan eksperimenteel bepaal word, maar as gevolg van die uniekhied daarvan tot verskillende sisteme moet dit vir elke tweeledige sisteem bepaal word. Op grond hiervan word 'n deterministiese model voorgestel om die effektiewe diffusiwiteit vir diffusie deur homogene en losstaande poreuse media te voorspel. Die model hang slegs af van die porositeit van die poreuse medium wat benader word as 'n veselbed of korrelstruktuur. Die diffusieproses deur dergelike strukture word beskou as homogeen en isotroop in die dwarsstroomrigting. Die veselbed- en korrelmodelle word beskou as twee- en driedimensionele modelle onderskeidelik en word gekombineer om 'n geweegde gemiddelde model te vorm wat dus by enige porositeit die verlangde porositeit gee. Die model is geverifieer deur vergelyking met analitiese- en numeriese modelle asook eksperimentele data vanuit die literatuur. 'n Numeriese program is gebruik om verdere resultate te verkry vir verskeie skikkings van homogene, anisotrope en dwarsverskuifde poreuse media. Die numeriese resultate is gekontroleer deur vergelyking met 'n analitiese model vanuit die literatuur. 'n Spesifieke geval is uitgewys waarvoor hierdie model nie toepasbaar is nie, maar waarvoor die voorgestelde geweegde gemiddelde model goeie resultate lewer. Die uitkomste dui aan dat die analitiese model goed ooreenstem met die numeriese en eksperimentele data en kan dus direk toegepas word om die effektiewe diffusiwiteit te verkry van 'n tweeledige sisteem waarvan die porositeit bekend is.

Acknowledgements

Thank you so much to my family, friends (extended family), supervisor and fellow students for making life a wonderfully interesting journey! Yes, that *is* a compliment. Baie dankie vir jul ondersteuning en liefde!

Tusen takk til Dr. Britt Halvorsen og Høgskolen i Telemark for muligheten til å få kunnskap og erfaring ved HiT og en fantastisk sjanse til å utforske Norge!

The financial assistance of the South African National Energy Research Institute towards this research is hereby acknowledged. Opinions expressed and conclusions arrived at, are those of the author and are not necessarily to be attributed to SANERI.

Contents

Nomenclature

General symbols:

C	specific heat capacity	$[L^2/T]$
c	mass concentration of mixture	$[mol/L^3]$
c_A	molar concentration of species A in a mixture	$[mol/L^3]$
d	length of square RUC	$[L]$
d_s	length of RUC solid cube	$[L]$
$d_\perp$	transverse cell length	$[L]$
$d_\parallel$	stream-wise cell length	$[L]$
$d_{s_\perp}$	transverse solid length	$[L]$
$d_{s_\parallel}$	stream-wise solid length	$[L]$
D	molecular diffusion coefficient of a binary system	$[L^2/T]$
D_{eff}	effective diffusion coefficient of a binary system	$[L^2/T]$
D_{SP}	effective diffusion coefficient of SP model	$[L^2/T]$
D_{PS}	effective diffusion coefficient of PS model	$[L^2/T]$
D_i	diffusion coefficient of element i of composite	$[L^2/T]$
h	transverse pore-width used in Bell & Crank (1973)	$[-]$
$\underline{j}_A$	molecular mass flux (diffusive flux) of species A	$[M/L^2T]$
$\underline{J}_A$	molar flux of species A	$[M/L^2T]$
k	coefficient of thermal conductivity	$[L^2/T]$
L	length of fibre bed cell	$[L]$
Le	Lewis number	$[-]$
l_i	length of element i of composite	$[L]$
l	total length of composite	$[L]$
Nu	Nusselt number	$[-]$
$\underline{\hat{n}}$	direction of net diffusion	[-]
$\underline{n}_A$	absolute mass flux of species A	$[M/L^2T]$

$\underline{n}$	unit vector normal to surface	$[-]$
Pr	Prandtl number	$[-]$
Pe	Peclet number	$[-]$
$\underline{q}$	heat flux	$[L^2/T]$
Re	Reynolds number	$[-]$
r	chemical production or consumption	$[mol/T]$
Sc	Schmidt number	$[-]$
Sh	Sherwood number	$[-]$
s	width of composite	$[L]$
t	time	$[T]$
U_0	total volume of RUC	$[L^3]$
U_s	volume of solid phase within RUC	$[L^3]$
U_f	volume of fluid phase within RUC	$[L^3]$
$U_{\|\|}$	fluid volume with streamwise net diffusion within RUC	$[L^3]$
$U_\perp$	fluid volume with transverse net diffusion within RUC	$[L^3]$
U_t	fluid volume unbounded by solid phase within RUC	$[L^3]$
U_g	fluid volume with stagnant convective flow within RUC	$[L^3]$
V	volume	$[L^3]$
V_a	general volume	$[L^3]$
$\underline{v}$	mass average velocity	$[L/T]$
$\underline{v}_a$	velocity of general volume	$[L/T]$
$\underline{v}_i$	average velocity of species i	$[L/T]$
$\underline{v}^*$	molar average velocity	$[L/T]$
$\underline{w}$	velocity of surface of general volume, V_a	$[L/T]$
x	Cartesian coordinate	$[-]$
y	Cartesian coordinate	$[-]$

Greek letters:

α	thermal diffusivity	$[L^2/T]$
γ_A	molar fraction of species A	$[-]$
ϵ	porosity	$[L^3]$
η	outwardly drawn normal to boundary	$[-]$
θ	weighted average coefficient used in Bell & Crank (1973)	$[-]$
μ	coefficient of dynamic viscosity	$[L^2/T]$

ν	kinematic viscosity	$[L^2/T]$
ρ	mass concentration of mixture	$[M/L^3]$
ρ_A	mass concentration of species A in a mixture	$[M/L^3]$
σ	streamwise solid length in the unit cell as used in Bell & Crank (1973)	$[-]$
τ	shear stress	$[N/L^2]$
Φ	variable used in discretisation technique in Patankar (1980)	$[-]$
ϕ	property of system	$[-]$
χ	tortuosity	$[-]$
ψ	geometric factor of RUC model	$[-]$
ω_A	mass fraction of species A	$[-]$

Acronyms:

PS	parallel-series
RUC	Representative Unit Cell
TDMA	tri-diagonal matrix algorithm
SP	series-parallel

Chapter 1

Introduction

The study of multiphase processes in porous media requires a thorough investigation into the various mechanisms that combine to create complex flow processes. To this end a complex multiphase system may be separated into simpler processes which, once understood, may be combined again in an effort to model the entire process successfully. The study of macroscopic diffusion is vital as it has a marked influence on more complex processes such as dispersion, combustion and chemical reaction.

Different types of diffusion occur in nature and industry and is dependent on the structure of a system as well as the properties of the diffusing chemical species. The presence of Knudsen diffusion may be detected in systems with very small concentrations of gas species or in which the host solid structure consists of pores of extremely small length scales. The random motion of molecules is labelled as Knudsen diffusion when individual molecules of a species are more likely to collide with the solid walls of a host or external solid structure than with other like molecules. A combination of Knudsen and molecular diffusion may take place in porous media with non-uniform pore sizes. Open systems may also be subject to surface diffusion in which the superficial molecules diffuse into the surrounding species and vice versa.

Molecular diffusion, in contrast to Knudsen diffusion, is present when the individual molecules of a species tend to collide with other like molecules more frequently than with the host or external solid structure and display a net movement in a particular direction. In a porous medium this occurs when the average free path of a molecule is comparatively short compared to the pore size and a concentration gradient of the diffusing species exists across these pores. This class of diffusion is also referred to as bulk, transport or Fickian diffusion

due to the governing mathematical laws determined by Adolf Fick, a German scientist of the 1800's. Fick developed the rate equation of molecular diffusion - Fick's first law, as well as the diffusion equation (or Fick's second law) which describes the diffusive transport of mass of a species.

Fick's first law linearly relates the mass flux to the concentration gradient of a species. The proportionality constant in this law is the diffusion coefficient, denoted by D. This coefficient is valid in the absence of an obstacle, such as the solid phase of a porous medium. The presence of an impermeable obstacle would decrease the mass flux. In such a case an effective diffusivity, D_{eff}, would compensate for the change in mass flux. A unique effective diffusivity can be determined experimentally for a specific system, but cannot be applied to another system with different constituents. As the diffusivity of a system is widely assumed to be dependent on the structure of the porous medium, whether it be a packed bed of glass spheres or the solid phase of a porous catalyst, it is valuable to have accurate, trusted models to predict the effective diffusivity of a system without the need of further experimental studies.

The application of an effective diffusivity model is vast in scope. Numerous studies exist to predict this coefficient for processes present in the fields of, amongst others, food engineering - see studies by Singh & Gupta (2007), energy research (Shi et al. (2009)), chemical engineering (Wakao & Smith (1962)), and fluid dynamics (Beyenal & Lewandowski (2000)). It is an established research area, but one in which there is constant investigation into the development of better models.

The diffusion coefficient, D, as well as the effective diffusivity, D_{eff}, require investigation as both are unique to a system. It is thus useful to combine these two coefficients in a diffusivity ratio, i.e. D_{eff}/D. Various models of D_{eff}/D exist in the literature. Statistical models, such as Monte-Carlo simulations of diffusion in a system (Kim & Torquato (1992)), concentrate on finding the statistical distributions of various phases within a system. Deterministic models may focus on the porous microstructure of a host solid and determine the effective diffusivity in a unit cell that is representative of the greater system (Crank (1975)). In this work such a deterministic model is proposed to predict the diffusivity ratio. The Representative Unit Cell (RUC) model is applied to an isotropic, macroscopic diffusion process through an impermeable, unconsolidated porous medium, following on considerable success of the RUC model on application to drag during convection in a porous medium by Woudberg et al. (2006).

The pore-scale RUC model, in which the solid phase is modelled as squares, is applied to an

unconsolidated porous medium in which the diffusion process is assumed to be isotropic (Whitaker (1999b)). The resulting expressions for the effective diffusivity ratio is tested against a computational fluid dynamics model using the tri-diagonal matrix algorithm of Patankar (1980). The same numerical model is used to predict the diffusivity of arrays of unconsolidated rectangles in which the diffusion process is not necessarily isotropic. The diffusivity of these arrays are predicted through a deterministic model developed by Crank (1975) and Bell & Crank (1973) which is also tested against the numerical model.

The governing equations of macroscopic diffusion are outlined in the first chapter. The analogous processes of mass, heat and momentum transfer are also explored to further understanding of the diffusion process. This process is regarded in detail in Chapter 3, where the diffusion equation is derived using the general transport theorem. In Chapter 4 the problem of diffusion in homogeneous porous media is discussed and the analytical RUC model is proposed as a means to predict the diffusivity ratio. An alternative method of regarding porous media which considers a composite medium consisting of multiple elements is held forth in Chapter 5 and the results of application of such a method are detailed in Chapter 6. The numerical method applied is discussed in Chapter 7, while all the numerical results generated through this method are given in Chapter 8. These numerical data are compared with the analytical RUC model as well as the models proposed by Bell & Crank (1973).

The results of this work have been published in the proceedings of the Fifth International Conference on Computational and Experimental Methods in Multiphase and Complex Flow (Du Plessis & Woudberg (2009)), held at the Wessex Institute of Technology, $15 - 17$ June 2009 in New Forest, United Kingdom and presented as a poster, titled "Modelling of single-phase diffusive transport in porous environments", at the International Conference on Coal Science and Technology in Cape Town, South Africa, $26 - 29$ October 2009. A paper has also been submitted to the Chemical Engineering Science journal and has been provisionally accepted for publication subject to minor corrections. An academic visit to the Høgskolen i Telemark in Porsgrunn, Norway in 2008, during which time flow through various packing materials in fluidised beds was studied, resulted in another publication in the proceedings Fifth International Conference on Computational and Experimental Methods in Multiphase and Complex Flow (Rautenbach et al. (2009)), which is unrelated to this work.

Chapter 2

Diffusion

The migration of molecules of a substance through those of another is known as diffusion. It takes place when the concentration of that substance is higher in one region than another causing its molecules to migrate until there is a uniform concentration profile throughout the system. This process leads to the transport of mass of a given species in a system. The path that each molecule takes in this diffusive motion is random, but the net migration of this substance will be in the direction of decreasing concentration.

Often the diffusive movement induces a bulk motion of matter. This bulk motion, or convection, contributes significantly to the transport of mass within a system. In different fields of study this bulk motion may be called advection, in which case the term convection is defined differently.

Since the type of diffusion in question occurs on the molecular scale, it is intuitive that diffusion of gases should be faster than liquids, which in turn should be faster than that of solids. The same equations are valid for all three phases (under certain conditions), since diffusion of each one remains a molecular process. There are, however, differences in the properties of the parameters in the mathematical description of diffusion. The diffusion coefficient, D, cannot be determined in the same way for diffusion in each phase. The particular application of this work is to diffusion within a porous medium, such as a gas through the channels of a host solid which may be considered stationary so that no bulk motion is induced. The solid phase itself is assumed to be impermeable.

This chapter introduces the principles of diffusion which lead to Fick's first and second laws. The problem of diffusion through a porous medium is also introduced, but is discussed in further detail in Chapter 4. The concept of mass average velocity is explored as its applica-

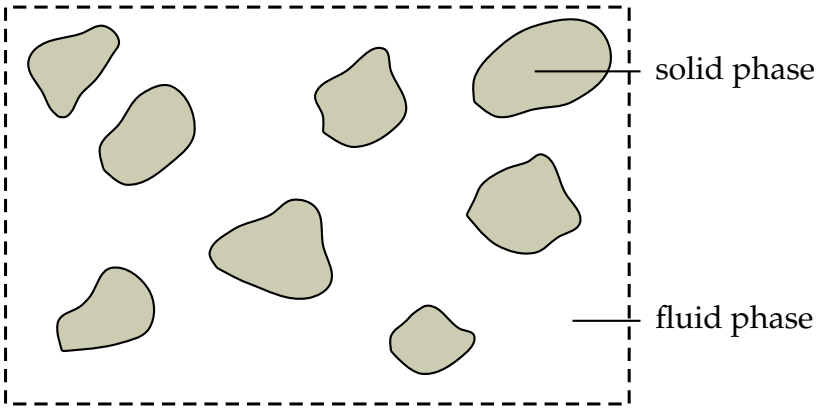

Figure 2.1: Porous medium with irregular solids.

tion to molecular diffusion. The analogy of molecular diffusion to the processes of heat and momentum transfer and results of these comparisons are also discussed.

2.1 Structure

Diffusion may take place in a porous medium where there is a fixed host solid together with another diffusing species in a system. Figure 2.1 is an example of a porous medium with irregular solid particles fixed in space. Figure 2.2 is an approximation of this porous medium with solid particles represented by uniform squares in a staggered array. The diffusion coefficient specific to the geometry of such an array is found through application of the methods discussed in subsequent chapters.

2.2 Fick's first law of diffusion

In considering molecular diffusion it is possible to draw comparisons with the transfer of heat through conduction. Conduction takes place through the collisions of molecules with differing temperatures, where higher temperatures indicate higher molecular energies. The

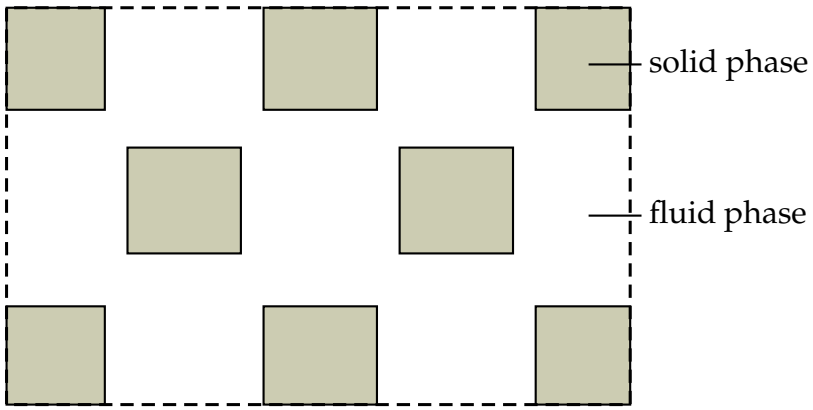

Figure 2.2: Model of a porous medium.

heat transfer rate may then be viewed as linearly proportional to the temperature gradient (also known as Fourier's law). Analogous to this is the mechanism of diffusion. The rate of diffusion is thus also linearly proportional to the concentration gradient of a chemical species in a system. This rate equation is known as Fick's law (or Fick's first law of diffusion) and has the form

$$\underline{j}_A = -\rho D \nabla \omega_A, \tag{2.1}$$

where $\underline{j}_A$ is the molecular mass flux of species A and ρ the total mass concentration of all species in the system. The proportionality constant, D, is the diffusion coefficient or diffusivity which is specific to a given system. The mass fraction of species A, denoted by ω_A, is a fraction of the entire system's mass concentration, i.e. $\omega_A = \rho_A/\rho$.

The molecular mass flux, $\underline{j}_A$, is the quantity of species A that is transported in the direction of diffusion per unit time and unit area. When the total mass concentration, ρ, is constant, Fick's first law becomes

$$\underline{j}_A = -D \nabla \rho_A. \tag{2.2}$$

A physical interpretation of Fick's law is presented in Figure 2.3, which shows that the mass fraction or concentration gradient is opposite to the direction of diffusion.

Fick's first law, in this form, is applicable to an isotropic medium. When diffusion occurs in an anisotropic medium, the orientation of that medium may alter the rate of diffusion significantly. In such a case the diffusivity tensor $\underline{\underline{D}}$ is applicable in the following manner:

$$\underline{j}_A = -\rho \underline{\underline{D}} \cdot \nabla \omega_A. \tag{2.3}$$

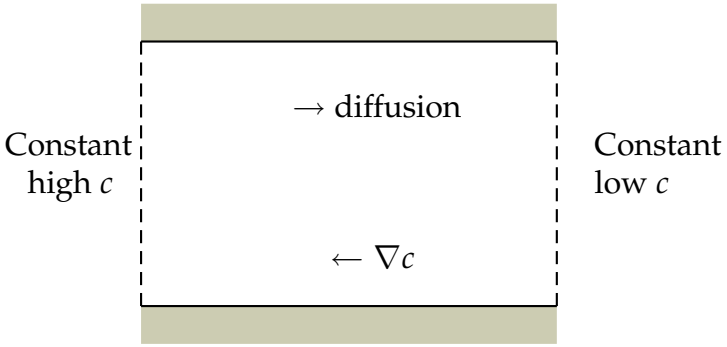

Figure 2.3: Fick's first law of diffusion: the gradient of mass concentration c is proportional, but opposite in direction to the diffusion.

A full study of the governing diffusion equations in tensor notation was conducted by Bear & Bachmat (1991).

2.2.1 Mass average velocity

In a multi-component system the molecular diffusive movement may lead to a bulk motion of all the species, resulting in mass transfer through convection (bulk motion). In considering such a system, there needs to be noted that the motion of each species may be different to the others as well as to the mixture as a whole. The concept of a mass average velocity is therefore used to refer to the average velocity of the center of mass of the entire system and, for a multi-component system of N species, is defined as

$$\underline{v} = \frac{1}{\rho}\sum_{i=1}^{N}\rho_i\underline{v}_i = \sum_{i=1}^{N}\omega_i\underline{v}_i, \tag{2.4}$$

where $\underline{v}_i$ refers to the average velocity of species i and $\omega_i = \rho_i/\rho$ the mass fraction of species i (with ρ the mass concentration of the whole mixture). For a binary mixture equation (2.4) is thus

$$\underline{v} = \omega_A\underline{v}_A + \omega_B\underline{v}_B. \tag{2.5}$$

The quantity $\rho\underline{v}$ is the total rate at which mass flows through a cross-sectional area perpendicular to the direction of flow due to the bulk motion, in other words, the mass flux due to convection. The diffusive flux of species A relative to the bulk motion may thus be defined as

$$\underline{j}_A = \omega_A(\underline{v}_A - \underline{v}), \tag{2.6}$$

which is then another form of Fick's first law.

As mentioned, the bulk motion of a mixture contributes to the mass transfer taking place. The absolute mass transfer of species A, $\underline{n}_A$, is therefore given by the diffusive mass transfer together with the convective mass transfer, i.e.

$$\underline{n}_A = \underline{j}_A + \rho_A \underline{v} = -\rho D \nabla \omega_A + \rho_A \underline{v}. \tag{2.7}$$

Equation (2.7) is valid for a control volume, i.e. a volume that is fixed relative to a specific coordinate system. If, however, a general volume of which the boundaries may move with time is used, equation (2.7) becomes

$$\underline{n}_A = -\rho D \nabla \omega_A + \rho_A (\underline{v} - \underline{w}). \tag{2.8}$$

In this case $\underline{w}$ is the velocity of the surface of the general volume, V_a, used to measure the properties of the fluid and which is not fixed in space.

2.3 Fick's second law of diffusion

Fick's second law of diffusion may be applied to a system with stationary, incompressible fluids and a constant diffusion coefficient with no sources of chemical production. Also known as the diffusion equation, it is given by

$$\frac{\partial \rho_A}{\partial t} = D \nabla^2 \rho_A. \tag{2.9}$$

The diffusion equation describes the mass transport of a specific species. It may be derived from the general transport theorem using Fick's first law. This derivation is looked at in further detail in Chapter 3.

2.4 Diffusion coefficient

In Fick's law, a proportionality constant is present in the form of the diffusion coefficient D. This coefficient is the diffusivity of a system and is similar to the proportionality constants in momentum and energy transfer.

In a system with two species, A and B, the diffusivity D is a property of the pair (and is thus sometimes represented as D_{AB} in the literature), rather than a property of exclusively

species A or B. It is unique to such a pair and is generally dependent on the composition of the system, as well as its temperature and pressure.

The difficulty lies in the estimation of the diffusivity. It may be determined empirically for certain pairs of species, but that method requires intensive testing and difficult measurement. Different models exist for different combinations of phases in binary systems since a model constructed for a binary mixture of gases would not be applicable to a mixture of a gas and a solid, for instance. Specifically, in the case of gases, the diffusivity could change with a change in temperature. Models of the form $D \sim p^{-1}T^{3/2}$ for ideal gases are discussed in Bird et al. (2007), where the diffusivity is dependent on the temperature T and pressure p of a system.

The diffusivity of mixtures of liquids is generally found through experimental measurement since the analytical models developed for such systems are complex and are not sufficiently accurate. In certain mixtures where the diffusing species has small concentrations, it may be found that the diffusivity increases with an increase in temperature (Bergman et al. (2007)). Bird et al. (2007) discuss two alternative approaches to find models that predict the diffusivity. The hydrodynamic theory is based on the Nernst-Einstein equation, which describes the diffusivity in terms of each particle's potential to gain velocity due to unit forces acting on it. The other theory that comes under discussion in Bird et al. (2007) is the Eyring activated-state theory which models a liquid as a crystal lattice.

As stated, this work concentrates on diffusion within a binary system where one phase forms the solid phase within a a porous medium and the other an incompressible Newtonian fluid and it will be assumed that the diffusion coefficient in such a system is independent of temperature and pressure. The model considered is a spatially periodic one whereby the diffusivity ratio of a section of the porous medium is found and is assumed to be representative of the whole, since the specific geometry of that section, as well as its diffusive properties, is repeated throughout the medium. Published models for diffusion in a porous medium are looked at in more depth is Chapter 4.

2.5 Mass and molar concentrations

The transport of mass may be approached mathematically by considering either mass or molar units. Both sets of notation are necessary and depend on the further specifications of the problem to be modelled. If the system includes chemical reactions the governing

	mass form	molar form
Fick's law	$\underline{j}_A = -\rho D \nabla \omega_A$	$\underline{J}_A = -cD\nabla\gamma_A$
	$\underline{j}_A = \omega_A(\underline{v}_A - \underline{v})$	$\underline{J}_A = \gamma_A(\underline{v}_A - \underline{v}^*)$

Table 2.1: Comparison of governing diffusion equations in molar and mass units.

diffusion equations would be written in the form of molar concentrations.

The mass concentration ρ_A has been defined as the mass of species A per unit volume of the mixture. The molar concentration c_A is defined similarly as the number of moles of species A per unit volume of the mixture. The mass fraction ω_A gives the ratio of the mass concentration of species A to the mass concentration of the entire mixture, ρ. Analogous to this is the mole fraction, γ_A, which is defined as the ratio of the molar concentration of species A to the total molar concentration, c.

Equations (2.6) and (2.7), which are in terms of the mass average velocity, may be written in terms of the molar average velocity $\underline{v}^*$. The two forms of Fick's law, equations (2.1) and (2.6), are given in Table 2.1 in their respective mass and molar forms.

2.6 Mass, heat and momentum transfer

As mentioned in Section 2.2, the problem of molecular diffusion, or mass transfer, may be compared with that of heat transfer as well as momentum transfer. In all three cases a property gradient exists which causes a transfer process of the specific property. This gradient thus acts as the driving force behind the property flux which is in the direction of decreasing potential. In the case of mass transfer, this driving force is a concentration gradient.

In Section 2.2, Fick's first law is given in equation (2.1). The principle assumption in establishing Fick's law is that of a linear proportionality between the concentration gradient and the flux. Similar equations are derived for heat and momentum transfer where the relationship between the gradient and flux is also assumed to be linear.

The rate equation for heat transfer (Bird et al. (2007)),

$$\underline{q} = -k\nabla T, \tag{2.10}$$

is called Fourier's law of heat conduction with k the coefficient of thermal conductivity and

T the temperature. The linear proportionality in Fourier's law can be demonstrated experimentally while the direction of conduction is consistent with the second law of thermodynamics.

Newton's equation of viscosity (Bird et al. (2007)),

$$\tau = \mu \frac{\partial u}{\partial y}, \tag{2.11}$$

describes the shear stresses between the layers of a Newtonian fluid that move at different velocities, u, in the x-direction. This change in x-direction velocity is assumed to be linear - the linear proportionality constant is μ, the coefficient of dynamic viscosity. Equation (2.11) is therefore the rate equation for the molecular transfer of momentum perpendicular to the direction of flow.

2.6.1 Diffusivities

The rate equations for heat, mass and momentum transfer are described by equations (2.10), (2.1) and (2.11) respectively. The linear proportionality constants k and μ may be used to define other transfer process coefficients with the same dimensions as the diffusivity D, namely $[L^2/T]$.

The kinematic viscosity (momentum diffusivity) of a Newtonian fluid is defined as (Bergman et al. (2007))

$$\nu \equiv \frac{\mu}{\rho}, \tag{2.12}$$

with ρ the density of the fluid. The thermal diffusivity of heat transfer is defined as

$$\alpha \equiv \frac{k}{\rho C}, \tag{2.13}$$

with ρ again the density of the fluid and C the specific heat capacity. Along with D, these three transfer coefficients form the diffusivities of the respective transfer processes.

2.6.2 Dimensionless numbers

In the study of transfer processes it is useful to be able to understand the interactions between the three processes and quantify their effect on each other. The diffusivities defined

in Subsection 2.6.1 are used to this end in defining dimensionless numbers that relate the three processes.

The Prandtl number, Pr, is defined as the ratio between the momentum and energy diffusivities (Bird et al. (2007)),

$$\mathrm{Pr} \equiv \frac{\nu}{\alpha}. \tag{2.14}$$

Thus, a large Prandtl number would be indicative of a more effective energy transfer process compared to the heat transfer capability.

The Lewis number, Le, is defined as the ratio between the thermal and mass diffusivities,

$$\mathrm{Le} \equiv \frac{\alpha}{D}, \tag{2.15}$$

where a large Lewis number would occur in a process where the transfer of heat is faster than the transfer of mass.

The Schmidt number, Sc, relates the kinematic viscosity to the mass diffusivity and is defined as

$$\mathrm{Sc} \equiv \frac{\nu}{D}. \tag{2.16}$$

Similarly to equations (2.14) and (2.16), a large Sc-value would indicate a faster transfer of momentum than mass.

These three dimensionless numbers are of particular use in characterising the boundary layers present in systems with simultaneous transfer processes.

The Schmidt number is further used in conjunction with the Reynolds number Re in the definition of the Peclet number, $Pe = \mathrm{ReSc}$, which relates the rate of convection to the rate of macroscopic diffusion in a system and is used extensively in computational fluid dynamics. An analogous Peclet number is defined using the Prandtl number, i.e. $Pe = \mathrm{RePr}$.

Dimensionless numbers pertaining to the boundary layer are also defined. The Sherwood number, $Sh = h_m L/D$, gives the ratio of diffusive to convective mass transport which occurs at the concentration boundary layer, where h_m is a mass transfer coefficient and L a characteristic length of the system (Bergman et al. (2007)). The equivalent heat and momentum dimensionless numbers are the Nusselt and Stanton numbers, respectively.

2.6.3 General transport equation

The general transport equation may be applied to all three transport process discussed above. It relates the rate of change in time and space of a property to external sources of that same property, i.e.

$$\frac{\partial \rho \phi}{\partial t} = \nabla \cdot (D \nabla \phi) - \nabla \cdot (\rho \underline{u} \phi) + S, \tag{2.17}$$

where the second term denotes the flux of property ϕ, the third the convection of ϕ and the fourth any sources or sinks of ϕ, such as chemical production or consumption.

In this chapter Fick's first and second laws were briefly examined. The diffusion coefficient, the proportionality constant in Fick's first law, was introduced and discussed. The analogous processes of heat, mass and momentum transfer were also considered in order to provide further background and understanding of the process of molecular diffusion.

Chapter 3

Mass transport

The diffusive motion of molecules is essentially the transport of mass of a given species through space. Throughout the rest of this work the diffusion of a two-component system is of interest. This chapter explores these concepts and their application in mathematically describing the transport of mass within a system.

3.1 General transport theorem

The general transport theorem (Whitaker (1999a)) for an arbitrary volume $V_a(t)$ is given by

$$\frac{d}{dt}\iiint_{V_a(t)} f dV = \iiint_{V_a(t)} \frac{\partial f}{\partial t} dV + \iint_{\partial V_a(t)} \underline{n} \cdot \underline{w} f dS, \tag{3.1}$$

where $f = f(\underline{r}, t)$ and represents either mass, momentum or energy, with $\underline{r}$ being the position vector. In this theorem the general volume $V_a(t)$ does not depend on the actual matter within the volume, but rather on the velocity of its boundary or surface, $\underline{w}$.

The first term of the general transport theorem describes the total change in quantity of the function being measured in time, whether it be mass, momentum or energy. Physically, the terms on the right hand side should then ultimately describe the same total change that has taken place. The second term is the local time derivative of f summed over the entire volume resulting in the amount of f in the volume at present. The third and last term describes the movement of f across the surface of the volume, thus giving the amount of f that come into or exited the volume V_a. Together, these two terms give the amount of f that has entered or

left the volume V_a added to that which was already within the volume.

3.2 Application to diffusion

In applying equation (3.1) to diffusion, the transport of mass is of interest. For the total transport of mass the function f in equation (3.1) is chosen as $f = \rho\omega_A = \rho_A$ so that

$$\frac{d}{dt}\iiint_{V_a(t)} \rho_A dV = \iiint_{V_a(t)} \frac{\partial \rho_A}{\partial t} dV + \iint_{\partial V_a(t)} \underline{n} \cdot \underline{w}\rho_A dS. \tag{3.2}$$

If an arbitrary volume is selected mass may enter or exit the volume through diffusion or through convection. However, mass may also be produced (or consumed) due to chemical reactions between the two species in the system. The total change in mass thus has to adhere to the conservation law

$$\frac{d}{dt}\iiint_{V_a(t)} \rho_A dV = \iiint_{V_a(t)} r_A dV - \iint_{\partial V_a(t)} \underline{n} \cdot \underline{n}_A dS, \tag{3.3}$$

where r_A is the chemical production of species A within the arbitrary volume and $\underline{n}_A$ is the flux of the same species across the boundary of the volume (with $\underline{n}$ the vector normal to the surface). Together with the divergence theorem, i.e.

$$\iiint_{V} \nabla \cdot \underline{v} dV = \oiint_{\partial V} \underline{n} \cdot \underline{v} dS, \tag{3.4}$$

equation (3.3) may be substituted into equation (3.2) to find

$$\iiint_{V_a(t)} \left[\frac{\partial \rho_A}{\partial t} + \nabla \cdot (\rho_A \underline{w}) + \nabla \cdot \underline{n}_A - r_A \right] dV = 0. \tag{3.5}$$

Since the volume $V_a(t)$ is arbitrary, equation (3.5) must hold for any representative volume chosen. This will only be true if the integrand of equation (3.5) is zero, thus

$$\frac{\partial \rho_A}{\partial t} + \nabla \cdot (\rho_A \underline{w}) + \nabla \cdot \underline{n}_A - r_A = 0. \tag{3.6}$$

Equation (3.6) (Bird et al. (2007)) describes a conservation law for the system that is applicable in situations with both advection and diffusion. It can thus be simplified further until it is in an appropriate form for a system with only diffusion present.

The absolute mass flux of species A, $\underline{n}_A$, was described in Section 1.1 by equation (2.8) and thus, after its substitution and further simplification of the result, equation (3.6) becomes

$$\frac{\partial \rho_A}{\partial t} + \nabla \cdot (\rho_A \underline{v}) - \nabla \cdot (D \nabla \rho_A) - r_A = 0. \tag{3.7}$$

Note that in this form none of the terms include the velocity of the volume $V_a(t)$, and the same result would have followed had a material volume been used in the general transport theorem. Here the first term is the rate of change in time of the mass concentration of species A and r_A denotes the rate of chemical production or consumption as mentioned earlier. The second and third terms describe the dispersion of mass concentration due to the bulk and molecular motions respectively. Equation (3.7) may be simplified further in the case of an incompressible mixture, where the bulk velocity is the same throughout, hence

$$\frac{\partial \rho_A}{\partial t} + \underline{v} \cdot \nabla \rho_A - D \nabla^2 \rho_A - r_A = 0, \tag{3.8}$$

and is applicable to systems where diffusion occurs in dilute liquid solutions at a constant temperature and pressure (Bird et al. (2007)).

Finally, in the case where there is no convection (no bulk motion) and no sources of chemical production (or consumption), equation (3.8) simplifies to

$$\frac{\partial \rho_A}{\partial t} - \nabla \cdot D \nabla \rho_A = 0, \tag{3.9}$$

which is known as either the diffusion equation or Fick's second law of diffusion and is applicable to systems with diffusion through a host solid or in stationary liquids. Further, for a steady-state process in an incompressible mixture with no bulk motion or chemical production and a constant diffusivity, the diffusion equation simplifies to the Laplace equation, i.e.

$$\nabla^2 \rho_A = 0. \tag{3.10}$$

This equation is valid for a single point and as such must be solved at every point in the area of concern.

Chapter 4

Diffusion in homogeneous porous media

Diffusion in a porous medium adheres to the governing diffusion equation, equation (3.9). If this equation is to be applied to an actual process, the diffusion coefficient D needs to be modelled as it is a variable depending on the constituents of the system. A general assumption made on which most models are based is that the diffusivity is dependent solely on the geometry of the porous medium, rather than a variable which arises from the process of diffusion (there are published models which contest this assumption).

Various models of D_{eff}/D exist which are based on the geometry of the porous medium. The geometry of a porous medium is contained in two particular parameters - the porosity and the tortuosity. The porosity ϵ, or void fraction, gives an indication of the ratio of fluid-filled space to solid space. The tortuosity χ, on the other hand, gives an indication of the spacing of the fluid phase in relation to the solid phase. Models based solely on the porosity are useful as it is relatively easy to determine. Such models may be of the form $D_{eff}/D = f(\epsilon)$, where $f(\epsilon)$ ranges from a function of the form ϵ^m to $a\epsilon + b$ as briefly discussed in Currie (1960), depending on the system to which it is to be applied. Currie (1960) found the diffusion coefficient of a gas through a granular medium to be dependent on the shape and spacing of the solid in addition to the porosity. The suggestion was an empirical equation of the form $D_{eff}/D = \gamma\epsilon^{\mu}$ with γ and μ functions of the type of granular solid.

Unlike the granular medium investigated by Currie (1960), the solid phase may be consolidated with porous spaces located within. Diffusion through such a solid is investigated by Gavalas & Kim (1981), who propose a periodic capillary model capable of including macroscopic, Knudsen and transient diffusion. In their work the spatial periodicity of the capillary model allowed them to concentrate on a unit cell representative of the whole.

Wakao & Smith (1962) studied diffusion in catalyst pellets which is a process where diffusion occurs between the pellets, but also through the pores within the pellets themselves (a so-called bi-disperse porous system). They proposed a model based on the porosities of the micropores and macropores to include both Knudsen and macroscopic diffusion. The resulting equation for D_{eff}/D of their model could be weighted according to the predominant type of diffusion occurring. A system with a low density of catalyst pellets where the effect of Knudsen diffusion through the macropores is negligible could thus be weighted so that only the macroscopic diffusion would be considered.

A spatially periodic model, such as that proposed by Gavalas & Kim (1981), Currie (1960) and Kim et al. (1987) cannot be homogeneous or isotropic (where homogeneous implies invariant under arbitrary translation and isotropic invariant under arbitrary rotation), whereas the actual porous medium may have these properties. Analysis of the diffusivity tensor by Ryan et al. (1981) revealed that although a porous medium model may be anisotropic, the diffusion process through it may be assumed to be invariant with respect to the streamwise and transverse directions as expressed in rectangular cartesian coordinates. This implies that in such a system the diffusion coefficient is independent of the direction of the individual molecules' path and may thus be modelled as a scalar instead of a tensor.

In this chapter, two pore-scale models, the RUC models, are proposed to predict the diffusivity ratio, D_{eff}/D, for diffusion in a porous medium. Various configurations of arrays of unconsolidated solid particles are introduced through which diffusion may take place. The RUC models are applicable to homogeneous, unconsolidated arrays of square solid particles as they rely on the assumption that the diffusion coefficient D is invariant with respect to the streamwise and transverse directions. The RUC models are tested against experimental data and other analytical models available in the literature.

4.1 Volume averaging

The diffusive transport of mass of a chemical species through a porous medium with a constant diffusion coefficient is described by the Laplace equation for mass transport, equation (3.10). The Laplace equation, however, only describes the mass transport at a point and not over a vector field and therefore has to be solved at every point within the porous medium. Equation (3.10) shall thus be volume averaged over a representative portion of the porous medium in order to obtain an equation that describes the diffusion process macroscopically.

Volume averaging is conducted over the fluid phase since the solid phase is assumed to be impermeable. The volume averaging process is fully described by Whitaker (1999b) and the volume-averaged forms of the governing diffusion equations derived by Ryan et al. (1981).

The result of application of the volume averaging method is an equation containing the effective diffusivity ratio which is dependent only on porosity, i.e.

$$\frac{D_{eff}}{D} = f(\epsilon), \tag{4.1}$$

where f denotes a function of the porosity alone.

4.2 Geometric pore-scale model

The geometrical properties of a porous medium may be modelled through use of control volumes which are representative of the porous medium as a whole. The rectangular Representative Unit Cell (RUC) model was introduced by Du Plessis (1997) and is defined as the smallest rectangular control volume U_o which contains the average geometrical properties of the specific porous medium.

4.2.1 Ordered arrays

A porous medium may be modelled as illustrated in Figures 2.1 and 2.2. The solid phase is represented by rectangular solids packed in an array. Depending on the arrangement of the solids being modelled, the array may be staggered or not. Staggering may occur in either the streamwise or transverse directions, where the streamwise direction refers to the net direction of diffusion, $\hat{\underline{n}}$, and the transverse direction to the direction normal to it. Arrays staggered in the transverse and streamwise directions are indicated in Figure 4.1. In a streamwise staggered array a row of cells is shifted in the streamwise direction and in the case of a transversally staggered array a column of cells is shifted in the transverse direction.

Only regular and fully staggered arrays are considered and within these arrays there may be overlapping of the solid phase in either the streamwise or transverse direction. Here overlapping does not imply physical overlapping of the solid phase, but rather overlapping with respect to a direction. In a regular array no staggering occurs, while a fully staggered array is one in which the unit cells of the row or column being staggered fall exactly halfway along the unit cells of the adjacent rows or columns. An example of a regular array is depicted in

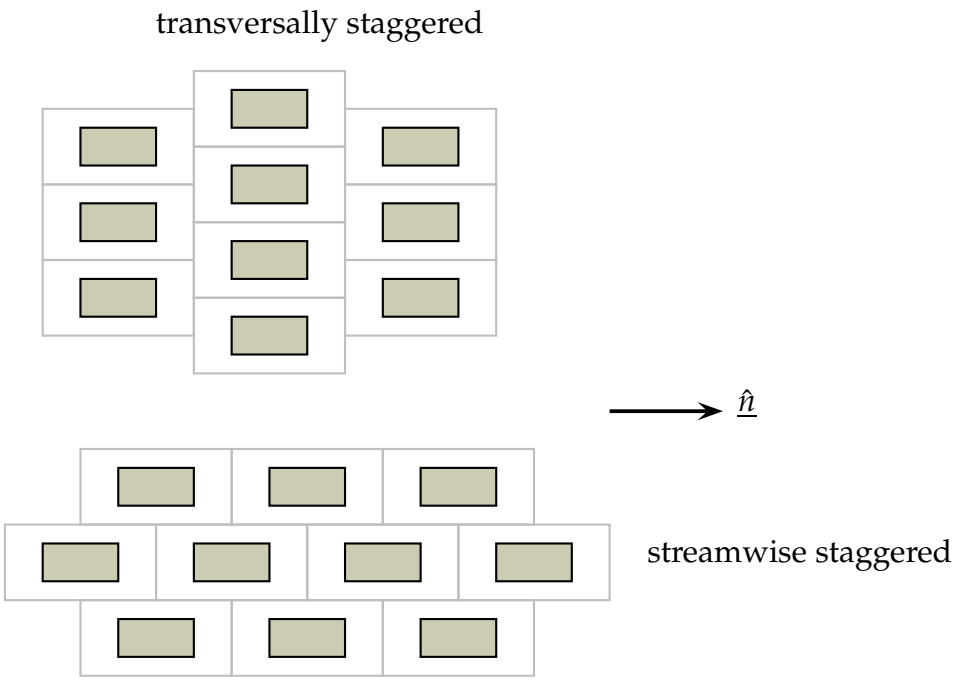

Figure 4.1: Staggering in the transverse and streamwise directions.

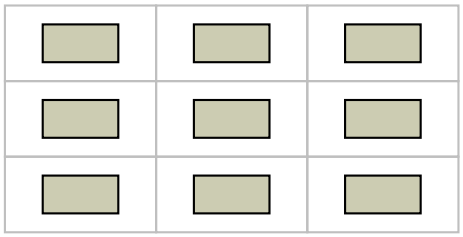

Figure 4.2: Example of a regular array.

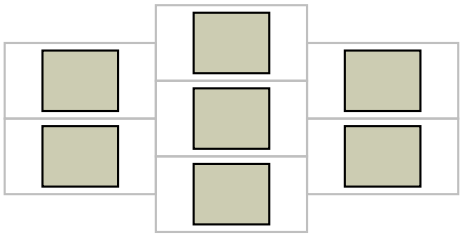

Figure 4.3: Example of a transversally staggered array with overlapping of the solid phase occurring in the streamwise direction.

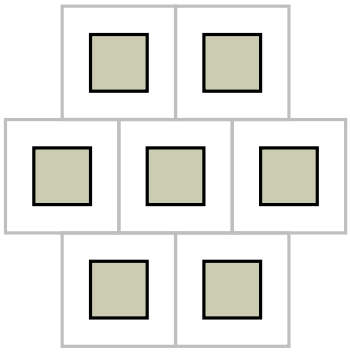

Figure 4.4: Example of a streamwise staggered array of squares.

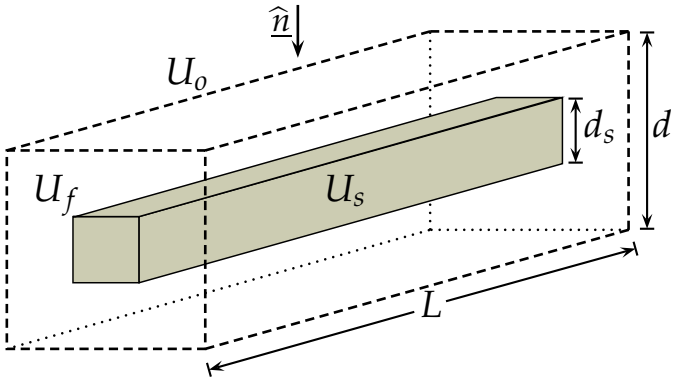

Figure 4.5: RUC model for fibre beds.

Figure 4.2 - note that in such an array it is impossible for any overlapping to occur. Figure 4.3, on the other hand, illustrates an example of a fully transversally staggered array with overlapping of the solid phase. As is visible in this figure, the overlapping of the solid phase occurs in the streamwise direction. Similarly, when an array is staggered in the streamwise direction, overlapping may occur in the transverse direction. Note that in both cases the overlapping cannot occur in the same direction as the staggering.

Ordered arrays may also consist of square solid particles instead of rectangular ones, as demonstrated in Figure 4.4. In these arrays of squares the diffusion is assumed to be the same in the streamwise and transverse directions, following findings of Whitaker (1999b). Such a system is referred to as transversally isotropic with respect to the diffusion process (Whitaker (1999b)). This is, however, not true for rectangular solids.

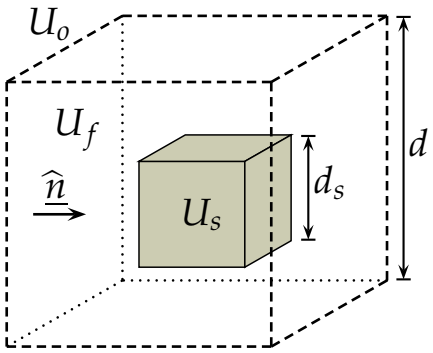

Figure 4.6: Granular RUC model.

4.2.2 Fibre bed and granular RUC models

The RUC model for unidirectional fibre beds is schematically illustrated in Figure 4.5 and that of a granular porous medium shown in Figure 4.6. In both figures $\underline{\hat{n}}$ denotes the net direction of diffusion, i.e.

$$\underline{\hat{n}} = \frac{\underline{j}}{|\underline{j}|}, \tag{4.2}$$

and U_o the total volume of the cell. The solid phase is indicated by U_s and the fluid phase by U_f.

The fibre bed model is useful in the diffusion problem when modelling the host solid as an array of unconsolidated rectangles. Similarly, the granular model is applicable when the host solid is considered to be an unconsolidated array of squares. These rectangles may or may not be staggered. The regular and fully staggered arrays described in the previous section are applicable to the RUC models. The diffusion process is assumed to be uniform along the length L of the solid fibre in Figure 4.5 and as such the fibre bed model may be considered a two-dimensional and transversally isotropic model. The granular model may thus be considered as a three-dimensional model, in contrast to the fibre bed model.

Table 4.1 summarizes the linear dimensions of the unit cell of the fibre bed and granular models in terms of the porosity.

4.2.3 Volume partitioning

The RUC model was applied to convective flow by Woudberg et al. (2006) and in keeping with the notation developed there in which piece-wise straight streamlines are assumed, the

Linear dimensions	**Fibre bed model**	**Granular model**
Solid particle size	$d_s = d\sqrt{1-\epsilon}$	$d_s = d(1-\epsilon)^{1/3}$
Cell size	$d = \frac{d_s}{\sqrt{1-\epsilon}}$	$d = \frac{d_s}{(1-\epsilon)^{1/3}}$
Pore size	$d - d_s = d(1-\sqrt{1-\epsilon})$	$d - d_s = d(1-(1-\epsilon)^{1/3})$

Table 4.1: Linear dimensions of the fibre bed and granular RUC models in terms of cell parameters and porosity.

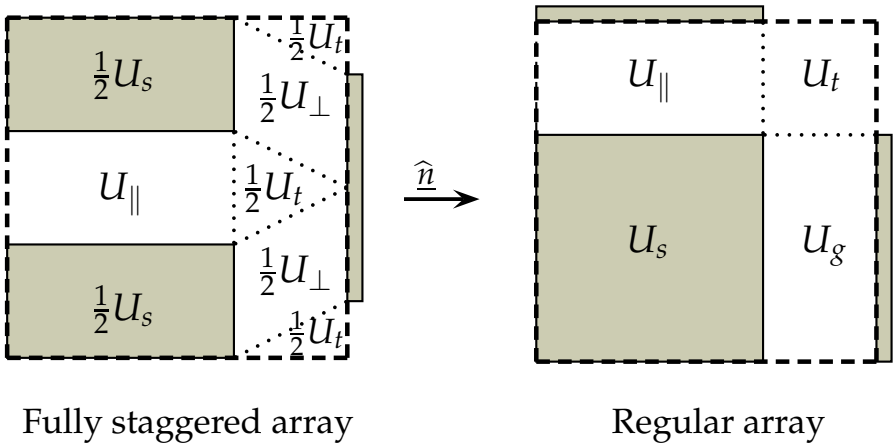

Figure 4.7: Volume partitioning of (a) a fully staggered array with overlapping in the stream-wise direction and (b) a regular array.

unit cell of fully staggered and regular arrays are partitioned into sub-volumes with uniform flow properties. In this work, however, the streamlines for convective flow are replaced with piece-wise straight diffusive lines. This is merely an assumption since diffusion is a random process wherein individual particles do not necessarily follow straight path lines. An example of such volume partitioning is given in Figure 4.7. This example demonstrates volume partitioning in RUC notation when applied to a fully staggered array and a regular array.

In Figure 4.7, $U_{||}$ denotes those sections within the porous medium where the diffusive lines are parallel to the direction of diffusion and $S_{||}$ indicates the solid phase borders also parallel to $\underline{\hat{n}}$. $U_\perp$ denotes those partitions where the fluid volume falls between two walls

Parameter	Fibre bed model	Granular model
U_0	d^2L	d^3
U_s	d_s^2L	d_s^3
U_f	$(d^2 - d_s^2)L$	$d^3 - d_s^3$
U_t	$(d - d_s)^2L$	$(d - d_s)^3$
$U_{\|\|}$	$d_s(d - d_s)L$	$d_s(d - d_s)^2$
$U_\perp$		
Regular	0	0
Fully staggered	$d_s(d - d_s)L$	$d_s(d - d_s)^2$
U_g		
Regular	$d_s(d - d_s)L$	$d_s(d - d_s)^2$
Fully staggered	0	0

Table 4.2: Volume partitioning of the RUC models for fibre beds and granular porous media.

perpendicular to $\underline{\hat{n}}$. U_g refers to areas which also fall between two walls perpendicular to $\underline{\hat{n}}$, but which are considered to be stagnant for convective flow (Woudberg et al. (2006)). For the process of diffusion the diffusive flux will not be zero in these fluid regions and will therefore be treated like the transverse fluid volumes $U_\perp$. Lastly, U_t denotes a transfer volume which does not border any part of the solid phase and therefore in which no wall friction occurs for convective flow. In the case of diffusion U_t will be treated in the same manner as the streamwise volumes $U_{||}$ as purely the direction of the diffusive lines are important.

A summary of the dimensions of each sub-volume of the fibre bed model in Figure 4.5 is given in Table 4.2.

4.2.4 Tortuosity

Tortuosity is a useful parameter when modelling a porous medium as it gives an indication of the geometry of that medium. In the RUC model the tortuosity, χ, is defined as (e.g.

Diedericks & Du Plessis (1995))

$$\chi = \frac{d_e}{d}, \qquad \chi \geq 1, \tag{4.3}$$

where d denotes the length of a unit cell and d_e the path followed by a fluid particle. The tortuosity is thus the ratio between these two parameters and a larger χ-value indicates a more staggered or tortuous path. Equation (4.3) may also be written in terms of the volume partitioning in Table 4.2. In this form it becomes

$$\chi = \frac{U_{||} + U_t + U_{\perp}}{U_{||} + U_t}, \tag{4.4}$$

where the stagnant regions, U_g, are not included.

Ideally an expression of the tortuosity in terms of the porosity of the RUC is required. Since porosity is defined as the ratio of fluid volume to the total volume, $\epsilon = U_f / U_o$, the relationship

$$d_s = d\sqrt{1-\epsilon} \tag{4.5}$$

is valid for fibre beds. Through this equation and the expressions presented in Table 4.2, the tortuosity of a staggered array for fibre beds, χ_f, may be expressed in terms of the porosity as

$$\chi_{fibre} = \frac{\epsilon}{1-\sqrt{1-\epsilon}}. \tag{4.6}$$

The effect of stagnant regions may also be accounted for, in which case equation (4.4) becomes

$$\psi = \frac{U_{||} + U_t + U_{\perp} + U_g}{U_{||} + U_t}, \tag{4.7}$$

where ψ is a geometric factor introduced by Lloyd et al. (2004) to indicate that all stagnant volumes are also considered in the model. Similarly to equation (4.6), the geometric factor for fibre beds, ψ_f, may be written in terms of the porosity as

$$\psi_{fibre} = \frac{\epsilon}{1-\sqrt{1-\epsilon}}. \tag{4.8}$$

Expressions for the tortuosity and geometric factor for granular media are calculated similarly. The expressions found for regular and staggered arrays of each model are given in Table 4.3.

4.2.5 Effective diffusion coefficient

A model is constructed according to the RUC theory to predict the effective diffusivity of an array of solid square particles. It is assumed that the diffusion through such an array is

	χ	ψ
Fibre bed model		
Regular array	1	$\frac{\epsilon}{1-\sqrt{1-\epsilon}}$
Staggered array	$\frac{\epsilon}{1-\sqrt{1-\epsilon}}$	$\frac{\epsilon}{1-\sqrt{1-\epsilon}}$
Granular model		
Regular array	1	$\frac{\epsilon}{1-(1-\epsilon)^{2/3}}$
Staggered array	$\frac{\epsilon}{1-(1-\epsilon)^{2/3}}$	$\frac{\epsilon}{1-(1-\epsilon)^{2/3}}$

Table 4.3: Expressions for the tortuosity and geometric factors of the granular and fibre bed models in terms of porosity.

transversally isotropic with respect to the diffusion process. Kim et al. (1987) states, based on the results of Ryan et al. (1981), that simple, two-dimensional models can be used to predict the transport characteristics of isotropic systems. Since the porosity alone has in previously published attempts (Wakao & Smith (1962)) not been deemed sufficient in predicting the diffusivity, the ratio of effective diffusivity D_{eff} to diffusivity D is modelled as

$$\frac{D_{eff}}{D} = \frac{\epsilon}{\chi}, \tag{4.9}$$

which is the ratio of porosity to tortuosity (Kim et al. (1987)).

Application of this model to a staggered, overlapping array of the fibre bed model yields a ratio of

$$\frac{D_{eff}}{D}_{\chi,fibre} = 1 - \sqrt{1-\epsilon}, \tag{4.10}$$

if equation (4.6) is substituted into equation (4.9). Equation (4.10) is only applicable to a staggered array with overlapping, since the tortuosity of regular and non-overlapping staggered arrays is unity.

In the preceding section the geometric factor was introduced as a means of including stagnant fluid volumes into the model. An alternate model is thus given by

$$\frac{D_{eff}}{D} = \frac{\epsilon}{\psi}, \tag{4.11}$$

	$\frac{D_{eff}}{D} = \frac{\epsilon}{\chi}$	$\frac{D_{eff}}{D} = \frac{\epsilon}{\psi}$
Fibre bed model		
Regular array	ϵ	$1 - \sqrt{1-\epsilon}$
Staggered array	$1 - \sqrt{1-\epsilon}$	$1 - \sqrt{1-\epsilon}$
Granular model		
Regular array	ϵ	$1 - (1-\epsilon)^{2/3}$
Staggered array	$1 - (1-\epsilon)^{2/3}$	$1 - (1-\epsilon)^{2/3}$

Table 4.4: Ratios of D_{eff}/D for the granular and fibre bed models in terms of porosity.

which, when applied to both the regular and staggered arrays of fibre beds, irrespective of overlapping, yields

$$\frac{D_{eff}}{D}_{\psi,fibre} = 1 - \sqrt{1-\epsilon}, \tag{4.12}$$

which is the same expression as equation (4.10).

Since all volumes present in any configuration of solids is included in the geometric factor model, equation (4.11) is valid for regular and staggered arrays irrespective of overlapping. The diffusivity ratios for all combinations of array and model type are available in Table 4.4. A comparison of these expressions will reveal the importance of the geometric factor: for both fibre beds and granular media the expressions for regular and staggered arrays are the same. According to Kim et al. (1987) the effective diffusion coefficient in the streamwise and transverse directions of a fully staggered array differ by less than 1%. Since diffusion in the transverse direction of a transversally staggered array corresponds to diffusion in the streamwise direction of a regular array (and vice versa for a streamwise fully staggered array), the RUC model based on the geometric factor, ψ, agrees with the findings of Kim et al. (1987).

A weighted average of the fibre bed and granular models in terms of the geometric factor, i.e. equation (4.11), is proposed as an alternative model in predicting the diffusivity ratio for isotropic processes:

$$\frac{D_{eff}}{D}_{RUC} = (1-\epsilon)\frac{D_{eff}}{D}_{fibre} + \epsilon\frac{D_{eff}}{D}_{granular}. \tag{4.13}$$

The manner in which equation (4.13) is weighted is motivated by the trend in data and other

models to be discussed in the following section, in which was found that the fibre bed model favours areas of low porosity, while the granular model favours the higher porosity regions. The two models are thus weighted according to these findings.

4.2.6 Model Validation

The RUC model is tested against alternative models found in the literature which, like the RUC model, are functions of only the porosity.

The micropore-macropore model of Wakao & Smith (1962) suggests a quadratic function of porosity to predict the effective diffusivity, i.e.

$$\frac{D_{eff}}{D} = \epsilon^2, \tag{4.14}$$

when macroscopic diffusion is dominant and Knudsen diffusion negligible.

Kim et al. (1987) propose

$$\frac{D_{eff}}{D} = \epsilon^{1.4} \tag{4.15}$$

as a model for the effective diffusivity rather than equation (4.14), as they found the model proposed by Wakao & Smith (1962) to underestimate the ratio of D_{eff}/D.

Kim et al. (1987) also discuss the first effective diffusivity model, proposed by Maxwell (1881), who studied a dilute suspension of spheres. As this model was originally developed for very high porosities, it functions as a convenient upperbound for all other porosities. This models suggests an effective diffusivity of the form

$$\frac{D_{eff}}{D} = \epsilon[1 + \frac{1}{2}(1-\epsilon)]^{-1}. \tag{4.16}$$

Weissberg (1963) determined a model tested on a bed of spheres. Their expression for the effective diffusivity is given by

$$\frac{D_{eff}}{D} = \epsilon[1 - \frac{1}{2}\ln\epsilon]^{-1}. \tag{4.17}$$

Sáez et al. (1991) cite a statistical model developed for disordered media by Torquato (1985) and Weissberg (1987) of the form

$$\frac{D_{eff}}{D} = \frac{\epsilon - 0.5\epsilon\zeta}{1.5 - 0.5\epsilon - 0.5\epsilon\zeta}, \tag{4.18}$$

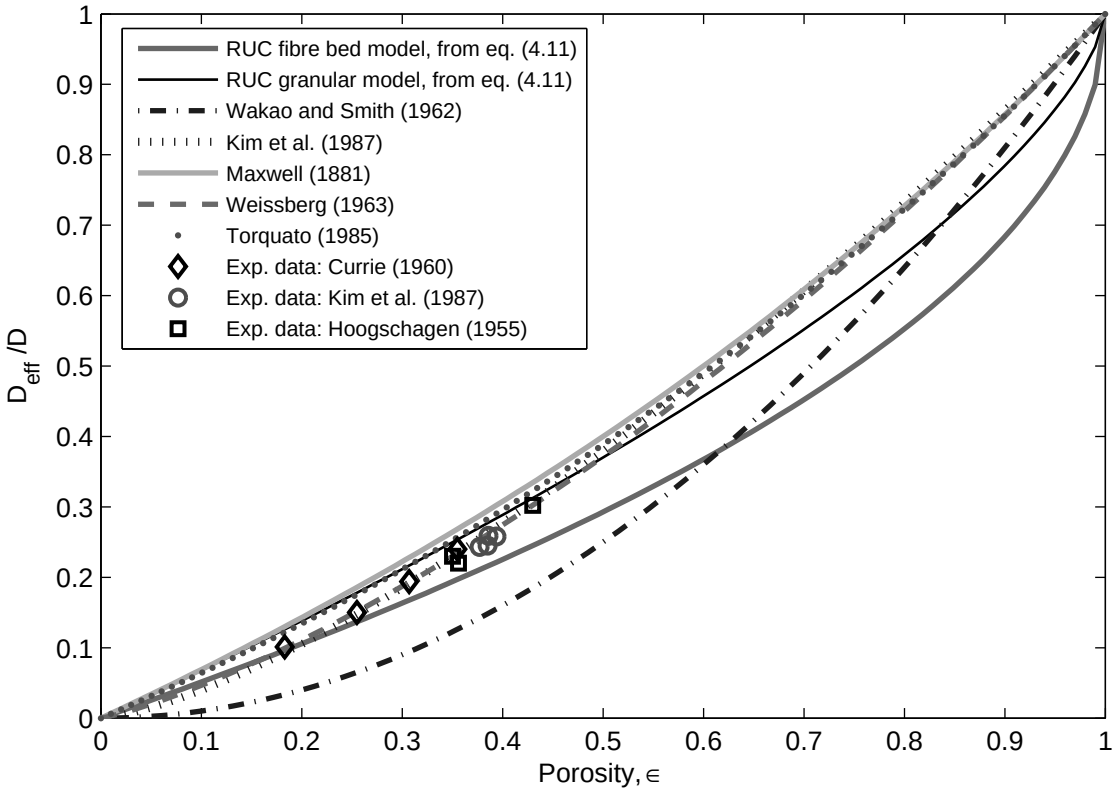

Figure 4.8: Comparison of the effective diffusivity ratio predicted by the RUC models with analytical models and experimental data from literature.

where $\zeta = 0.21068(1-\epsilon) - 0.04693(1-\epsilon)^2 + 0.00247(1-\epsilon)^3$.

A comparison of the models listed above with both the fibre bed and granular RUC models based on the geometric factor implementation (equation (4.11)) is shown in Figure 4.8. Experimental data gained from packed beds of glass spheres from Currie (1960), Kim et al. (1987) and Hoogschagen (1955) is also shown.

In Figure 4.8, it is evident that equation (4.14) under-predicts the experimental data. The fibre bed model also under-predicts the data, but is a slightly better fit than the granular RUC model model when the porosity is less than 0.5. The granular RUC model slightly over-predicts the data at porosities below 0.5, but is generally in good agreement with the data as well as the other analytical models. Both RUC models appear to under-predict the D_{eff}/D ratio for high porosities as they follow a different trend to the other analytical models, but this cannot be tested without available data for those porosities. The granular RUC model appears, however, to be significantly more accurate than the fibre model at high porosities. The granular RUC model on its own is thus an adequate predictor of the diffusivity ratio for all porosities, but to provide more accurate results the RUC weighted average model

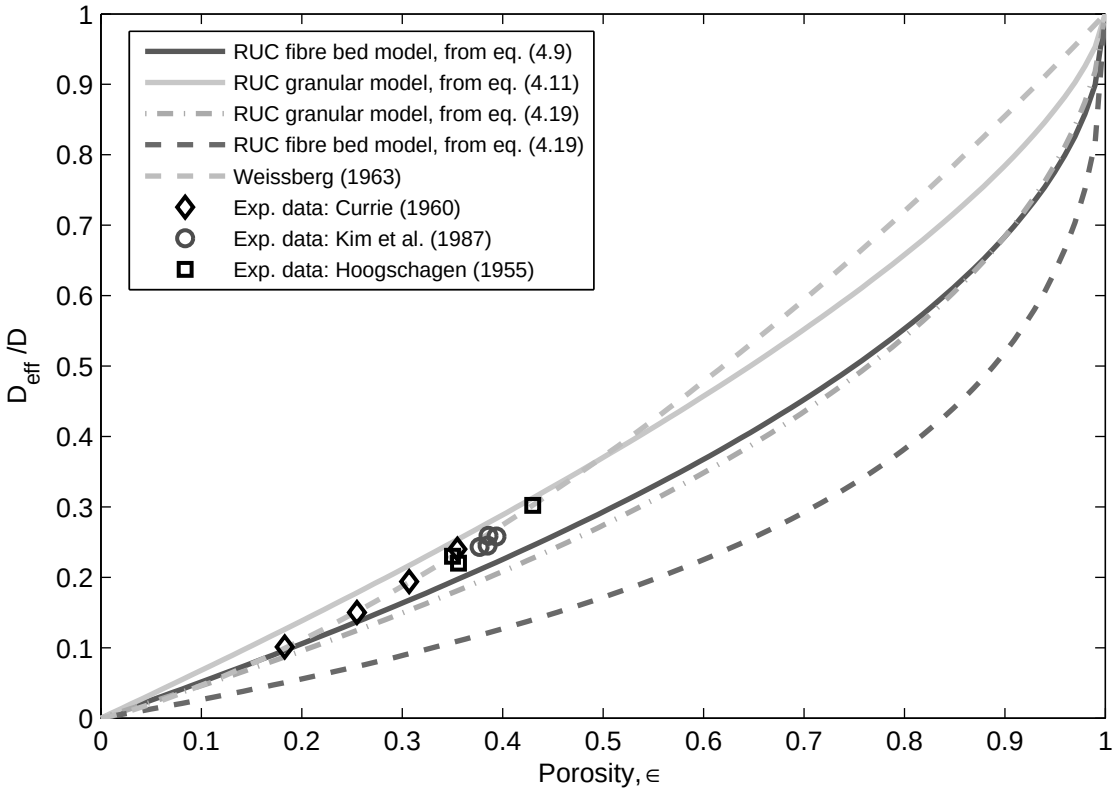

Figure 4.9: Comparison of the effective diffusivity ratio predicted by the fibre bed and granular RUC models through implementation of equations (4.9) and (4.19).

described by equation (4.13) was constructed specifically so that the granular model is the predominant model in the high porosity region and the fibre bed model in the low porosity region.

Currie (1960) suggests a theoretical model in terms of porosity and tortuosity of the form

$$\frac{D_{eff}}{D} = \frac{\epsilon}{\chi^2}. \tag{4.19}$$

Both RUC models are implemented using equation (4.19) and tested against the traditional form of the diffusivity ratio of equations (4.9) and (4.11) in Figure 4.9. Note that application of equations (4.9) and (4.11) results in the same expression in the case of a fully staggered array (see Table 4.4). In this figure it is evident that the fibre bed model applied to equation (4.19) severely under-predicts the data, while both RUC models as applied to equation (4.9) are in good agreement with the available experimental data.

The RUC weighted average model, equation (4.13), is tested against the fibre bed and granular models based on equation (4.11) in Figure 4.10. The weighted average model is in good agreement with the experimental data. In the lower porosity region it follows the trend of

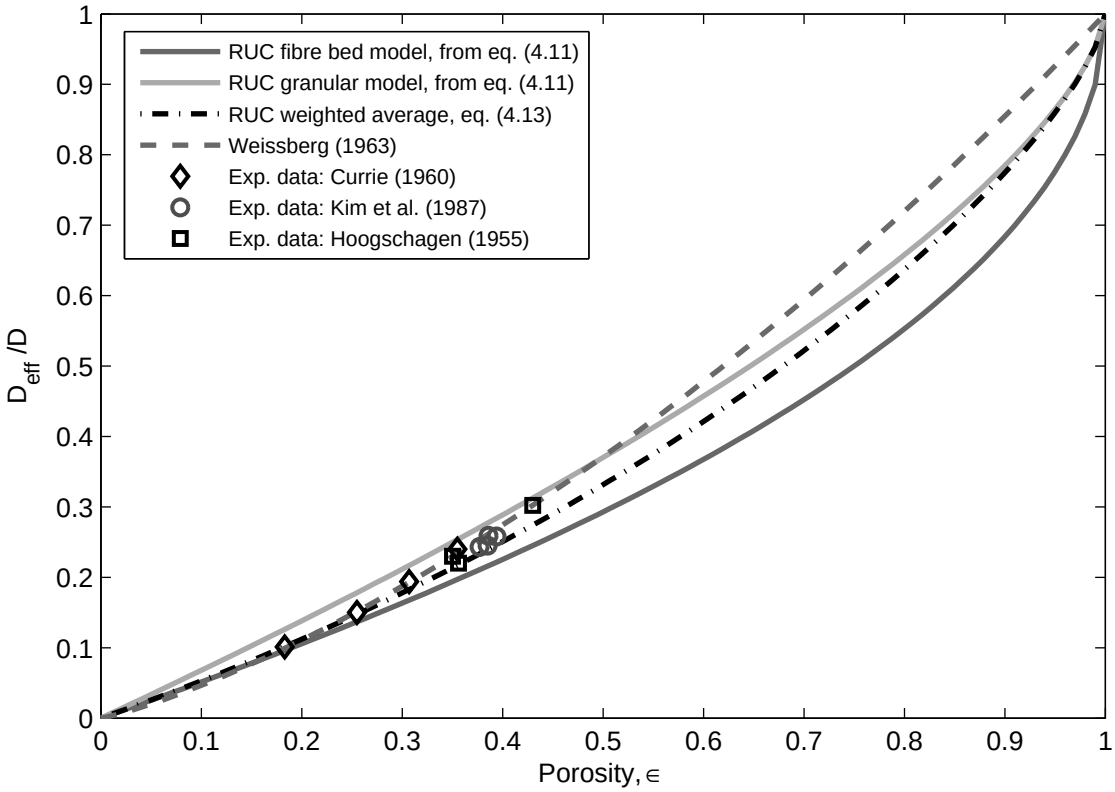

Figure 4.10: Comparison of the effective diffusivity ratio predicted by the granular and fibre bed RUC models and weighted average RUC model with analytical models and experimental data from literature.

the fibre bed model, but approximates the granular model in the high porosity region. Although it is evident that the granular model is sufficient to model the diffusivity ratio, the RUC weighted average appears to be better. The RUC weighted average is thus not superfluous. To further test the accuracy of the model, more data that falls in the high porosity region is required.

In this chapter the concept of a geometric pore scale model was introduced. The fibre bed and granular RUC models were introduced as such pore scale models. These consist of homogeneous, ordered arrays of solids whose average properties are contained within a representative unit cell. The method of volume partitioning was applied, along with the concept of tortuosity, in order to describe the path followed by a diffusing molecule. As the volume partitioning was developed for conduction, it was necessary to introduce the geometric factor, ψ, to replace the tortuosity, χ. The geometric factor was used in conjunction with the RUC models to predict the diffusivity ratio for regular and staggered arrays.

The diffusivity ratio was modelled according to equations (4.9) and (4.11), where it was

found that the geometric factor was in fact superior to the tortuosity.

A further RUC weighted average function was introduced, combining the fibre bed and granular models in an effort to obtain a single model applicable to regular and staggered arrays. This weighted average was found to be a better model than either the fibre bed or granular models alone.

Chapter 5

Diffusion through ordered array of solids

The estimation of the diffusivity which is assumed to be solely dependent on the geometry of a medium may be approached by considering a composite medium (Crank (1975)). This method assumes steady-state diffusion through a composite consisting of rectangular elements with each element having a different diffusivity. Within each of these elements the diffusion is assumed to be unidirectional.

The purpose of this chapter is to introduce this method used by Crank (1975) and Bell & Crank (1973) to predict the diffusivity ratio through a porous medium and to discuss the analytical models which are obtained through application of this method.

5.1 Diffusion through stacked composites

In order to find the effective diffusivity, two formulae developed in Bell & Crank (1973) are proposed which calculate the diffusivity of rectangular elements stacked either in series (Figure 5.1) or parallel (Figure 5.2). As depicted in Figures 5.1 and 5.2, the diffusion is unidirectional and each element i of length l_i possesses its own diffusivity D_i and mass concentration ρ_i.

The flux in the $\underline{\hat{n}}$ direction through the composite in Figure 5.1, with mass concentration ρ_A, is given by Fick's law, i.e.

$$j_A = D_{eff}\frac{\Delta\rho_A}{L}, \tag{5.1}$$

with D_{eff} the effective diffusivity of the composite and L its total length. Since the diffusive flux through each element must be the same, Fick's law may be applied to each element so

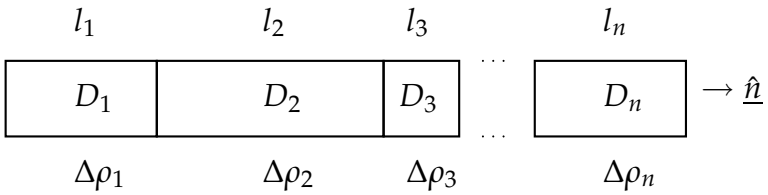

Figure 5.1: Series stacking with $\hat{n}$ a unit vector in the direction of the diffusive flux.

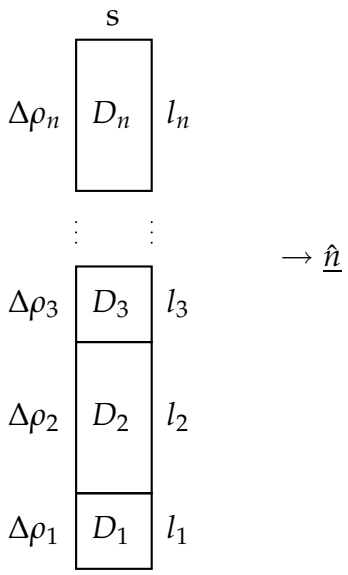

Figure 5.2: Parallel stacking with $\hat{n}$ a unit vector in the direction of the diffusive flux and s the width of the composite.

that

$$j_A = D_{eff}\frac{\Delta\rho_A}{L} = D_1\frac{\Delta\rho_1}{l_1} = D_2\frac{\Delta\rho_2}{l_2} = \cdots = D_n\frac{\Delta\rho_n}{l_n}. \tag{5.2}$$

Since the total change in mass concentration ρ_A is the sum of the change in mass concentration over the entire composite, the relationship of L/D may, according to equation (5.2), be expressed as

$$\begin{aligned}\frac{L}{D_{eff}} &= \frac{\Delta\rho_A}{j_A},\\ &= \frac{\sum\Delta\rho_i}{j_A},\\ &= \sum_{i=1}^{n}\frac{l_i}{D_i}.\end{aligned} \tag{5.3}$$

This equation represents the formula for series stacking and will be applied to the arrays used in this work.

For a composite consisting of rectangular elements stacked in parallel, the total diffusive flux is the sum of the individual fluxes of each element. With the parameters as indicated in Figure 5.2 and using Fick's law, the total diffusive flux is given by

$$\begin{aligned} j_A &= \sum_{i=1}^{n} j_i, \\ &= \frac{\sum l_i D_i \Delta\rho_i}{s}, \end{aligned} \tag{5.4}$$

with s the width of the composite. From equation (5.4) the formula for parallel stacking is found to be

$$LD_{eff} = \sum_{i=1}^{n} l_i D_i. \tag{5.5}$$

5.2 Series and parallel formulae

As derived in Section 5.1, the formula for a composite created by stacking in series is given by

$$\frac{l}{D_{eff}} = \frac{l_1}{D_1} + \frac{l_2}{D_2} + \frac{l_3}{D_3} + \cdots + \frac{l_n}{D_n}, \tag{5.6}$$

and similarly for a composite created by stacking in parallel

$$lD_{eff} = l_1 D_1 + l_2 D_2 + l_3 D_3 + \cdots + l_n D_n. \tag{5.7}$$

These formulae are to be applied to specific arrays of solids presented and discussed in the following chapter. Representative unit cells are chosen for each array. Each unit cell is divided into both a series of rows and columns to which equations (5.6) and (5.7) are applied in turn. After application of the formulae, two models of the effective diffusivity are found, namely the series-parallel (SP) model and the parallel-series (PS) model (Crank (1975)).

5.2.1 Notation

The notation used in Bell & Crank (1973) is explained in Figure 5.3. For this unit cell and others, the parameter h is the length of the transverse pore-width and a the streamwise

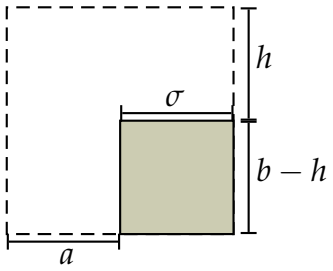

Figure 5.3: Notation used in Bell & Crank (1973).

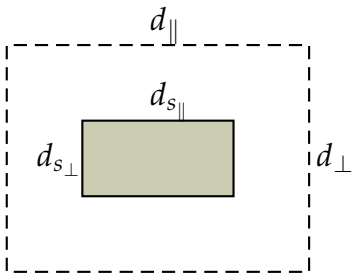

Figure 5.4: Representative unit cell notation.

pore-width. The solid dimensions are characterised by σ and $b - h$. For the cases studied in Bell & Crank (1973), $b = 1$ and $a + \sigma = 1$.

In Figure 5.4 the RUC notation used in this work is given, where the unit cell as a whole has the dimensions of $d_{\parallel}$ and $d_{\perp}$, and the solid $d_{s_{\parallel}}$ and $d_{s_{\perp}}$. For arrays of solid squares $d_{\parallel} = d_{\perp} = d$ and $d_{s_{\parallel}} = d_{s_{\perp}} = d_s$.

5.2.2 SP model

An example of an arbitrary unit cell containing no solid phase and divided into columns is given in Figure 5.5 whereas Figure 5.6 represents the same cell that has been divided into rows.

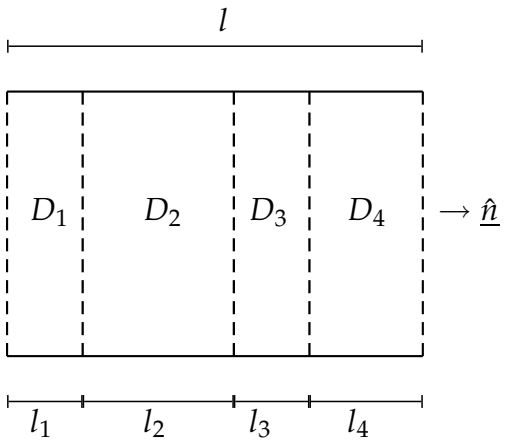

Figure 5.5: Division of a unit cell in series.

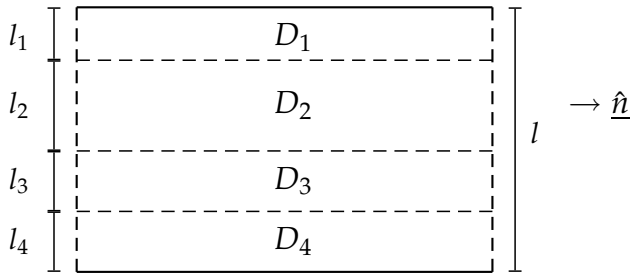

Figure 5.6: Division of a unit cell in parallel.

The series-parallel (SP) model is found through application of the parallel equation (equation (5.7)) to each column of Figure 5.5. The resulting diffusion coefficients are then substituted into equation (5.6), the series formula, as applied to the rows of Figure 5.6. The resulting diffusivity ratio is denoted by D_{SP}/D.

5.2.3 PS model

The parallel-series (PS) model is found in a similar fashion as the SP model. The series equation (equation (5.6)) is applied to each row of Figure 5.5. The resulting diffusion coefficients are then substituted into the parallel formula (equation (5.7)). The final diffusivity ratio of the PS model is indicated as D_{PS}/D.

5.2.4 Weighted average of SP and PS models

Both the series-parallel (SP) and parallel-series (PS) models are applied to specific ordered arrays of rectangles as studied in Bell & Crank (1973). Previous results obtained by Bell & Crank (1973) indicate that neither of these models is an accurate means of predicting the effective diffusivity of a given geometry. Specifically, results showed that one model consistently over-predicted the diffusivity while the other under-predicted it. A logical approach was thus to combine the results of these models and incorporate them into a weighted average function.

The weighted average function used in this work is that first proposed by Crank (1975). This function was developed in an attempt to obtain a single general function that would provide good results for all geometries, rather than implement a function weighted differently for each case. The weighted average function is given as

$$\frac{D_{eff}}{D} = \theta\frac{D_{SP}}{D} + (1-\theta)\frac{D_{PS}}{D}, \tag{5.8}$$

where

$$\theta = 0.56 - 0.5(0.5d_{s_\parallel}) + 0.4(0.5(d_\perp - d_{s_\perp})), \tag{5.9}$$

in RUC notation (see Figure 5.4). In terms of the notation used in Crank (1975) (see Figure 5.3), this is

$$\theta = 0.56 - 0.5\sigma + 0.4h,$$

where h is the transverse pore-width or "window height" and σ the streamwise solid length in the unit cell.

This chapter discussed the method introduced by Crank (1975). Application of the series-parallel and parallel-series formulae, derived by viewing a porous medium as stacked composites, lead to the SP and PS models for the diffusivity ratio. A combination of these two models resulted in the weighted average, introduced by Crank (1975).

Chapter 6

Effective diffusion coefficients for ordered arrays

In this work various ordered arrays of rectangles are considered, namely regular arrays, streamwise fully staggered arrays with and without overlapping and transversally fully staggered arrays with and without overlapping, all of which are described in detail in Appendix A.

In this chapter the effective diffusion coefficients for the various ordered arrays used are found using the SP and PS models. For both models an effective diffusion coefficient is found using equations (5.6) and (5.7), which are applied to the dimensions of the unit cell of the particular ordered array under consideration.

It was found that the effective diffusivity found through this method is solely dependent on the geometry of the array, that is, its direction of staggering and possible overlapping of solids. The same equation for the diffusivity was found irrespective of the orientation of the rectangle. The same equation is thus valid whether $d_{s_\parallel} > d_{s_\perp}$ or $d_{s_\perp} > d_{s_\parallel}$. A particular staggered array's diffusivity may change when overlapping occurs. The unit cell of an overlapping array is divided differently into its parallel and series segments.

A complete set of the calculations for all the arrays of solid rectangles as mentioned above is available in Appendix A, of which a single example is presented below. In Appendix B the same calculations to determine D_{eff}/D are performed for arrays of solid squares.

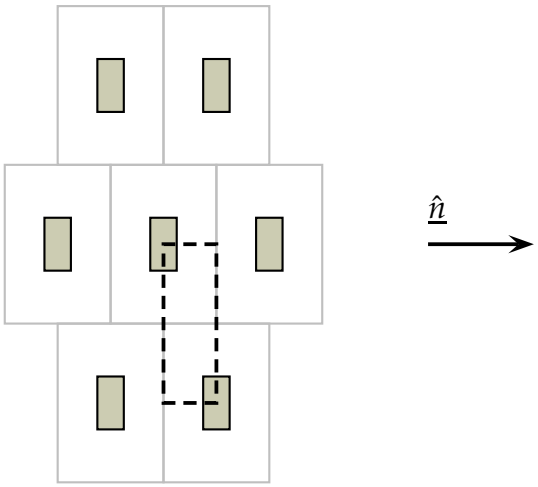

Figure 6.1: Non-overlapping, streamwise staggered array with unit cell indicated by the bold dashed frame.

6.1 Example: Streamwise staggered array with no overlapping of solid phase

This particular streamwise staggered array, as depicted in Figure 6.1, consists of vertical, rectangular solids, i.e. $d_{s_\perp} > d_{s_\parallel}$. Here the solids do not overlap, hence the resulting effective diffusivity is not applicable to the overlapping case. Both SP and PS methods are discussed below.

Non-overlapping SP model

The SP model is obtained through application of the parallel formula on the unit cell in Figure 6.2, followed by the series formula.

Application of the parallel formula, equation (5.7), on column i of Figure 6.2 yields

$$d_\perp D_i = (d_\perp - \frac{1}{2} d_{s_\perp}) D,$$

thus

$$D_i = \left(\frac{d_\perp - \frac{1}{2} d_{s_\perp}}{d_\perp} \right) D. \tag{6.1}$$

Similarly, for column ii

$$d_\perp D_{ii} = d_\perp D,$$

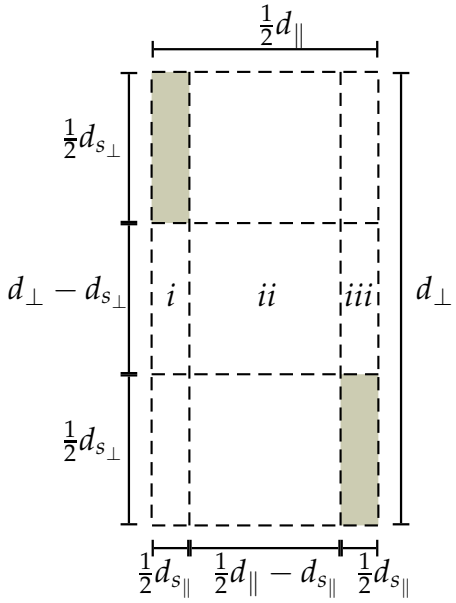

Figure 6.2: Unit cell of non-overlapping, streamwise staggered array using the SP model.

thus

$$D_{ii} = D \tag{6.2}$$

and column *iii*

$$d_\perp D_{iii} = (d_\perp - \frac{1}{2}d_{s_\perp})D,$$

which yields

$$D_{iii} = \left(\frac{d_\perp - \frac{1}{2}d_{s_\perp}}{d_\perp}\right) D. \tag{6.3}$$

Substitution of equations (6.1), (6.2) and (6.3) into equation (5.6), the series formula, yields

$$\frac{\frac{1}{2}d_{\parallel}}{D_{SP}} = \frac{d_{s_\parallel}/2}{D_i} + \frac{\frac{1}{2}d_{\parallel} - d_{s_\parallel}}{D_{ii}} + \frac{d_{s_\parallel}/2}{D_{iii}},$$

thus

$$\frac{D}{D_{SP}} = \frac{2d_\perp d_{s_\parallel}}{d_{\parallel}(d_\perp - \frac{1}{2}d_{s_\perp})} + \frac{d_{\parallel} - 2d_{s_\parallel}}{d_{\parallel}}. \tag{6.4}$$

Through further simplification of equation (6.4), the diffusion coefficient of this array, according to the SP model, is found to be

$$\frac{D_{SP}}{D} = \left[1 + \frac{d_{s_\parallel} d_{s_\perp}}{d_{\parallel}(d_\perp - \frac{1}{2}d_{s_\perp})}\right]^{-1}. \tag{6.5}$$

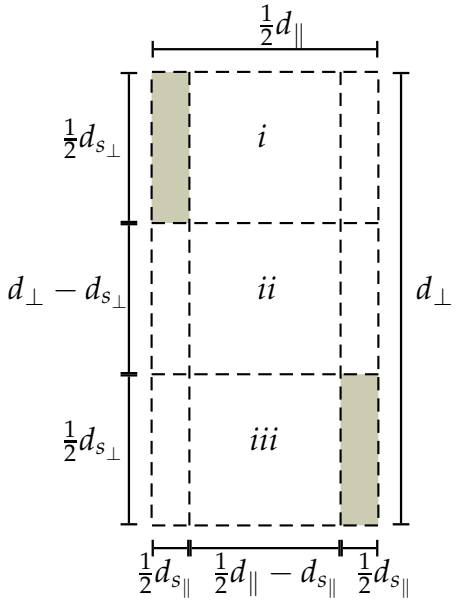

Figure 6.3: Unit cell of non-overlapping, streamwise staggered array using the PS model.

Non-overlapping PS model

The PS model is obtained through application of the series formula on the unit cell in Figure 6.3 followed by the parallel formula.

Application of the series formula on columns i and iii of Figure 6.3 yields specific diffusion coefficients of zero, i.e.

$$D_i = D_{iii} = 0, \tag{6.6}$$

while for column ii

$$D_{ii} = D. \tag{6.7}$$

Substitution of equations (6.6) and (6.7) into the parallel formula, equation (5.7), yields

$$d_\perp D_{PS} = (d_\perp - d_{s_\perp})D. \tag{6.8}$$

Through simplification of equation (6.8), the diffusion coefficient of this array, according to the PS model, is found to be

$$\frac{D_{PS}}{D} = 1 - \frac{d_{s_\perp}}{d_\perp}. \tag{6.9}$$

6.2 Results

The results of all the calculations in Appendix A to determine the diffusivity ratio for all the arrays of rectangles, i.e. where $d_{s_\parallel} \neq d_{s_\perp}$, considered are presented in Table 6.1.

The effective diffusion coefficients for arrays with square solid particles, i.e. $d_{s_\parallel} = d_{s_\perp} = d_s$ and $d_\parallel = d_\perp = d$, are obtained either from application of the PS and SP model on the particular unit cells (see Appendix B), or from Table 6.1 by setting $d_{s_\parallel} = d_{s_\perp} = d_s$ and $d_\parallel = d_\perp = d$. The results are given in Table 6.2.

The results of Table 6.2 are expressed in terms of porosity in Table 6.3. For these two-dimensional arrays the porosity is given by

$$\epsilon = \frac{d^2 - d_s^2}{d^2}, \tag{6.10}$$

since porosity is the ratio between the fluid area and the total area of the unit cell.

Array	SP model	PS model
Regular array	$\frac{D_{SP}}{D} = \left[1 + \frac{d_{s_\parallel} d_{s_\perp}}{d_\parallel (d_\perp - d_{s_\perp})}\right]^{-1}$	$\frac{D_{PS}}{D} = \frac{d_\perp - d_{s_\perp}}{d_\perp}$
Streamwise staggered array		
Non-overlapping	$\frac{D_{SP}}{D} = \left[1 + \frac{d_{s_\parallel} d_{s_\perp}}{d_\parallel (d_\perp - \frac{1}{2} d_{s_\perp})}\right]^{-1}$	$\frac{D_{PS}}{D} = \frac{d_\perp - d_{s_\perp}}{d_\perp}$
Overlapping	$\frac{D_{SP}}{D} = \left[\frac{d_\perp^2 - \frac{3}{2} d_{s_\perp} d_\perp + \frac{d_{s_\parallel}}{d_\parallel} d_{s_\perp} d_\perp}{(d_\perp - \frac{1}{2} d_{s_\perp})(d_\perp - d_{s_\perp})}\right]^{-1}$	$\frac{D_{PS}}{D} = \frac{d_\perp - d_{s_\perp}}{d_\perp}$
Transversally staggered array		
Non-overlapping	$\frac{D_{SP}}{D} = \left[1 + \frac{d_{s_\parallel} d_{s_\perp}}{d_\parallel (d_\perp - d_{s_\perp})}\right]^{-1}$	$\frac{D_{PS}}{D} = \frac{d_\perp - 2 d_{s_\perp}}{d_\perp}$
Overlapping	$\frac{D_{SP}}{D} = \left[1 + \frac{d_{s_\parallel} d_{s_\perp}}{d_\parallel (d_\perp - d_{s_\perp})}\right]^{-1}$	$\frac{D_{PS}}{D} = 0$

Table 6.1: Diffusivity ratios for ordered arrays found using the SP and PS models.

Array	**SP model**	**PS model**
Regular array	$\frac{D_{SP}}{D} = \left[1 + \frac{d_s^2}{d(d-d_s)}\right]^{-1}$	$\frac{D_{PS}}{D} = \frac{d-d_s}{d}$
Streamwise staggered array		
Non-overlapping	$\frac{D_{SP}}{D} = \left[1 + \frac{d_s^2}{d(d-\frac{1}{2}d_s)}\right]^{-1}$	$\frac{D_{PS}}{D} = \frac{d-d_s}{d}$
Overlapping	$\frac{D_{SP}}{D} = \left[\frac{d}{d-d_s} - \frac{d_s}{d-\frac{1}{2}d_s}\right]^{-1}$	$\frac{D_{PS}}{D} = \frac{d-d_s}{d}$
Transversally staggered array		
Non-overlapping	$\frac{D_{SP}}{D} = \left[1 + \frac{d_s^2}{d(d-d_s)}\right]^{-1}$	$\frac{D_{PS}}{D} = \frac{d-2d_s}{d}$
Overlapping	$\frac{D_{SP}}{D} = \left[1 + \frac{d_s^2}{d(d-d_s)}\right]^{-1}$	$\frac{D_{PS}}{D} = 0$

Table 6.2: Diffusivity ratios for arrays of squares found using the SP and PS models.

Array	**SP model**	**PS model**
Regular array	$\frac{D_{SP}}{D} = \left[1 + \frac{1-\epsilon}{1-\sqrt{1-\epsilon}}\right]^{-1}$	$\frac{D_{PS}}{D} = 1 - \sqrt{1-\epsilon}$
Streamwise staggered array		
Non-overlapping	$\frac{D_{SP}}{D} = \left[1 + \frac{1-\epsilon}{1-\frac{1}{2}\sqrt{1-\epsilon}}\right]^{-1}$	$\frac{D_{PS}}{D} = 1 - \sqrt{1-\epsilon}$
Overlapping	$\frac{D_{SP}}{D} = \left[1 + \frac{3-\epsilon}{1-\epsilon-\sqrt{1-\epsilon}}\right]^{-1}$	$\frac{D_{PS}}{D} = 1 - \sqrt{1-\epsilon}$
Transversally staggered array		
Non-overlapping	$\frac{D_{SP}}{D} = \left[1 + \frac{1-\epsilon}{1-\sqrt{1-\epsilon}}\right]^{-1}$	$\frac{D_{PS}}{D} = 1 - 2\sqrt{1-\epsilon}$
Overlapping	$\frac{D_{SP}}{D} = \left[1 + \frac{1-\epsilon}{1-\sqrt{1-\epsilon}}\right]^{-1}$	$\frac{D_{PS}}{D} = 0$

Table 6.3: Diffusivity ratios for arrays of squares as functions of porosity.

Chapter 7

Numerical computations

Numerical computations are needed to test the validity of analytical models. For each array considered the analytical SP and PS models, as well as the weighted average of the two, were tested against numerical results. The results were also compared to those in Bell & Crank (1973).

The numerical method implemented is discussed in this chapter, along with certain aspects of the implementation which could influence the results, such as grid-dependence and convergence testing. The accuracy of the weighted average function as compared to the numerical results is also tested.

All numerical computations were done using computational fluid dynamics (CFD) coded in FORTRAN and all figures rendered using MATLAB.

7.1 Numerical model

A numerical model was implemented via computational fluid dynamics to compare the weighted average RUC model (equation (4.13)), the SP and PS models and their weighted average function developed by Crank (1975). Since the problem to be solved is steady state and does not include convection or chemical production, the governing equation to be solved is given by equation (3.10) expressed in Cartesian coordinates, i.e.

$$\nabla^2 \rho_A = \frac{\partial^2 \rho_A}{\partial x^2} + \frac{\partial^2 \rho_A}{\partial y^2} = 0. \tag{7.1}$$

Equation (7.1) must be discretised in order to be solved numerically. Considering the prob-

lem to be two-dimensional, the discretised equation

$$a_P\Phi_P = a_E\Phi_E + a_W\Phi_W + a_N\Phi_N + a_S\Phi_S + b, \tag{7.2}$$

follows, where Φ indicates the mass concentration, ρ_A, at a given node in the grid constructed using Cartesian coordinates, and the coefficients a_i as defined in Patankar (1980).

Equation (7.1) is accompanied by the eastern and western boundary conditions

$$\rho_A = 0,\ y = 0,\ 0 < x < L, \tag{7.3}$$
$$\rho_A = 0,\ y = H,\ 0 < x < L, \tag{7.4}$$
$$\tag{7.5}$$

where L is the length of the grid and H the height. Along the northern and southern walls the boundary conditions are implemented as

$$\rho_A = 1,\ x = 0,\ 0 < y < H, \tag{7.6}$$
$$\rho_A = 0,\ x = L,\ 0 < y < H. \tag{7.7}$$
$$\tag{7.8}$$

The discretised equation was solved using the TDMA (tri-diagonal-matrix algorithm), since equation (7.1) could be discretised in the form of equation (7.2). The TDMA calculates the value of Φ at a specific node in the grid according to its neighbouring nodes. If the boundary nodes have a given value, Φ takes on those values, whereas if they are unknown, the TDMA may be constructed in order to remove any influence those specific nodes may have had. In the case of the diffusion problem, the initial condition was a constant maximum Φ-value on the western boundary nodes and a constant minimum Φ-value on the eastern boundary nodes. The influence of the northern and southern boundary nodes was thus removed since there was no diffusive flux across these boundaries.

The TDMA was implemented on a grid constructed according to Practice B of Patankar (1980), where nodal points are centered within each control volume. A fully implicit scheme was applied along with the central difference scheme.

In generating numerical data for each array, the unit cell was used with effective diffusion coefficients calculated for every porosity. This was achieved by varying a parameter within the unit cell: for ordered rectangular arrays either $d_{s_\parallel}$ or $d_{s_\perp}$ was kept constant while the other was variable over the applicable range of that array. In the case of the arrays of squares

the variable was d_s, with d constant. The solids were implemented by setting the concentration the selected nodes to zero.

In order to compare the numerical model with the SP and PS models and especially the weighted average function, it was required that the unit cell implemented in the numerical code have equal parallel and perpendicular lengths as the weighted average function of Bell & Crank (1973) was developed solely for such a case.

The effective diffusivity, D_{eff}, was calculated from the numerical results as the ratio of the sum of the fluxes of all the cells within the porous matrix over the ratio of the total flux when no solids are present.

The numerical model was applied to a regular array as well as both staggered arrays (transverse and streamwise) as well as the regular and staggered arrays of squares.

7.1.1 Convergence

The sum of the fluxes in the y-direction was computed for every grid point in the x-direction. Convergence was achieved when the computed flux for each grid point in the x-direction met the convergence requirement of 1×10^{-10}.

7.2 Numerical dependencies

7.2.1 Grid type

The two grid types implemented were those of uniform and non-uniform grids. The uniform grid produced data points at regular intervals, while the non-uniform grid could be configured to concentrate data points at the extreme values of the array.

Figures 7.1 and 7.2 depict the change in effective diffusivity against the change in transverse pore-width, h in the Bell and Crank notation or $\frac{1}{2}(d_\perp - d_{s_\perp})$ in RUC notation of a regular array of rectangles for a uniform and non-uniform grid, respectively. The SP, PS and weighted average models of Bell & Crank (1973) are indicated in the figure. A smaller value of h implies a bigger solid and thus a smaller porosity and smaller effective diffusivity. The numerical data appears to follow the same trend in both figures and this is confirmed by Figures 7.3 and 7.4, which give the percent difference between the weighted average function

and numerical data as the transverse pore-width increases.

Comparison of Figures 7.1 with 7.2 and Figures 7.3 with 7.4 thus show that the implementation of a non-uniform grid does not necessarily yield numerically differing results, rather merely a concentration of data points in a preferred region. A non-uniform grid could thus be of use when certain regions of porosity are of particular interest. This, however, was not the case and as such all further results discussed were generated using a uniform grid.

Percent difference

Figures 7.3 and 7.4 represent the percent difference between the weighted average function of the SP and PS models and the numerical data. This error margin was calculated according to

$$\%\ difference = \frac{|v_1 - v_2|}{\frac{1}{2}(v_1 + v_2)} \cdot 100, \tag{7.9}$$

where v_1 is a value obtained through one method and v_2 the value calculated through the other method. The percent difference formula was used instead of the percent error formula as both data points obtained through the SP and PS models and numerical computation are approximations.

In all percent difference graphs the error margins in the lowest values of the x-axis seem far bigger than the rest of the graph. This is due the fact that, even if the weighted average function is seemingly the same as the numerical value, the percent difference is large when the data point itself has a very small value. Thus, if the weighted average function has a diffusivity ratio 0.05 and the numerical value is calculated to be 0.055, the percent difference is almost 10%.

7.2.2 Grid size

The grid size was tested for all arrays. In each case the numerical results were independent of grid size. The grid size implemented was 71 by 71 for the rectangular arrays, while a grid size of 72 by 26 was implemented for the square arrays. These respective grid sizes were chosen after considering time constraints and the amount of data points required.

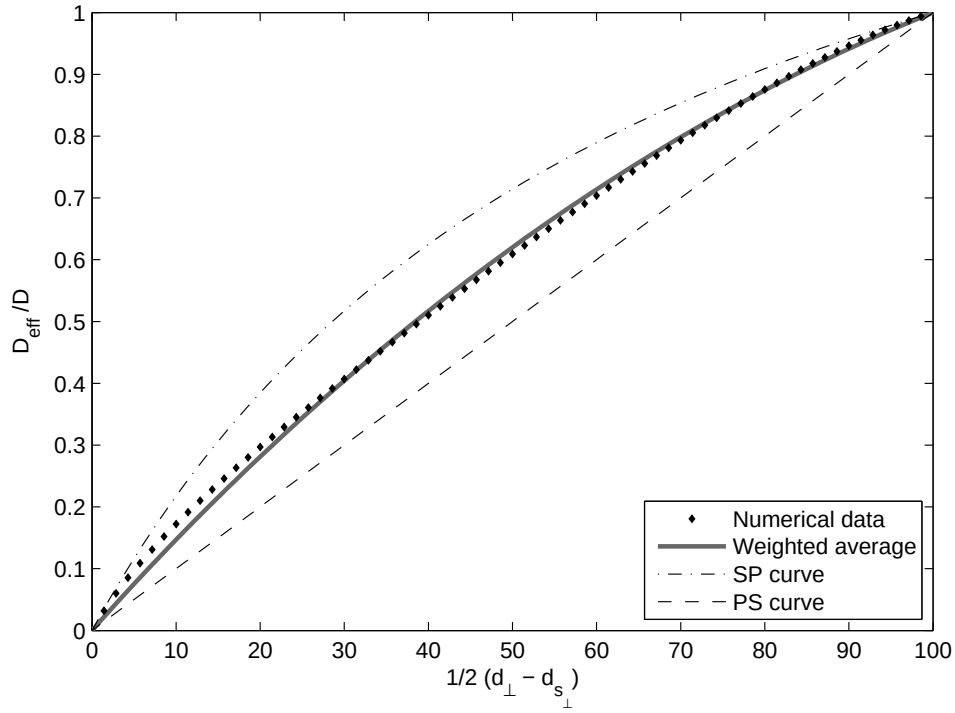

Figure 7.1: Regular array of rectangles with $\sigma = \frac{1}{2}d_{s_{\parallel}} = 0.4$ and numerical data calculated using a uniform grid.

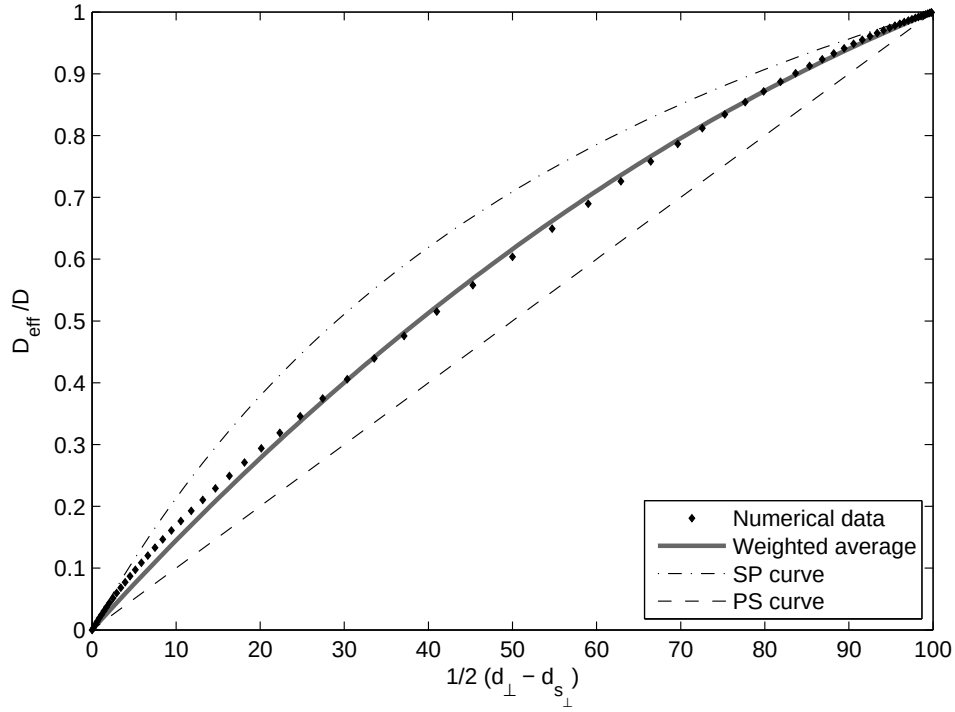

Figure 7.2: Regular array of rectangles with $\sigma = \frac{1}{2}d_{s_{\parallel}} = 0.4$ and numerical data calculated using a non-uniform grid.

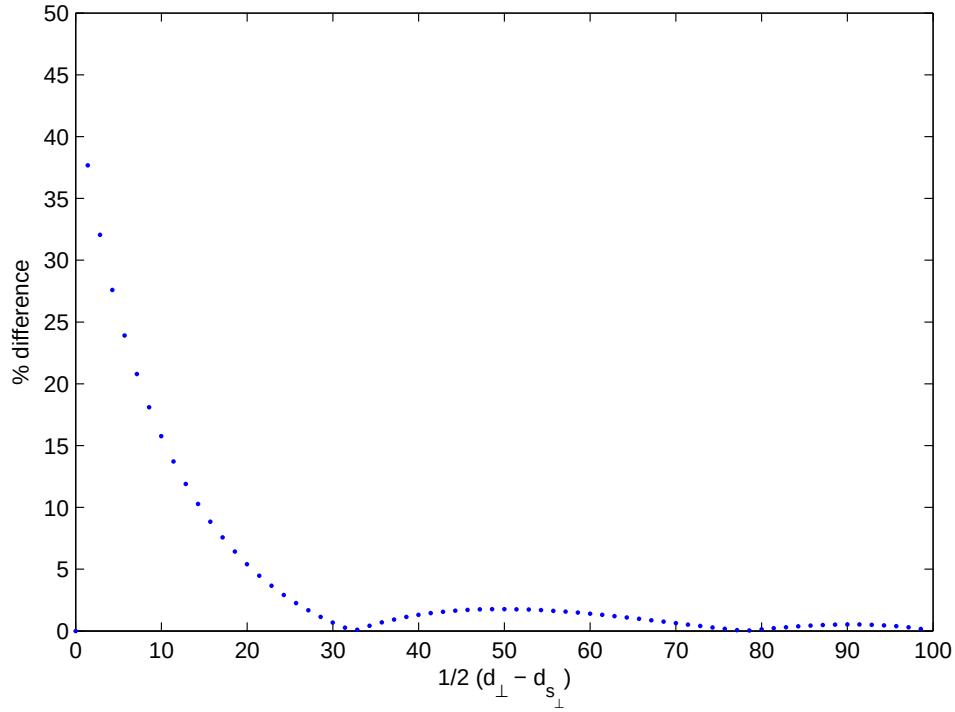

Figure 7.3: Percent difference between numerical data and weighted average function for a regular array with $\sigma = \frac{1}{2}d_{s_{\parallel}} = 0.4$ and a uniform grid.

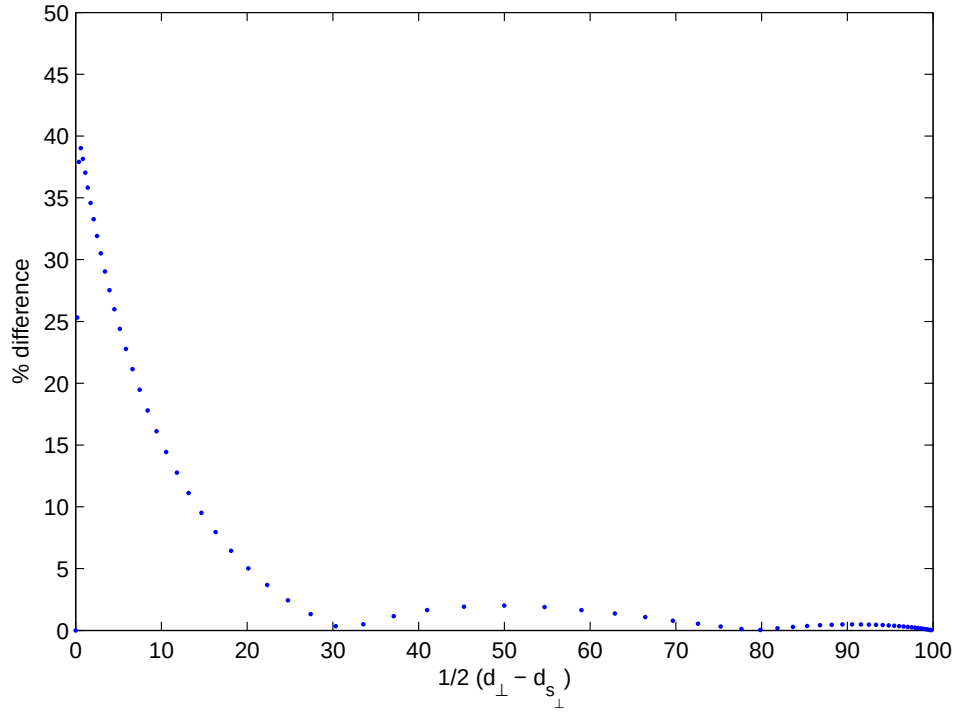

Figure 7.4: Percent difference between numerical data and weighted average function for a regular array with $\sigma = \frac{1}{2}d_{s_{\parallel}} = 0.4$ and a non-uniform grid.

Chapter 8

Results

The results of application of the SP and PS models as presented in Tables 6.1 and 6.3 and the weighted average function are compared with the numerical data obtained through the computations as explained in Chapter 7. The results are also compared with those obtained through application of the fibre bed and granular RUC models.

8.1 Arrays of rectangular solid particles

It is important to note the importance of the weighted average function of Bell & Crank (1973). The results discussed in this chapter all show that neither the SP or PS model provides an accurate prediction for the numerical data. The weighted average function, however, was the best model for the numerical data in each case of the arrays of rectangles. Included in the results is the percent difference between the numerical results and the weighted average function for each array.

As mentioned, the numerical data for the rectangular ordered arrays were generated by keeping either $d_{s_\parallel}$ or $d_{s_\perp}$ constant while varying the other, with the length of the unit cell in the numerical program chosen as 1. The variables h and σ are thus given as dimensionless lengths. The results were represented graphically as D_{eff}/D as a function of either the transverse pore-width h (in terms of the notation used in Crank (1975)), or as a function of $\frac{1}{2}d_{s_\parallel}$ (σ in Crank (1975)).

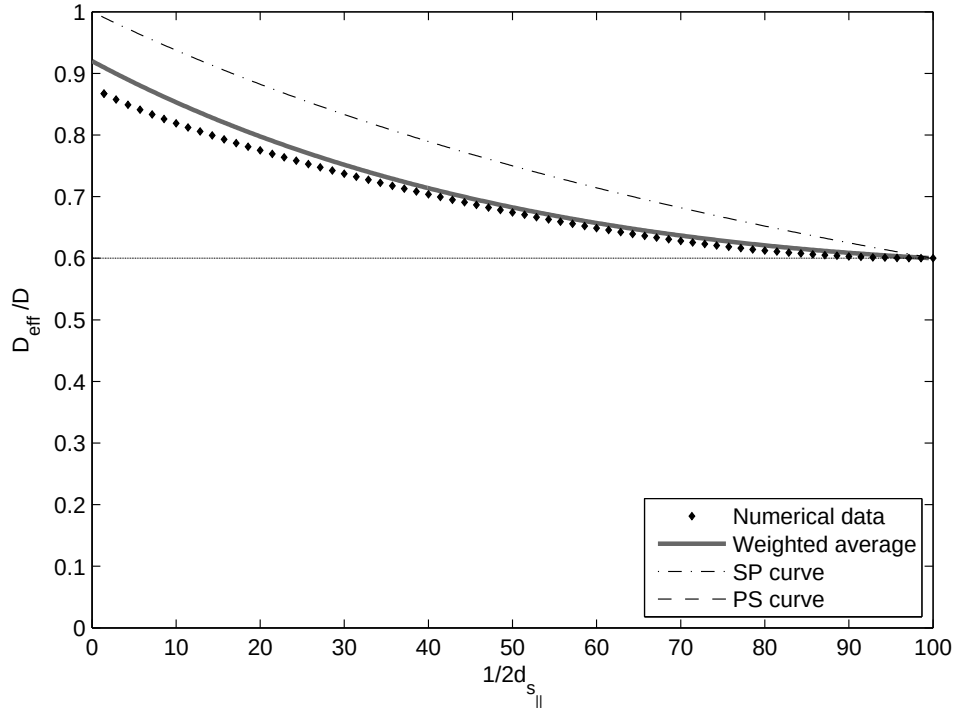

Figure 8.1: Comparison between numerical data and analytical models of Bell & Crank (1973) for a regular array with $\frac{1}{2}(d_\perp - d_{s_\perp}) = 0.4$.

8.1.1 Regular array

Two situations occur when generating data for a regular array. In the first $d_{s_\perp}$ is kept constant while $d_{s_\parallel}$ is varied over the applicable range. The resulting effective diffusion coefficients are then given as functions of the streamwise solid width $\frac{1}{2}d_{s_\parallel}$. In the second instance $d_{s_\perp}$ is kept constant with $d_{s_\parallel}$ being the variable. Here the results are functions of transverse pore-width h.

In Figure 8.1 the resulting data of a constant h value of 0.6 are compared to the analytical models. As expected, the weighted average function is the best predictor for the numerical results of the three models. In this case the weighted average function is a very good predictor for all porosity values, since, as given in Figure 8.2, the percent difference between this function and the numerical data remains less than five percent.

Figure 8.3 depicts the result of keeping $d_{s_\parallel}$ constant with a varying $d_{s_\perp}$, with a streamwise pore-width of 0.6. For a regular array with a varying transverse pore-width

$$h = \frac{1}{2}(d_\perp - d_{s_\perp}).$$

In this figure the weighted average function seems to match the numerical data closely.

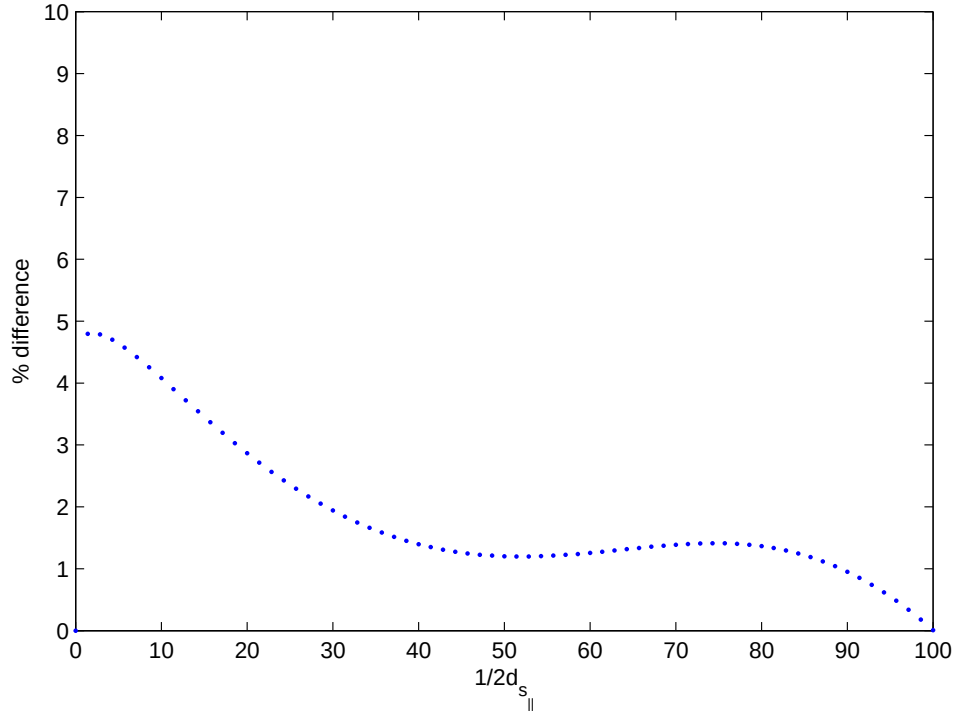

Figure 8.2: Percent difference between numerical data and weighted average function for a regular array with $\frac{1}{2}(d_\perp - d_{s_\perp}) = 0.4$.

However, in the region where h is small, it diverges significantly. This is deduced from Figure 8.4 where the percent difference between the two reaches up to forty percent for the very small porosity region. Except for this region, it still compares very well with the numerical data.

8.1.2 Streamwise staggered array

The numerical data for the streamwise staggered arrays were generated by keeping $d_{s_\perp}$ constant. In the results discussed below the data ranges from the non-overlapping case to that of overlapping. For a streamwise staggered array the transverse pore-width is given by

$$h = d_\perp - \frac{1}{2} d_{s_\perp}.$$

The point where overlapping of solids occurs is visible in Figure 8.5 where the SP model and weighted average model have discontinuities at $\frac{1}{2}d_{s_\parallel} = 50\%$. At this point the SP model takes on a different expression (see Appendix A), while the PS model is constant. In Figure 8.6 this change is reflected in the sudden drop in percent difference between the weighted

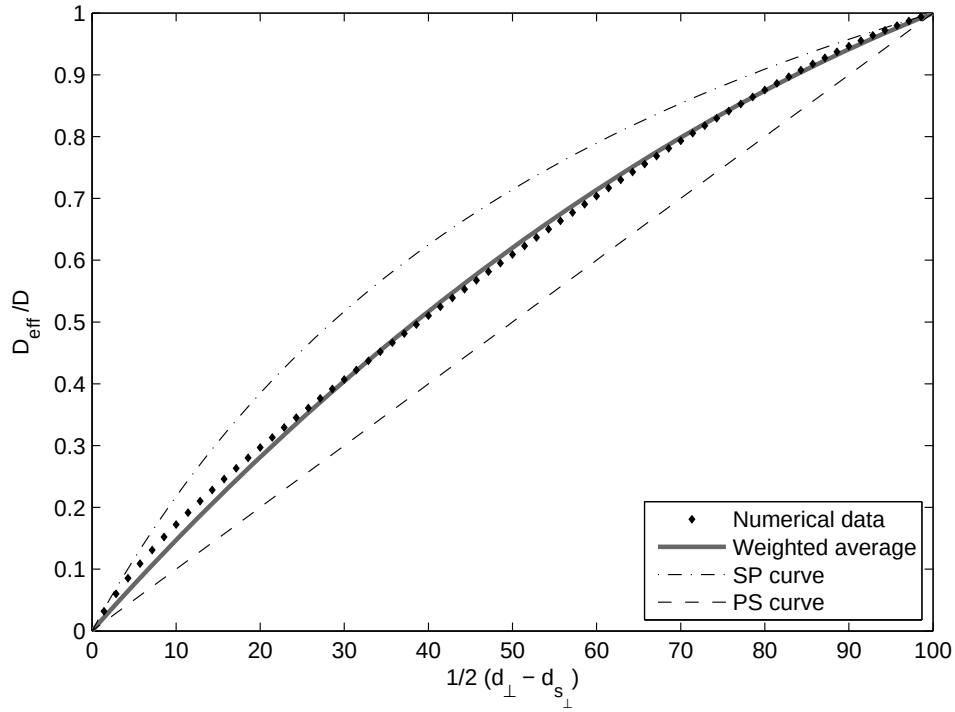

Figure 8.3: Comparison between numerical data and analytical models of Bell & Crank (1973) for a regular array with $\frac{1}{2}d_{s_{\parallel}} = 0.6$.

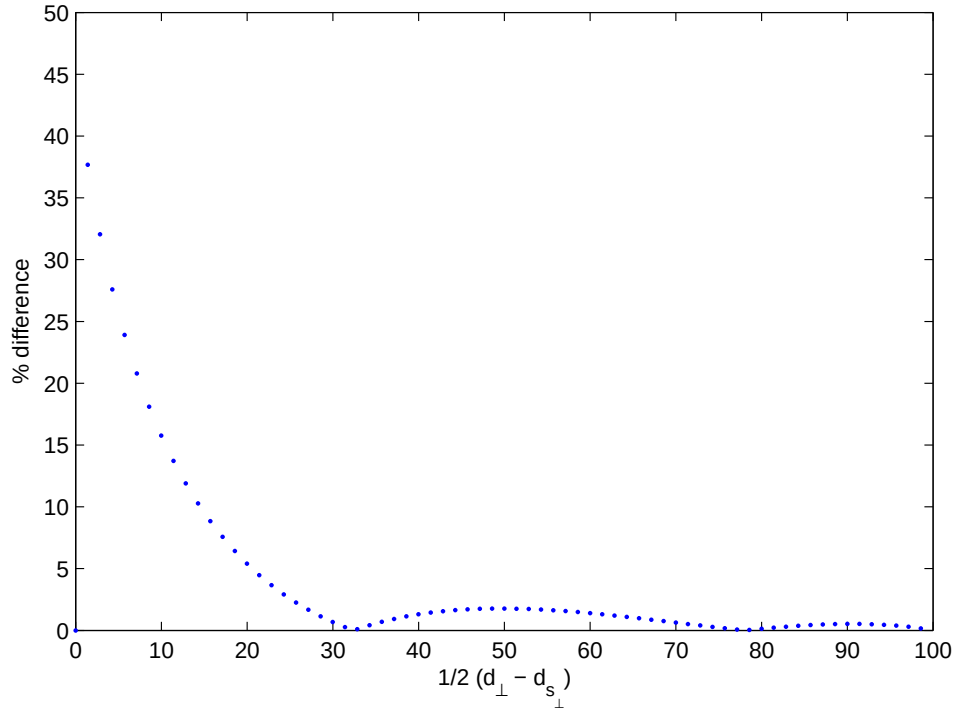

Figure 8.4: Percent difference between numerical data and weighted average function for a regular array with $\frac{1}{2}d_{s_{\parallel}} = 0.6$.

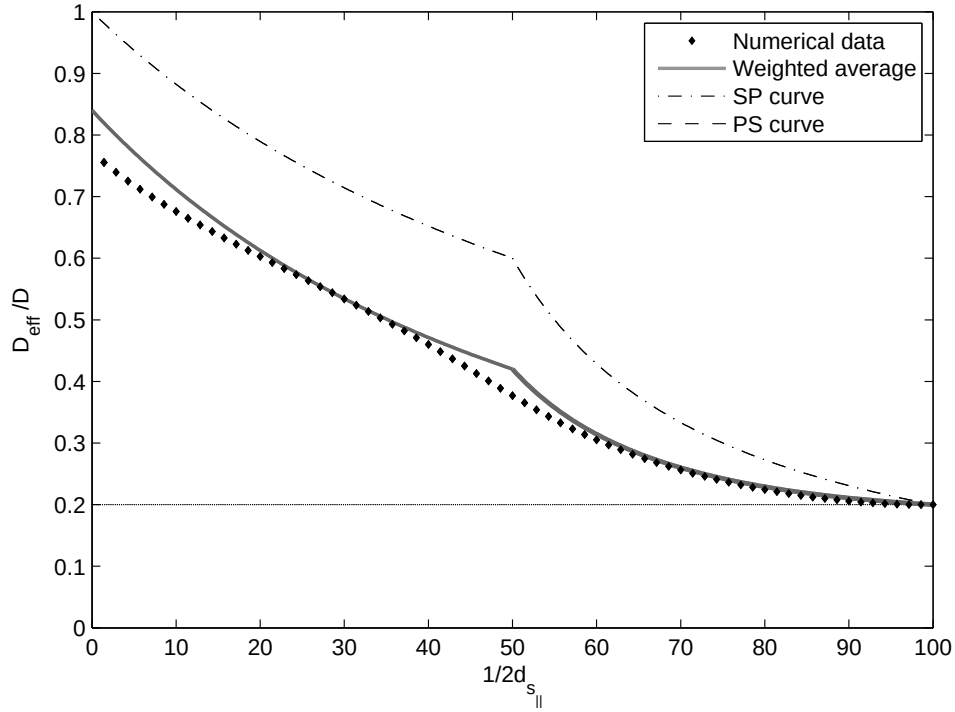

Figure 8.5: Comparison between numerical data and analytical models of Bell & Crank (1973) for a streamwise staggered array with $h = d_{\parallel} - \frac{1}{2}d_{s_{\parallel}} = 0.6$.

average function and numerical data. Note that the percent difference between the two is largest in the non-overlapping, high-porosity region. In the overlapping region the weighted average function is a very good predictor for the numerical data.

8.1.3 Transversally staggered array

For transversally staggered arrays the numerical data were generated by keeping $d_{s_{\parallel}}$ constant and varying $d_{s_{\perp}}$. As in the case of streamwise staggered arrays, the data ranges from non-overlapping to overlapping solid particles. Figure 8.7 depicts the results when compared to the analytical models.

For both the non-overlapping and overlapping regions of transversally staggered arrays

$$h = \frac{1}{2}(d_{\perp} - d_{s_{\perp}})$$

is applicable.

The change from overlapping to non-overlapping is evident in the discontinuities in the PS model and weighted average function at $\frac{1}{2}(d_{\perp} - d_{s_{\perp}}) = 50\%$ in Figure 8.7, unlike the

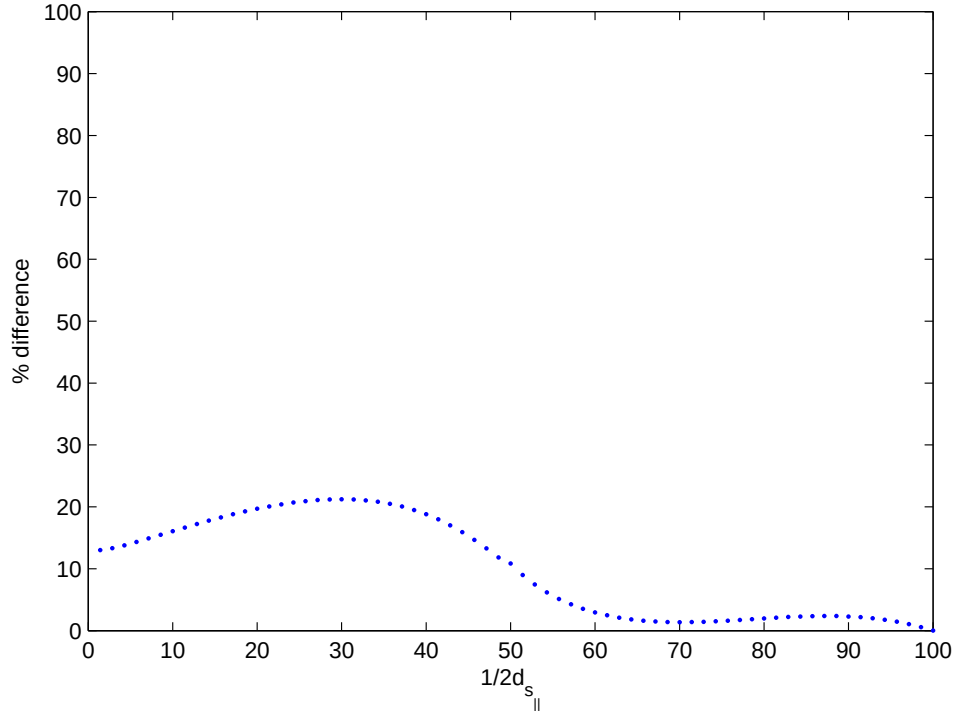

Figure 8.6: Percent difference between numerical data and weighted average function for a streamwise staggered array with $h = d_\parallel - \frac{1}{2}d_{s_\parallel} = 0.6$

streamwise staggered array, the SP model is continuous in this case, while the PS model is discontinuous due to a change from a linear trend for $h > 50\%$ to zero when $h < 50\%$. The PS model is zero in the stated region as the arrangement of the unit cell in question (see Figure B.14) leads to diffusion coefficients of zero upon application of the series formula. The weighted average thus does not predict the trend in numerical data exactly, but is still a good fit across the change from non-overlapping to overlapping, with the percent difference between them less than five percent as evidenced in Figure 8.8. However, for the region where the transverse pore-width is small, the percent difference is significantly larger than the rest. This behaviour is similar to that of the regular, non-staggered array with a varying transverse pore-width.

8.2 Arrays of solid squares

In comparing the analytical models to the numerical data the diffusion coefficients for arrays of square solid particles are functions of porosity. In this case $d_{s_\parallel} = d_{s_\perp} = d_s$ is varied, while the length $d_\parallel = d_\perp = d$ is chosen as 1 in the numerical program.

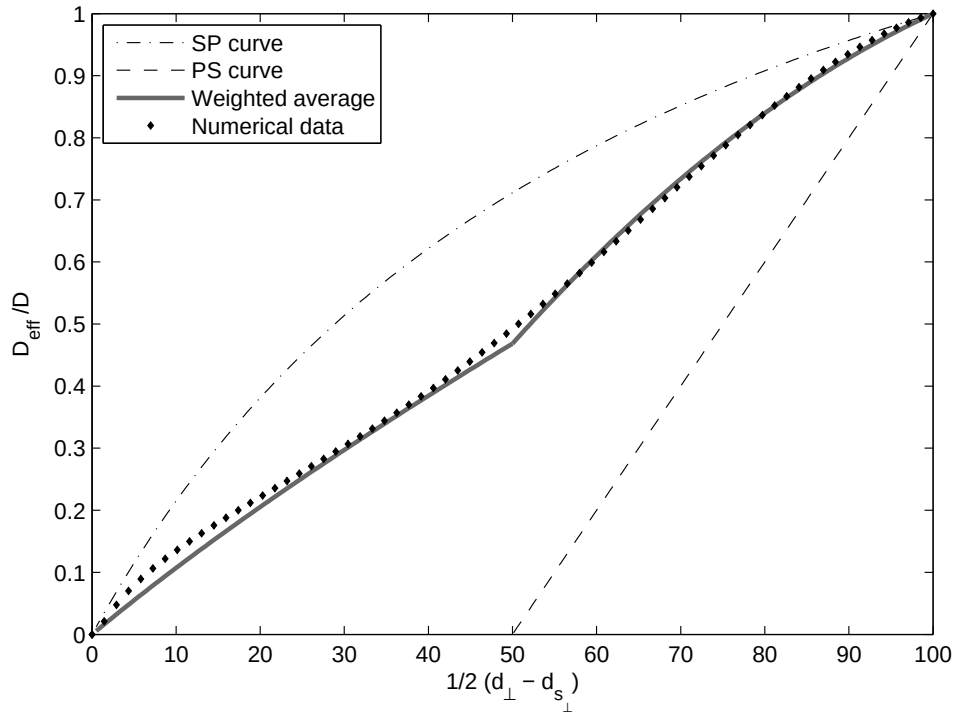

Figure 8.7: Comparison between numerical data and analytical models of Bell & Crank (1973) for a transversally staggered array with $\sigma = \frac{1}{2}d_{s_{\parallel}} = 0.2$.

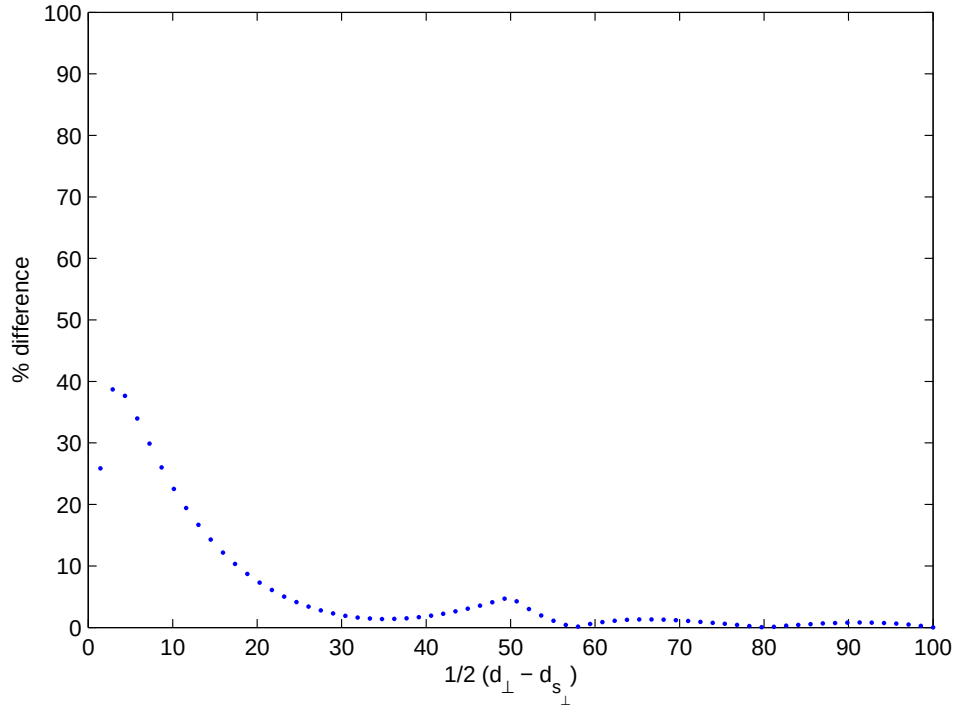

Figure 8.8: Percent difference between numerical data and weighted average function for a transversally staggered array with $\sigma = \frac{1}{2}d_{s_{\parallel}} = 0.2$

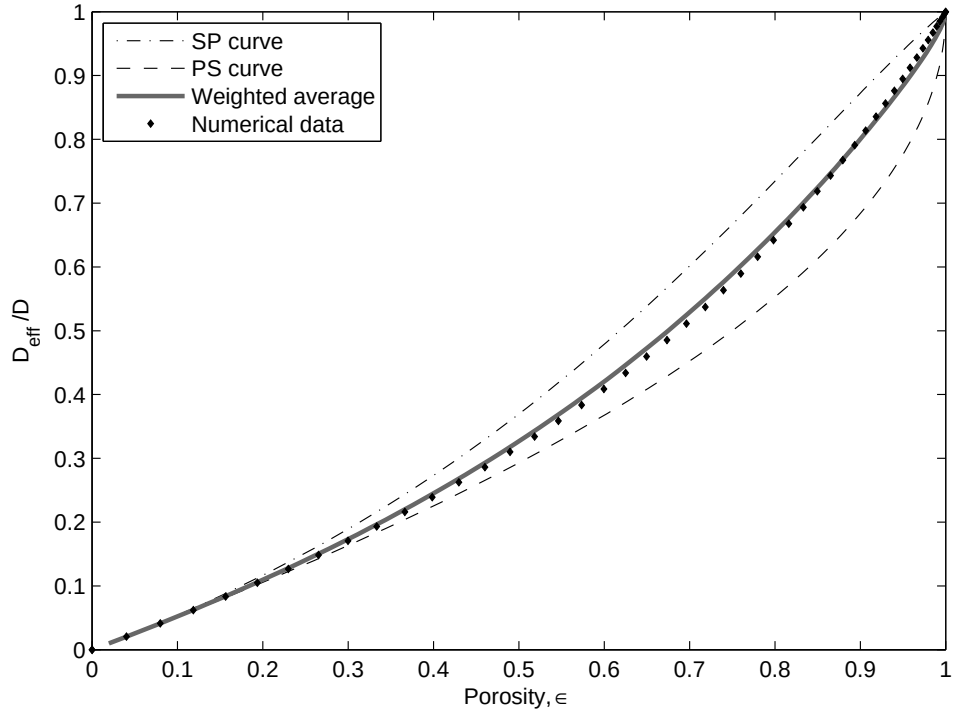

Figure 8.9: Regular array of squares with D_{eff}/D as a function of the porosity, ϵ.

8.2.1 Regular array

The numerical data generated for a regular array of square solid particles as compared to the application of the analytical models of Bell & Crank (1973) is shown in Figure 8.9. For small porosities all three analytical models are very good approximations for the numerical data, but as the porosity increases the weighted average function is once again the best. The percent difference between the weighted average and numerical data is presented in Figure 8.10. The percent difference is greater for larger porosities, but remains below ten percent.

8.2.2 Streamwise and transversally staggered arrays

The weighted average function from Bell & Crank (1973) was developed for arrays with square unit cells, but when an array of squares is staggered in either the streamwise or transverse directions the unit cell has to be rectangular to allow for the overlapping of solids (see Appendix B). The weighted average function should therefore not be a good approximation of the numerical results for either of these cases. This is confirmed in Figure 8.11 in which the results of a transversally staggered array are shown. The weighted average function does not fit the numerical data, with the SP model being the best approximation.

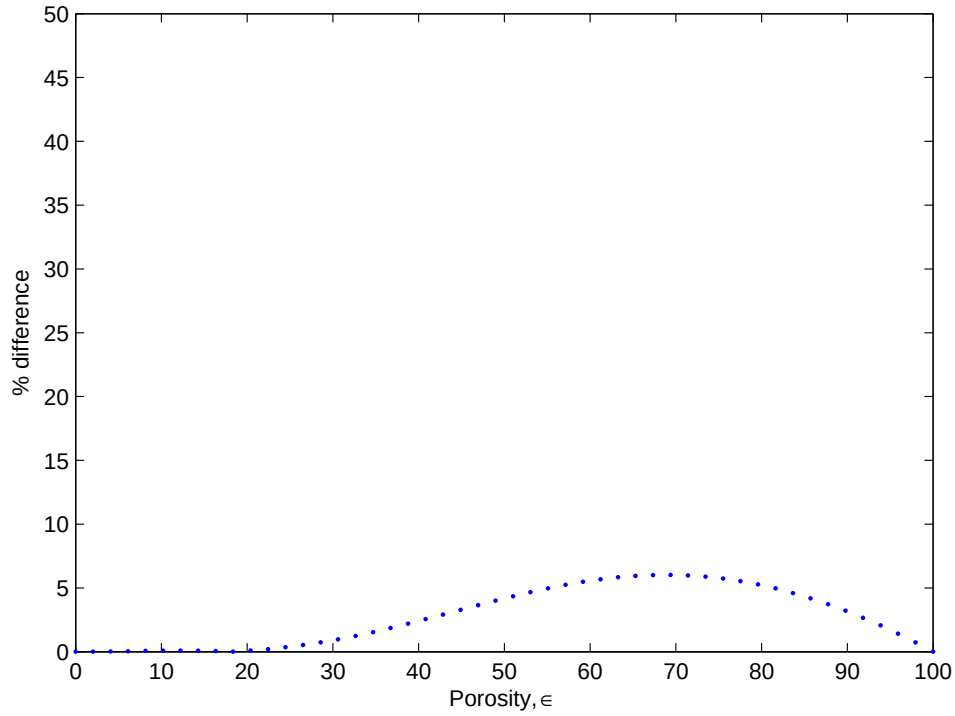

Figure 8.10: Percent difference between numerical data and weighted average function for a regular array of squares as a function of the porosity.

An alternate weighted average function could thus be developed for these streamwise and transversally staggered arrays.

8.2.3 RUC weighted average

The weighted average of the RUC models, equation (4.13), is tested against the SP and PS models and their weighted average function in Figure 8.13. The RUC model compares favourably with the numerical data and SP-PS weighted average function.

The weighted average of the RUC fibre bed and granular models is compared with the SP and PS model in Figure 8.13. This model is a reasonable predictor for the numerical diffusivities, and is a better fit than either of the SP or PS models, or especially the SP and PS weighted average function. There is thus need for a model such as the RUC weighted average.

Figure 8.12 illustrates the dominant behaviour present in the RUC weighted average model - in the lower porosity region the two-dimensional fibre bed model is dominant, while in the high porosity region the three-dimensional granular model is dominant. The numerical

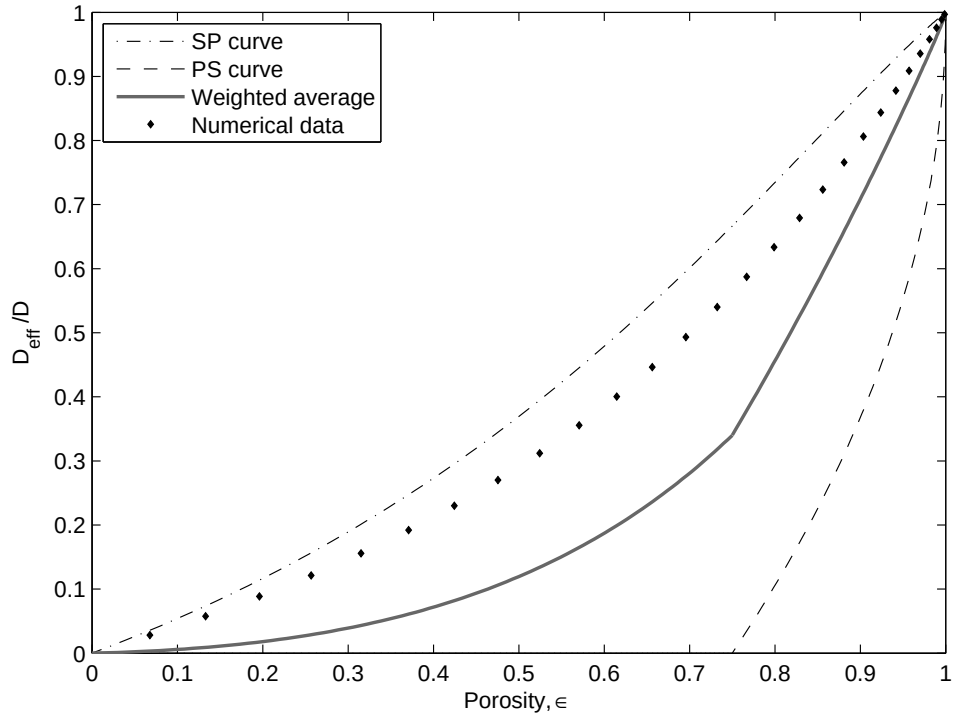

Figure 8.11: Transversally staggered array of squares with D_{eff}/D as a function of the porosity, ϵ.

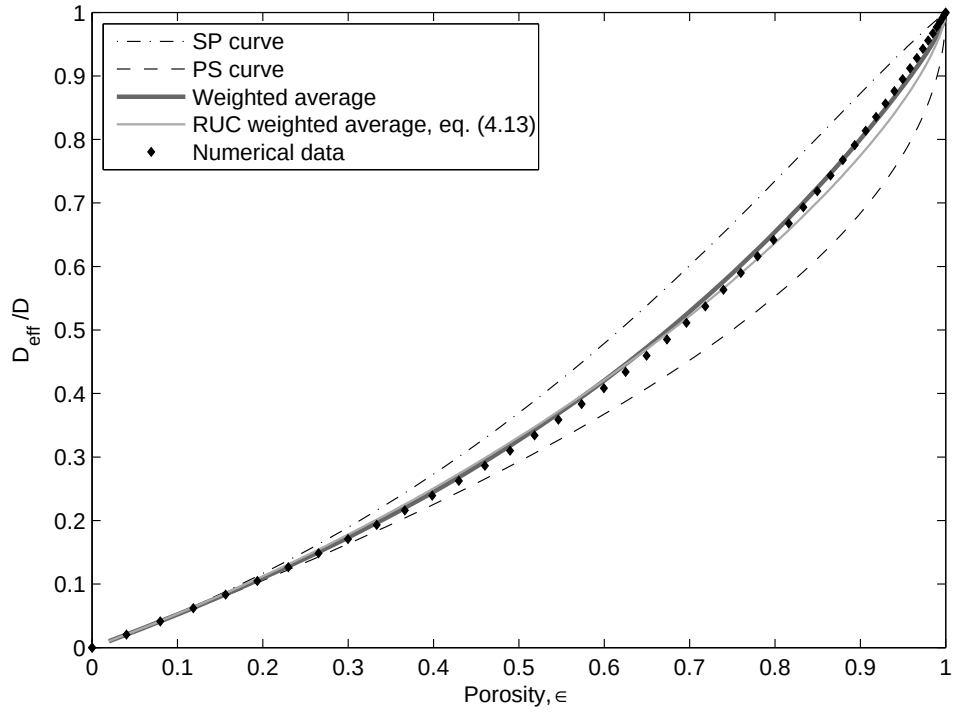

Figure 8.12: A comparison of the RUC weighted average model, equation (4.13), and the SP and PS models and weighted average function of Bell & Crank (1973) with the numerical data for a regular array of squares.

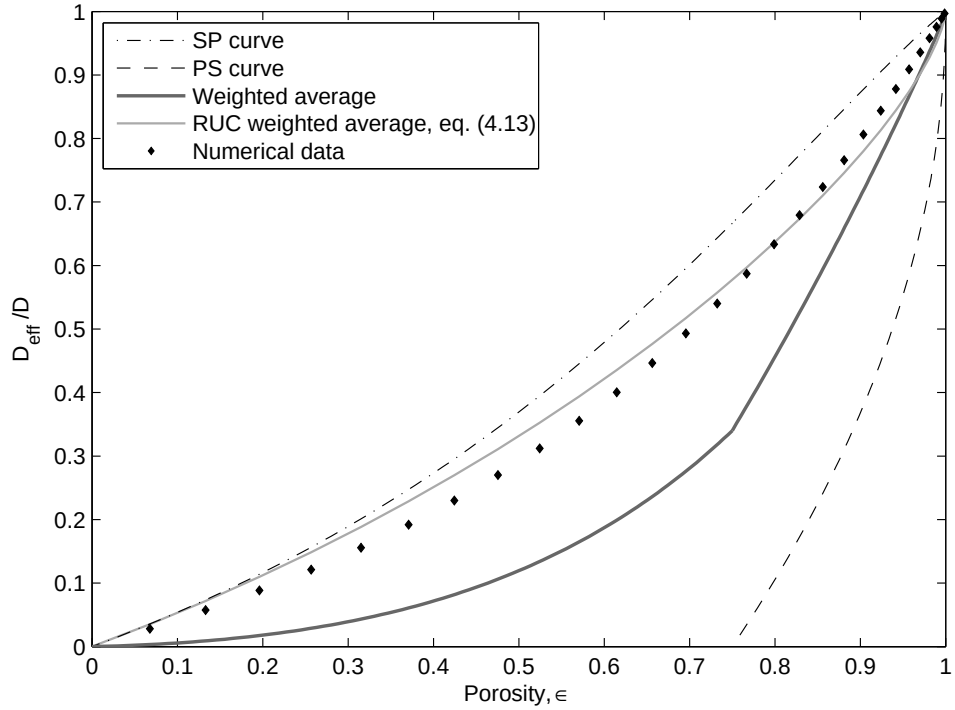

Figure 8.13: Transversally staggered array with D_{eff}/D as a function of the porosity, ϵ. A comparison of the RUC weighted average model, equation (4.13), and the SP and PS models and weighted average function of Bell & Crank (1973) with the numerical data for a transversally staggered array of squares.

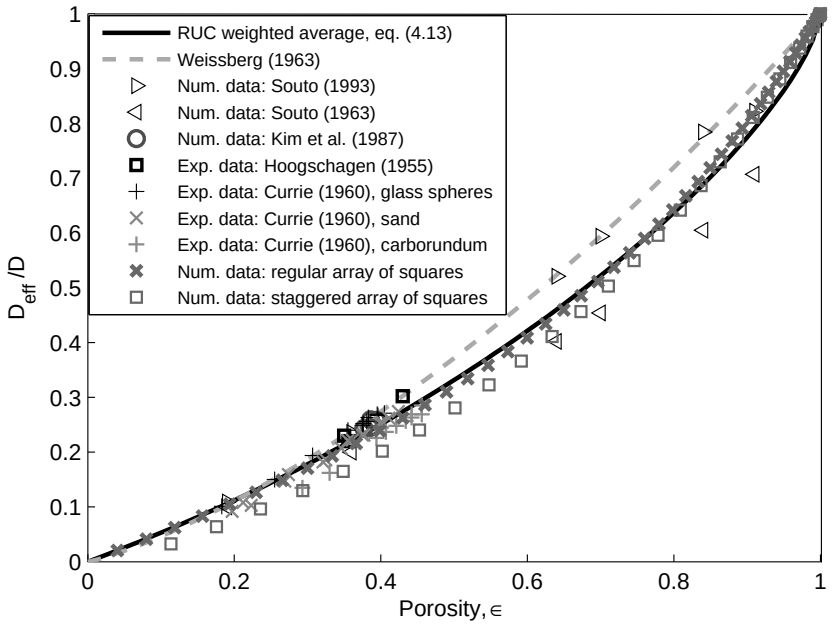

Figure 8.14: Comparison of the RUC weighted average model, equation (4.13), with numerical and experimental data from literature.

data reflects this trend, thus the construction of the weighted average according to equation (4.13) is justified.

The RUC weighted average model is tested against experimental data from the literature, and, as is evident in Figure 8.14, compares favourably with the data, despite the simple rectangular geometry of the model. The experimental data include those of Currie (1960) for spheres, sand and carborundum.

Figure 8.14 also indicates that the numerical data for the regular and staggered arrays of squares are unexpectedly similar. This result is in agreement with the numerical solution of Crank (1975) which find that the values of D_{eff}/D for aligned and staggered arrays differ by between two and three percent. Kim et al. (1987) also provide evidence that the effective diffusivities in regular and staggered arrays differ by less than 1%, even though the diffusive path through a fully staggered array is quite tortuous in comparison to the path through a regular array. This also justifies the use of the geometric factor ψ in the expression for D_{eff}/D which yields the same expression for both regular and staggered arrays.

Chapter 9

Conclusions

The implementation of the fibre bed and granular RUC models, which were used to represent two-dimensional and three-dimensional pore-scale models respectively, led to the construction of models to predict the diffusivity ratios of unconsolidated porous media which rely only on the porosity of the host solid. A weighted average of the two was used to predict the diffusivity ratio of homogeneous and transversally isotropic diffusion processes through arrays of unconsolidated solid squares. The specific weights of the RUC weighted average was determined through study of experimental data available in literature, where the fibre bed (two-dimensional) model was found to predict diffusivity ratios at low porosities best and the granular model found to be most accurate at high porosities. The two models were subsequently weighted to favour the appropriate model for each porosity region.

All three RUC models (fibre bed, granular and weighted average) were tested against experimental data from the literature, as well as various analytical, statistical and empirically deduced models of D_{eff}/D. The models were in good agreement with the data, with the RUC weighted average seemingly the most accurate for homogeneous and transversally isotropic diffusion processes. Comparison with published models from the literature models illustrated that such a pore-scale model could be effectively applied without the aid of complex statistical methods or expensive experimental testing when only the porosity of a porous medium is available.

A method developed by Crank (1975) was studied which enables the modelling of arrays of solids rectangles at the pore level. The resulting SP and PS models were combined in a weighted average function weighted according to a formula proposed by Bell & Crank (1973). This formula was however designed for square unit cells, which impedes modelling

of arrays of staggered solid squares as it was found that their unit cells cannot be square when allowing for staggering and overlapping of the solid phase. Thus, the weighted average function of Bell & Crank (1973) failed for these arrays, whereas the RUC weighted average performed well in contrast.

Numerical computations were conducted by means of the tri-diagonal matrix algorithm developed for computational fluid dynamics. Using this algorithm, the diffusive flux through an array of unconsolidated solids was computed for the entire porosity range. In the case of rectangular solids, either the parallel or streamwise solids length, $d_{s_{\parallel}}$ or $d_{s_{\perp}}$, was varied while the other remained constant in order to find D_{eff}/D for all porosities. The solid length, d_s, was varied on implementation of the numerical program for arrays of solid squares.

Comparison of the numerical results revealed the weighted average function of Bell & Crank (1973) to be a good model for arrays of unconsolidated rectangles for all regular, staggered and overlapping cases. The numerical results also confirmed the weighted average function to be unsuitable for staggered solid squares and the RUC weighted average to be a good predictive model for these arrays.

The performance of the RUC model upon comparison with the available experimental data, generated numerical results and published models from the literature provide confidence in the strength of the model to predict the diffusivity ratio. Building on these results, the scope may be widened to include anisotropic diffusion processes and possibly the effects of other diffusive processes, such as Knudsen diffusion in micro-pores, on the total transport of mass. Further extensions of the model could include convection in an effort to fully predict flow properties through porous media.

Appendix A

Effective diffusion coefficients of ordered arrays

The effective diffusion coefficients of ordered arrays are found through application of both the PS and SP models discussed in Chapter 5. The ordered arrays considered are regular arrays, non-overlapping and overlapping fully streamwise staggered arrays as well as non-overlapping and overlapping fully transversally staggered arrays.

A.1 Regular array

A regular array is one in which no staggering or overlapping of solids occur in either principle (streamwise or transversal) direction. A schematic representation of this array may be seen in Figure A.1, where the dashed lines indicate the representative unit cell chosen. Further, in Figures A.2 and A.3, the associated unit cells are shown in detail.

A.1.1 SP model

The SP model is obtained through application of the parallel formula on the unit cell in Figure A.2, followed by the series formula.

Application of the parallel formula, equation (5.7), on column i of Figure A.2 yields

$$d_{\perp} D_i = d_{\perp} D - d_{s_{\perp}} D,$$

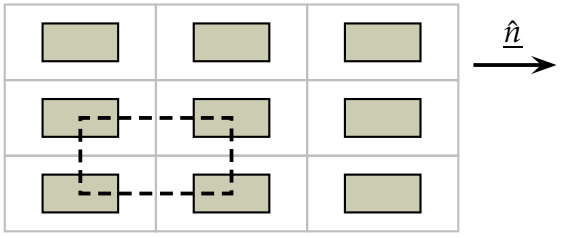

Figure A.1: Regular array with a unit cell indicated by the bold dashed frame.

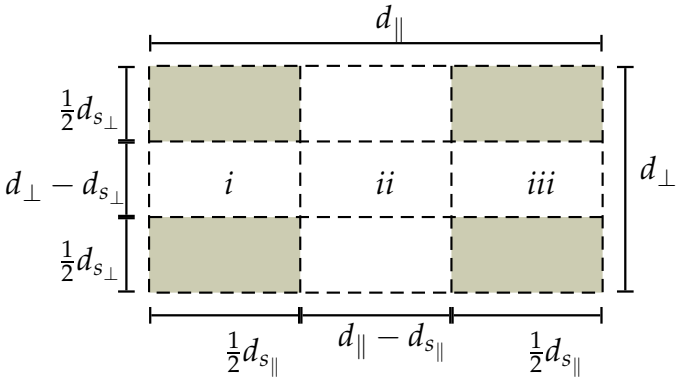

Figure A.2: Unit cell of regular array using the SP model.

thus

$$D_i = D\left(\frac{d_\perp - d_{s_\perp}}{d_\perp}\right). \tag{A.1}$$

Similarly, for column *ii*

$$d_\perp D_{ii} = d_\perp D,$$

thus

$$D_{ii} = D \tag{A.2}$$

and column *iii*

$$d_\perp D_{iii} = d_\perp D - d_{s_\perp} D,$$

which yields

$$D_{iii} = D\left(\frac{d_\perp - d_{s_\perp}}{d_\perp}\right). \tag{A.3}$$

Substitution of equations (A.1), (A.2) and (A.3) into equation (5.6), the series formula, yields

$$\frac{d_\parallel}{D_{SP}} = \frac{\frac{1}{2}d_{s_\parallel}}{D_i} + \frac{d_\parallel - d_{s_\parallel}}{D_{ii}} + \frac{\frac{1}{2}d_{s_\parallel}}{D_{iii}},$$

thus

$$d_\parallel \frac{D}{D_{SP}} = d_\perp \frac{\frac{1}{2}d_{s_\parallel}}{d_\perp - d_{s_\perp}} + (d_\parallel - d_{s_\parallel}) + d_\perp \frac{\frac{1}{2}d_{s_\parallel}}{d_\perp - d_{s_\perp}}. \tag{A.4}$$

Through further simplification of equation (A.4), the diffusion coefficient of this array, according to the SP model, is found to be

$$\frac{D_{SP}}{D} = \left[1 + \frac{d_{s_\parallel} d_{s_\perp}}{d_\parallel (d_\perp - d_{s_\perp})}\right]^{-1}. \tag{A.5}$$

A.1.2 PS model

The PS model is obtained through application of the series formula on the unit cell in Figure A.3, followed by the parallel formula.

Application of the series formula on columns *i* and *iii* of Figure A.3 yields diffusion coefficients of zero, i.e.

$$D_i = D_{iii} = 0, \tag{A.6}$$

while for column *ii*

$$\frac{d_\parallel}{D_{ii}} = \frac{\frac{1}{2}d_{s_\parallel}}{D} + \frac{d_\parallel - d_{s_\parallel}}{D} + \frac{\frac{1}{2}d_{s_\parallel}}{D},$$

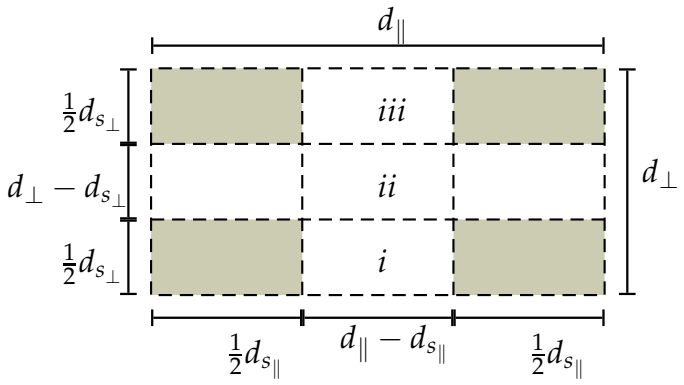

Figure A.3: Unit cell of regular array using the PS model.

thus

$$D_{ii} = D. \tag{A.7}$$

Substitution of equations (A.6) and (A.7) into the parallel formula, equation (5.7), yields

$$D_{PS}\, d_\perp = D(d_\perp - d_{s_\perp}). \tag{A.8}$$

Through simplification of equation (A.8), the diffusion coefficient of this array, according to the PS model, is found to be

$$\frac{D_{PS}}{D} = \frac{d_\perp - d_{s_\perp}}{d_\perp}. \tag{A.9}$$

A.2 Streamwise staggered arrays

A.2.1 $d_\parallel > d_\perp$

An example of a streamwise staggered array is represented in Figure A.4, in which case the streamwise cell length, $d_\parallel$, is greater than the transverse cell length, $d_\perp$.

Non-overlapping SP model

The SP model is obtained through application of the parallel formula on the unit cell in Figure A.5, followed by the series formula.

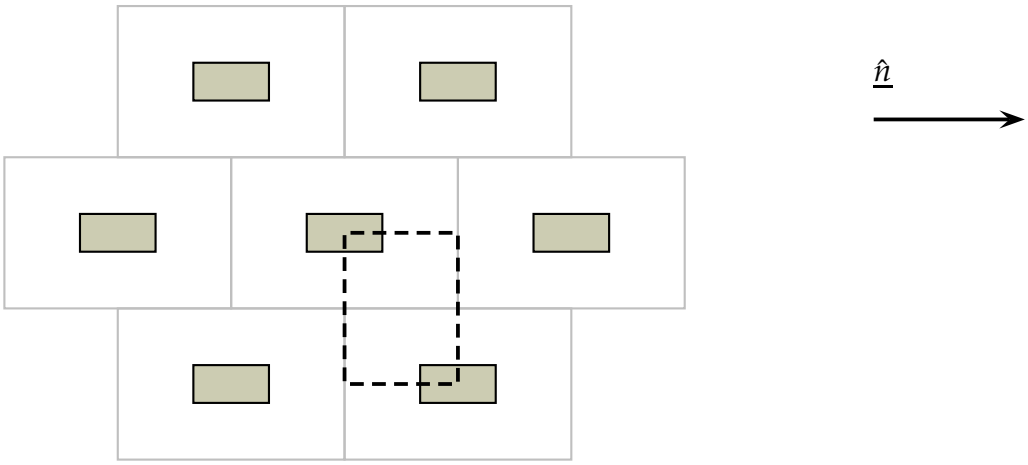

Figure A.4: Non-overlapping streamwise staggered array with unit cell indicated by the bold dashed frame.

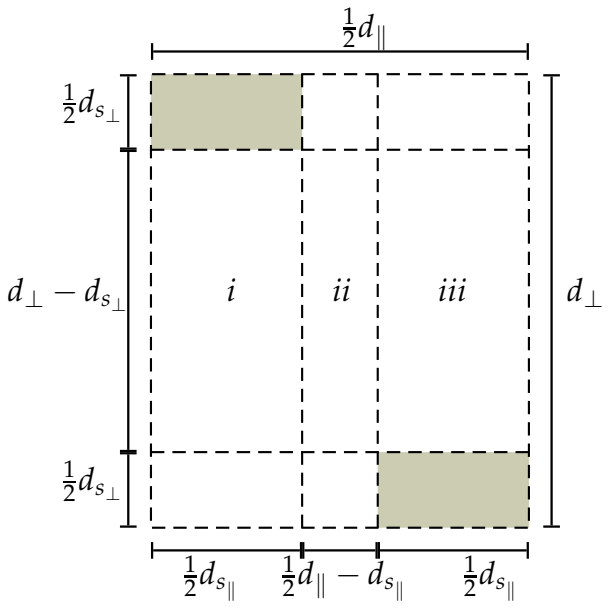

Figure A.5: Unit cell of non-overlapping, streamwise staggered array using the SP model.

Application of the parallel formula, equation (5.7), on column i of Figure A.5 yields

$$d_\perp D_i = (d_\perp - \frac{1}{2}d_{s_\perp})D,$$

thus

$$D_i = \left(\frac{d_\perp - \frac{1}{2}d_{s_\perp}}{d_\perp}\right) D. \tag{A.10}$$

Similarly, for column ii

$$d_\perp D_{ii} = d_\perp D,$$

thus

$$D_{ii} = D \tag{A.11}$$

and column iii

$$d_\perp D_{iii} = (d_\perp - \frac{1}{2}d_{s_\perp})D,$$

which yields

$$D_{iii} = \left(\frac{d_\perp - \frac{1}{2}d_{s_\perp}}{d_\perp}\right) D. \tag{A.12}$$

Substitution of equations (A.10), (A.11) and (A.12) into equation (5.6), the series formula, yields

$$\frac{\frac{1}{2}d_\parallel}{D_{SP}} = \frac{\frac{1}{2}d_{s_\parallel}}{D_i} + \frac{\frac{1}{2}d_\parallel - d_{s_\parallel}}{D_{ii}} + \frac{\frac{1}{2}d_{s_\parallel}}{D_{iii}},$$

thus

$$\frac{D}{D_{SP}} = \frac{2d_\perp d_{s_\parallel}}{d_\parallel(d_\perp - \frac{1}{2}d_{s_\perp})} + \frac{d_\parallel - 2d_{s_\parallel}}{d_\parallel}. \tag{A.13}$$

Through further simplification of equation (A.13), the diffusion coefficient of this array, according to the SP model, is found to be

$$\frac{D_{SP}}{D} = \left[1 + \frac{d_{s_\parallel} d_{s_\perp}}{d_\parallel(d_\perp - \frac{1}{2}d_{s_\perp})}\right]^{-1}. \tag{A.14}$$

Non-overlapping PS model

The PS model is obtained through application of the series formula on the unit cell in Figure A.6, followed by the parallel formula.

Application of the series formula on columns i and iii of Figure A.6 yields diffusion coefficients of zero, i.e.

$$D_i = D_{iii} = 0, \tag{A.15}$$

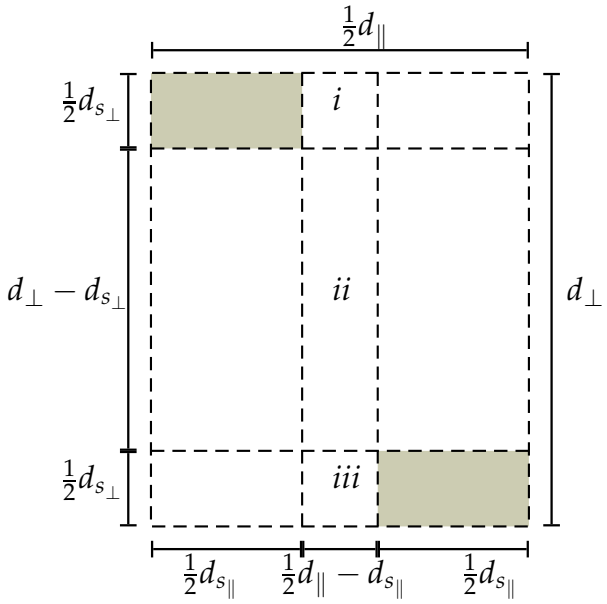

Figure A.6: Unit cell of non-overlapping, streamwise staggered array using the PS model.

while for column ii

$$D_{ii} = D. \tag{A.16}$$

Substitution of equations (A.15) and (A.16) into the parallel formula, equation (5.7), yields

$$d_\perp D_{PS} = (d_\perp - d_{s_\perp})D. \tag{A.17}$$

Through simplification of equation (A.17), the diffusion coefficient of this array, according to the PS model, is found to be

$$\frac{D_{PS}}{D} = 1 - \frac{d_{s_\perp}}{d_\perp}. \tag{A.18}$$

Overlapping SP model

An example of a streamwise staggered array in which overlapping occurs is given in Figure A.7

The SP model is obtained through application of the parallel formula on the unit cell in Figure A.8, followed by the series formula.

Application of the parallel formula, equation (5.7), on column i of Figure A.8 yields

$$d_\perp D_i = (d_\perp - \frac{1}{2}d_{s_\perp})D,$$

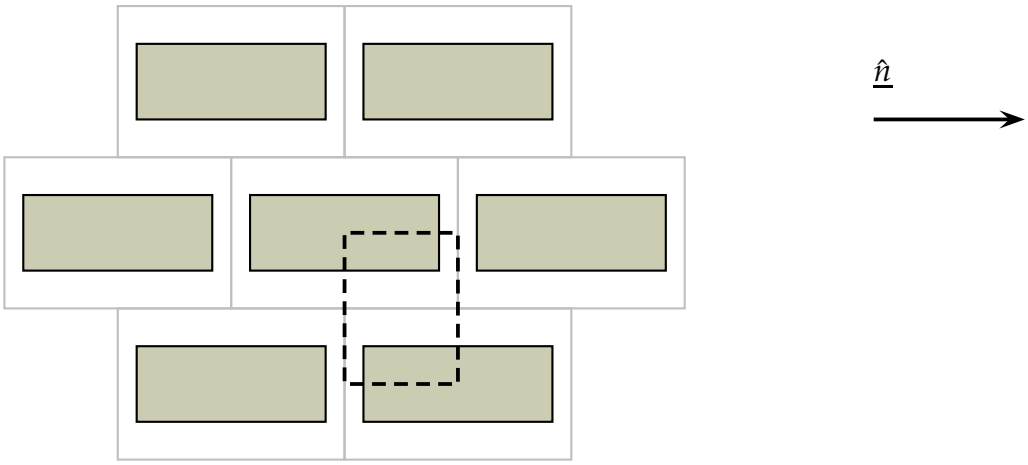

Figure A.7: Overlapping streamwise staggered array with unit cell indicated by the bold dashed frame.

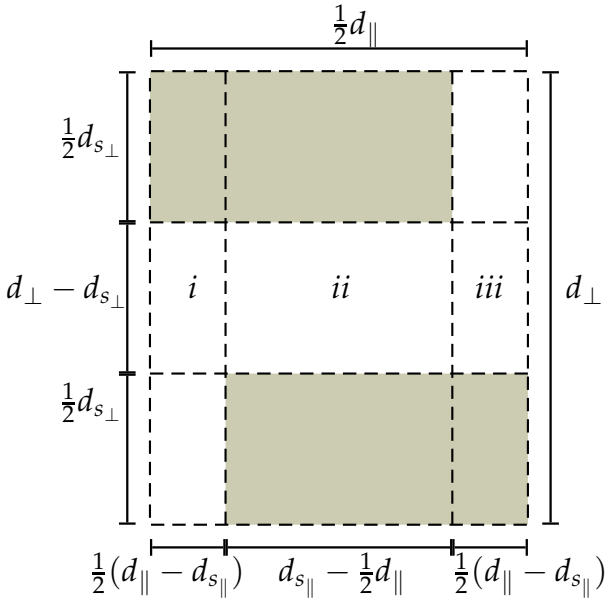

Figure A.8: Unit cell of overlapping, streamwise staggered array using the SP model.

thus

$$D_i = \left(\frac{d_\perp - \frac{1}{2} d_{s_\perp}}{d_\perp} \right) D. \tag{A.19}$$

Similarly, for column *ii*

$$d_\perp D_{ii} = (d_\perp - d_{s_\perp}) D,$$

thus

$$D_{ii} = \frac{d_\perp - d_{s_\perp}}{d_\perp} D \tag{A.20}$$

and column *iii*

$$d_\perp D_i = (d_\perp - \frac{1}{2} d_{s_\perp}) D,$$

which yields

$$D_{iii} = \left(\frac{d_\perp - \frac{1}{2} d_{s_\perp}}{d_\perp} \right) D. \tag{A.21}$$

Substitution of equations (A.19), (A.20) and (A.21) into equation (5.6), the series formula, yields

$$\frac{\frac{1}{2} d_\parallel}{D_{SP}} = \frac{\frac{1}{2}(d_\parallel - d_{s_\parallel})}{D_i} + \frac{d_{s_\parallel} - \frac{1}{2} d_\parallel}{D_{ii}} + \frac{\frac{1}{2}(d_\parallel - d_{s_\parallel})}{D_{iii}},$$

thus

$$\frac{D}{D_{SP}} = \frac{2 d_\perp (d_\parallel - d_{s_\parallel})}{d_\parallel (d_\perp - \frac{1}{2} d_{s_\perp})} + \frac{2 d_{s_\parallel} - d_\parallel}{d_\parallel (d_\perp - d_{s_\perp})}. \tag{A.22}$$

Through further simplification of equation (A.22), the diffusion coefficient of this array, according to the SP model, is found to be

$$\frac{D_{SP}}{D} = \left[\frac{d_\perp^2 - \frac{3}{2} d_{s_\perp} d_\perp + \frac{d_{s_\parallel}}{d_\parallel} d_{s_\perp} d_\perp}{(d_\perp - \frac{1}{2} d_{s_\perp})(d_\perp - d_{s_\perp})} \right]^{-1}. \tag{A.23}$$

Overlapping PS model

The PS model is obtained through application of the series formula on the unit cell in Figure A.9, followed by the parallel formula.

Application of the series formula on columns *i* and *iii* of Figure A.9 yields diffusion coefficients of zero, i.e.

$$D_i = D_{iii} = 0, \tag{A.24}$$

while for column *ii*

$$D_{ii} = D. \tag{A.25}$$

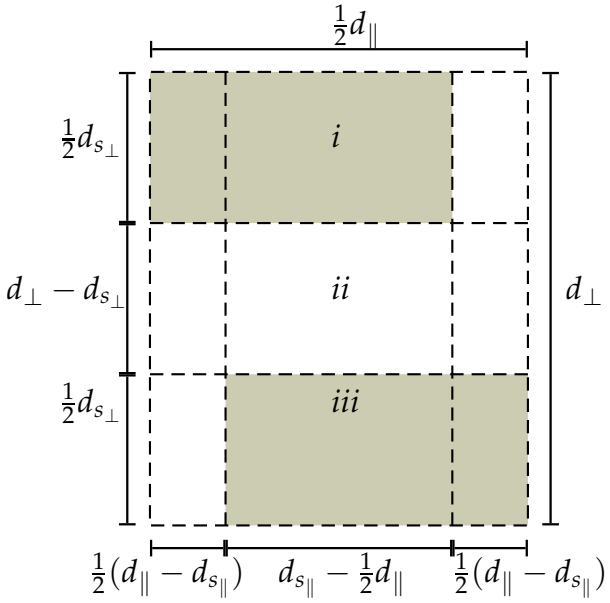

Figure A.9: Unit cell of overlapping, streamwise staggered array using the PS model.

Substitution of equations (A.24) and (A.25) into the parallel formula, equation (5.7), yields

$$d_\perp D_{PS} = (d_\perp - d_{s_\perp})D. \tag{A.26}$$

Through simplification of equation (A.26), the diffusion coefficient of this array, according to the PS model, is found to be

$$\frac{D_{PS}}{D} = 1 - \frac{d_{s_\perp}}{d_\perp}. \tag{A.27}$$

A.2.2 $d_\perp > d_{\parallel}$

In this section the diffusivity ratios of streamwise staggered arrays in which the transverse cell length is greater than the streamwise cell length are calculated. An example of such an array is given in Figure A.10.

Non-overlapping SP model

The SP model is obtained through application of the parallel formula on the unit cell in Figure A.11, followed by the series formula.

Application of the parallel formula, equation (5.7), on column i of Figure A.11 yields

$$d_\perp D_i = (d_\perp - \frac{1}{2}d_{s_\perp})D,$$

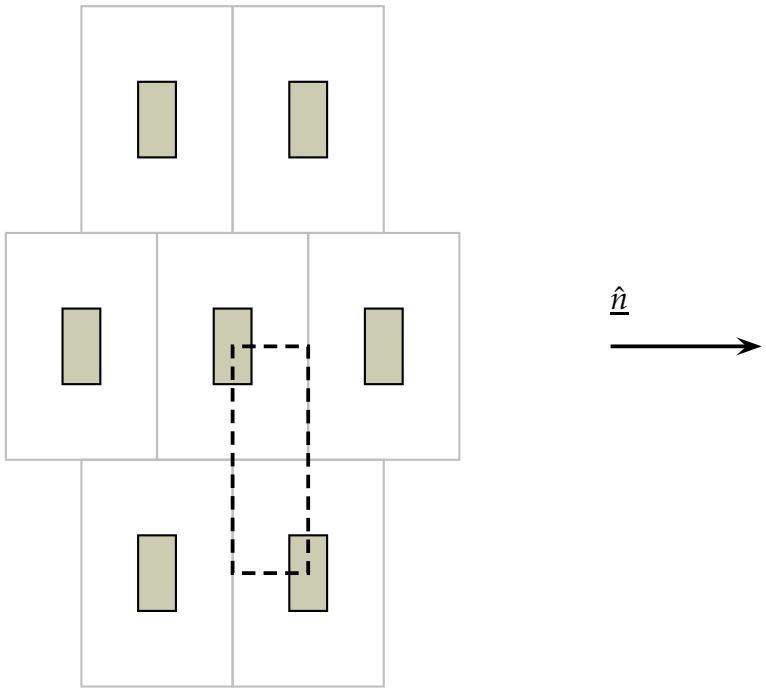

Figure A.10: Non-overlapping, streamwise staggered array with unit cell indicated by the bold dashed frame.

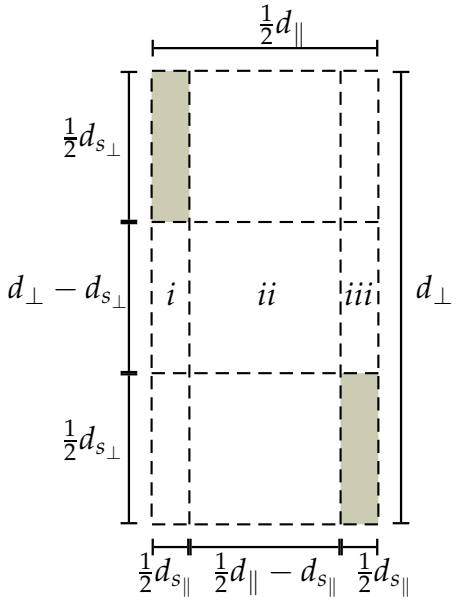

Figure A.11: Unit cell of non-overlapping, streamwise staggered array using the SP model.

thus

$$D_i = \left(\frac{d_\perp - \frac{1}{2} d_{s_\perp}}{d_\perp} \right) D. \tag{A.28}$$

Similarly, for column *ii*

$$d_\perp D_{ii} = d_\perp D,$$

thus

$$D_{ii} = D \tag{A.29}$$

and column *iii*

$$d_\perp D_{iii} = (d_\perp - \frac{1}{2} d_{s_\perp}) D,$$

which yields

$$D_{iii} = \left(\frac{d_\perp - \frac{1}{2} d_{s_\perp}}{d_\perp} \right) D. \tag{A.30}$$

Substitution of equations (A.28), (A.29) and (A.30) into equation (5.6), the series formula, yields

$$\frac{\frac{1}{2} d_\parallel}{D_{SP}} = \frac{\frac{1}{2} d_{s_\parallel}}{D_i} + \frac{\frac{1}{2} d_\parallel - d_{s_\parallel}}{D_{ii}} + \frac{\frac{1}{2} d_{s_\parallel}}{D_{iii}},$$

thus

$$\frac{D}{D_{SP}} = \frac{2 d_\perp d_{s_\parallel}}{d_\parallel (d_\perp - \frac{1}{2} d_{s_\perp})} + \frac{d_\parallel - 2 d_{s_\parallel}}{d_\parallel}. \tag{A.31}$$

Through further simplification of equation (A.31), the diffusion coefficient of this array, according to the SP model, is found to be

$$\frac{D_{SP}}{D} = \left[1 + \frac{d_{s_\parallel} d_{s_\perp}}{d_\parallel (d_\perp - \frac{1}{2} d_{s_\perp})} \right]^{-1}. \tag{A.32}$$

Non-overlapping PS model

The PS model is obtained through application of the series formula on the unit cell in Figure A.12, followed by the parallel formula.

Application of the series formula on columns *i* and *iii* of Figure A.12 yields diffusion coefficients of zero, i.e.

$$D_i = D_{iii} = 0, \tag{A.33}$$

while for column *ii*

$$D_{ii} = D. \tag{A.34}$$

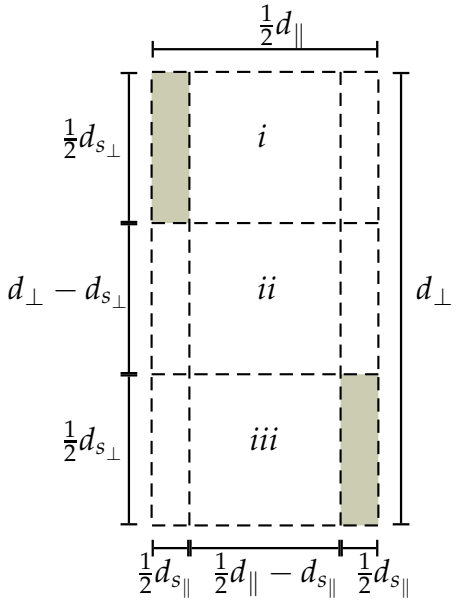

Figure A.12: Unit cell of non-overlapping, streamwise staggered array using the PS model.

Substitution of equations (A.33) and (A.34) into the parallel formula, equation (5.7), yields

$$d_\perp D_{PS} = (d_\perp - d_{s_\perp})D. \tag{A.35}$$

Through simplification of equation (A.35), the diffusion coefficient of this array, according to the PS model, is found to be

$$\frac{D_{PS}}{D} = 1 - \frac{d_{s_\perp}}{d_\perp}. \tag{A.36}$$

Overlapping SP model

Figure A.13 shows an example of an overlapping streamwise staggered array.

The SP model is obtained through application of the parallel formula on the unit cell in Figure A.14, followed by the series formula.

Application of the parallel formula, equation (5.7), on column i of Figure A.14 yields

$$d_\perp D_i = (d_\perp - \frac{1}{2}d_{s_\perp})D,$$

thus

$$D_i = \left(\frac{d_\perp - \frac{1}{2}d_{s_\perp}}{d_\perp}\right) D. \tag{A.37}$$

Similarly, for column ii

$$d_\perp D_{ii} = (d_\perp - d_{s_\perp})D,$$

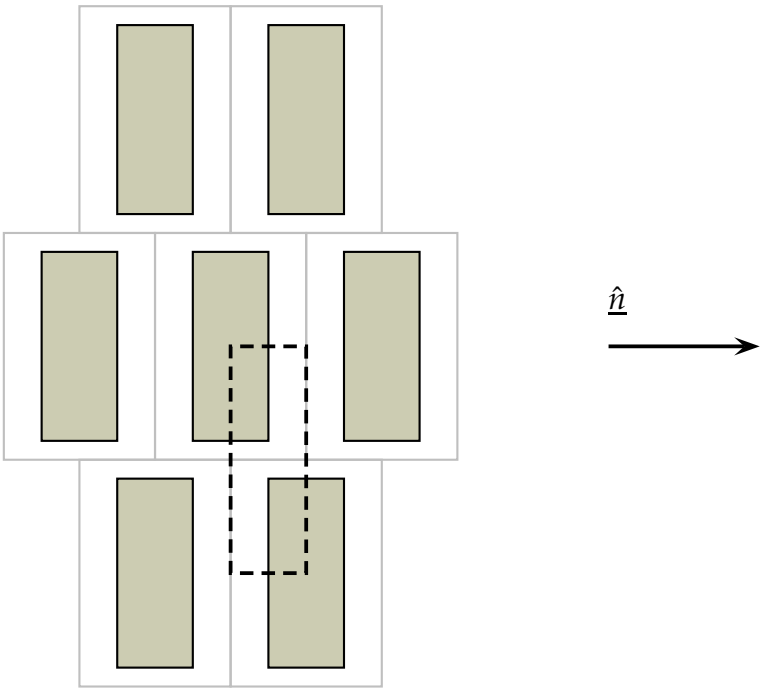

Figure A.13: Overlapping, streamwise staggered array with unit cell indicated by the bold dashed frame.

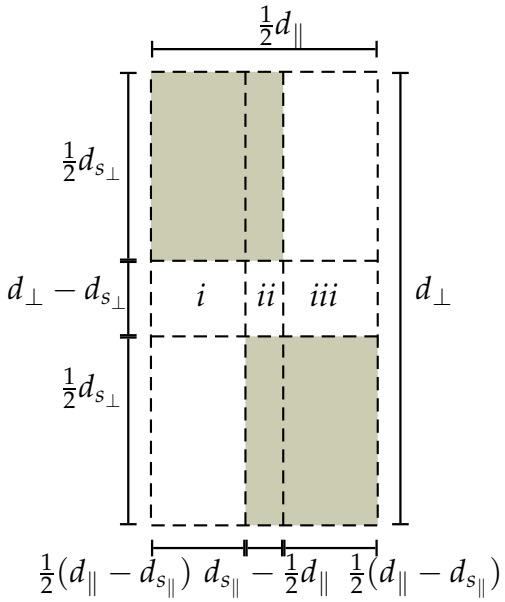

Figure A.14: Unit cell of overlapping, streamwise staggered array using the SP model.

thus

$$D_{ii} = \frac{d_\perp - d_{s_\perp}}{d_\perp} D \tag{A.38}$$

and column *iii*

$$d_\perp D_i = (d_\perp - \frac{1}{2} d_{s_\perp}) D,$$

which yields

$$D_{iii} = \left(\frac{d_\perp - \frac{1}{2} d_{s_\perp}}{d_\perp} \right) D. \tag{A.39}$$

Substitution of equations (A.37), (A.38) and (A.39) into equation (5.6), the series formula, yields

$$\frac{\frac{1}{2} d_\parallel}{D_{SP}} = \frac{\frac{1}{2}(d_\parallel - d_{s_\parallel})}{D_i} + \frac{d_{s_\parallel} - \frac{1}{2} d_\parallel}{D_{ii}} + \frac{\frac{1}{2}(d_\parallel - d_{s_\parallel})}{D_{iii}},$$

thus

$$\frac{D}{D_{SP}} = \frac{2 d_\perp (d_\parallel - d_{s_\parallel})}{d_\parallel (d_\perp - \frac{1}{2} d_{s_\perp})} + \frac{2 d_{s_\parallel} - d_\parallel}{d_\parallel (d_\perp - d_{s_\perp})}. \tag{A.40}$$

Through further simplification of equation (A.40), the diffusion coefficient of this array, according to the SP model, is found to be

$$\frac{D_{SP}}{D} = \left[\frac{d_\perp^2 - \frac{3}{2} d_{s_\perp} d_\perp + \frac{d_{s_\parallel}}{d_\parallel} d_{s_\perp} d_\perp}{(d_\perp - \frac{1}{2} d_{s_\perp})(d_\perp - d_{s_\perp})} \right]^{-1}. \tag{A.41}$$

Overlapping PS model

The PS model is obtained through application of the series formula on the unit cell in Figure A.15, followed by the parallel formula.

Application of the series formula on columns *i* and *iii* of Figure A.15 yields diffusion coefficients of zero, i.e.

$$D_i = D_{iii} = 0, \tag{A.42}$$

while for column *ii*

$$D_{ii} = D. \tag{A.43}$$

Substitution of equations (**??**) and (A.43) into the parallel formula, equation (5.7), yields

$$d_\perp D_{PS} = (d_\perp - d_{s_\perp}) D. \tag{A.44}$$

Through simplification of equation (A.44), the diffusion coefficient of this array, according to the PS model, is found to be

$$\frac{D_{PS}}{D} = 1 - \frac{d_{s_\perp}}{d_\perp}. \tag{A.45}$$

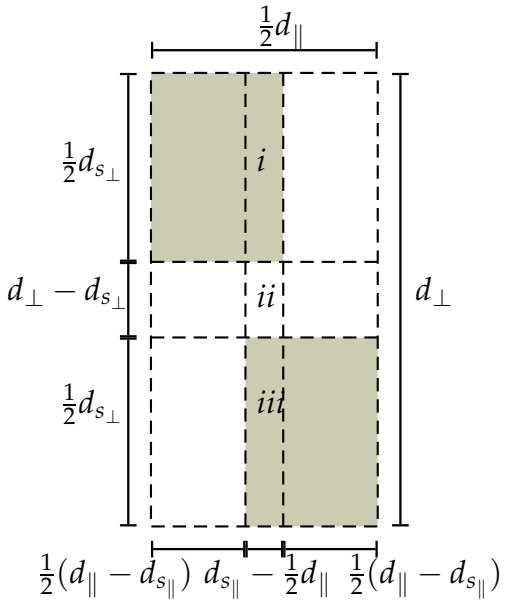

Figure A.15: Unit cell of overlapping, streamwise staggered array using the PS model.

A.3 Transversally staggered arrays

A.3.1 $d_{\parallel} > d_{\perp}$

An example of a non-overlapping transversally staggered array in which the streamwise cell lengths, $d_{\parallel}$, are greater than the transverse cell lengths, $d_{\perp}$, is given in Figure A.16.

Non-overlapping SP model

The SP model is obtained through application of the parallel formula on the unit cell in Figure A.17, followed by the series formula.

Application of the parallel formula, equation (5.7), on column i of Figure A.17 yields

$$\frac{1}{2}d_{\perp}D_i = \frac{1}{2}(d_{\perp} - d_{s_{\perp}})D,$$

thus

$$D_i = \left(\frac{d_{\perp} - d_{s_{\perp}}}{d_{\perp}}\right)D. \tag{A.46}$$

Similarly, for column ii

$$\frac{1}{2}d_{\perp}D_{ii} = \frac{1}{2}d_{\perp}D,$$

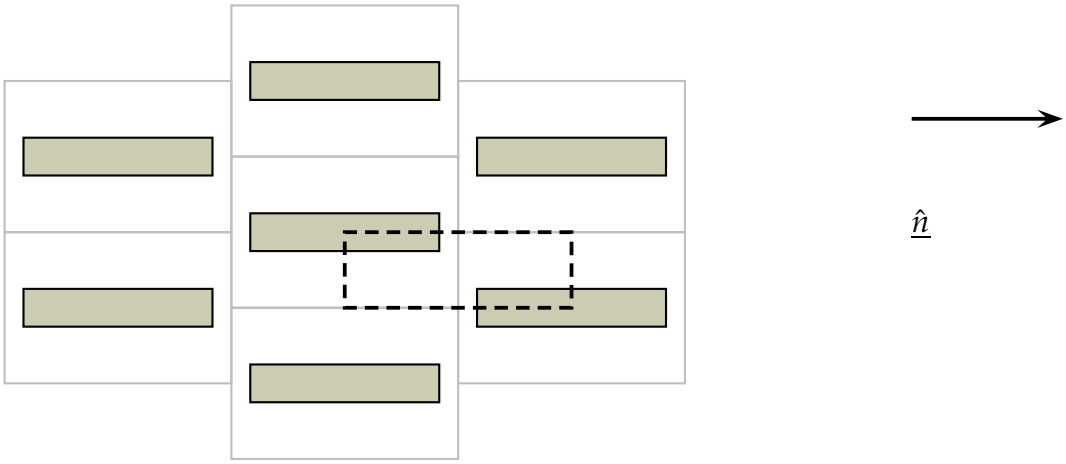

Figure A.16: Non-overlapping fully transversally staggered array with unit cell indicated by the bold dashed frame.

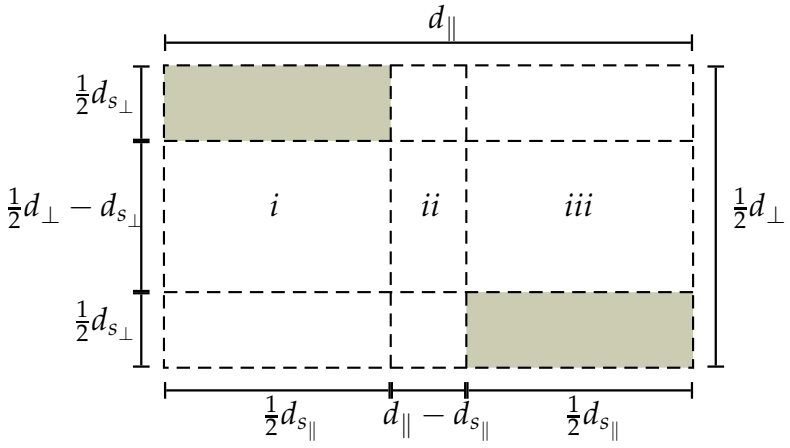

Figure A.17: Unit cell of non-overlapping transversally staggered array using the SP model.

thus

$$D_{ii} = D \tag{A.47}$$

and column *iii*

$$\frac{1}{2}d_{\perp}D_{iii} = \frac{1}{2}(d_{\perp} - d_{s_{\perp}})D,$$

which yields

$$D_{iii} = \left(\frac{d_{\perp} - d_{s_{\perp}}}{d_{\perp}}\right)D. \tag{A.48}$$

Substitution of equations (A.46), (A.47) and (A.48) into equation (5.6), the series formula, yields

$$\frac{d_{\parallel}}{D_{SP}} = \frac{\frac{1}{2}d_{s_{\parallel}}}{D_i} + \frac{d_{\parallel} - d_{s_{\parallel}}}{D_{ii}} + \frac{\frac{1}{2}d_{s_{\parallel}}}{D_{iii}},$$

thus

$$d_{\parallel}\frac{D}{D_{SP}} = d_{\perp}\frac{\frac{1}{2}d_{s_{\parallel}}}{d_{\perp} - d_{s_{\perp}}} + (d_{\parallel} - d_{s_{\parallel}}) + d_{\perp}\frac{\frac{1}{2}d_{s_{\parallel}}}{d_{\perp} - d_{s_{\perp}}}. \tag{A.49}$$

Through further simplification of equation (A.49), the diffusion coefficient of this array, according to the SP model, is found to be

$$\frac{D_{SP}}{D} = \left[1 + \frac{d_{s_{\parallel}}d_{s_{\perp}}}{d_{\parallel}(d_{\perp} - d_{s_{\perp}})}\right]^{-1}. \tag{A.50}$$

Non-overlapping PS model

The PS model is obtained through application of the series formula on the unit cell in Figure A.18, followed by the parallel formula.

Application of the series formula on columns *i* and *iii* of Figure A.18 yields diffusion coefficients of zero, i.e.

$$D_i = D_{iii} = 0, \tag{A.51}$$

while for column *ii*

$$D_{ii} = D. \tag{A.52}$$

Substitution of equations (A.51) and (A.52) into the parallel formula, equation (5.7), yields

$$\frac{1}{2}d_{\perp}D_{PS} = (\frac{1}{2}d_{\perp} - d_{s_{\perp}})D. \tag{A.53}$$

Through simplification of equation (A.53), the diffusion coefficient of this array, according to the PS model, is found to be

$$\frac{D_{PS}}{D} = 1 - \frac{2d_{s_{\perp}}}{d_{\perp}}. \tag{A.54}$$

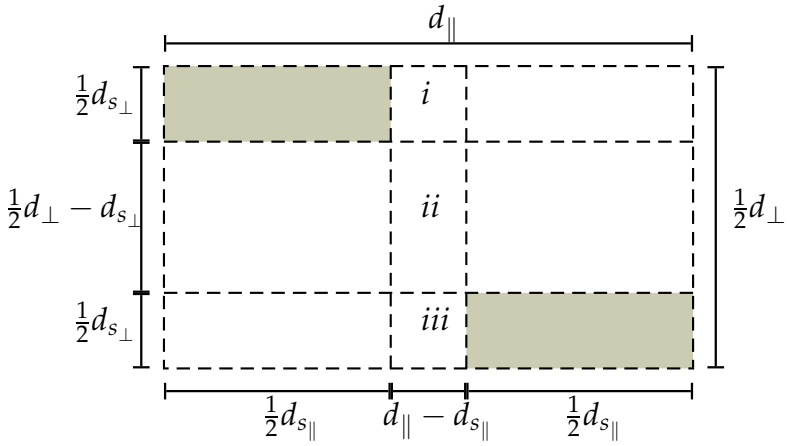

Figure A.18: Unit cell of non-overlapping transversally staggered array using the PS model.

Overlapping SP model

Figure A.19 demonstrates an example of a transversally staggered array in which overlapping occurs.

The SP model is obtained through application of the parallel formula on the unit cell in Figure A.20, followed by the series formula.

Application of the parallel formula, equation (5.7), on column i of Figure A.20 yields

$$\frac{1}{2}d_\perp D_i = \frac{1}{2}(d_\perp - d_{s_\perp})D,$$

thus

$$D_i = \left(\frac{d_\perp - d_{s_\perp}}{d_\perp}\right) D. \tag{A.55}$$

Similarly, for column ii

$$\frac{1}{2}d_\perp D_{ii} = \frac{1}{2}d_\perp D,$$

thus

$$D_{ii} = D \tag{A.56}$$

and column iii

$$\frac{1}{2}d_\perp D_{iii} = \frac{1}{2}(d_\perp - d_{s_\perp})D,$$

which yields

$$D_{iii} = \left(\frac{d_\perp - d_{s_\perp}}{d_\perp}\right) D. \tag{A.57}$$

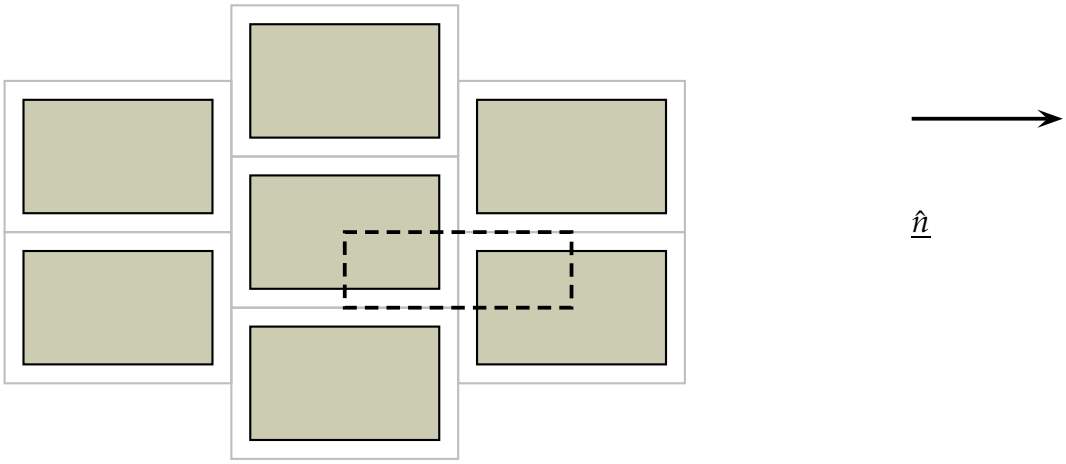

Figure A.19: Overlapping transversally staggered array with unit cell indicated by the bold dashed frame.

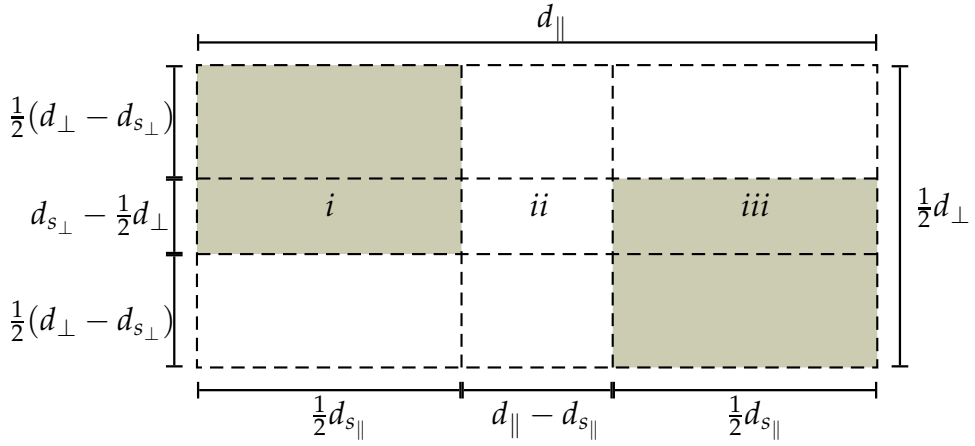

Figure A.20: Unit cell of overlapping, transversally staggered array using the SP model.

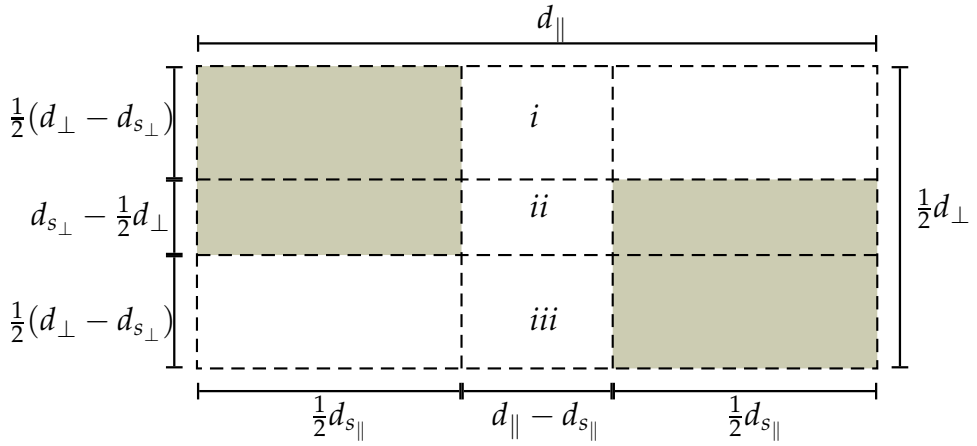

Figure A.21: Unit cell of overlapping, transversally staggered array using the PS model.

Substitution of equations (A.55), (A.56) and (A.57) into equation (5.6), the series formula, yields

$$\frac{d_{\parallel}}{D_{SP}} = \frac{\frac{1}{2}d_{s_{\parallel}}}{D_i} + \frac{d_{\parallel} - d_{s_{\parallel}}}{D_{ii}} + \frac{\frac{1}{2}d_{s_{\parallel}}}{D_{iii}},$$

thus

$$\frac{D}{D_{SP}} = \frac{d_{\perp}d_{s_{\parallel}}}{d_{\parallel}(d_{\perp} - d_{s_{\perp}})} + \frac{d_{\parallel} - d_{s_{\parallel}}}{d_{\parallel}}. \tag{A.58}$$

Through further simplification of equation (A.58), the diffusion coefficient of this array, according to the SP model, is found to be

$$\frac{D_{SP}}{D} = \left[1 + \frac{d_{s_{\parallel}}d_{s_{\perp}}}{d_{\parallel}(d_{\perp} - d_{s_{\perp}})}\right]^{-1}. \tag{A.59}$$

Overlapping PS model

The PS model is obtained through application of the series formula on the unit cell in Figure A.21, followed by the parallel formula.

Application of the series formula on columns *i* and *iii* of Figure A.21 yields diffusion coefficients of zero, i.e.

$$D_i = D_{ii} = D_{iii} = 0. \tag{A.60}$$

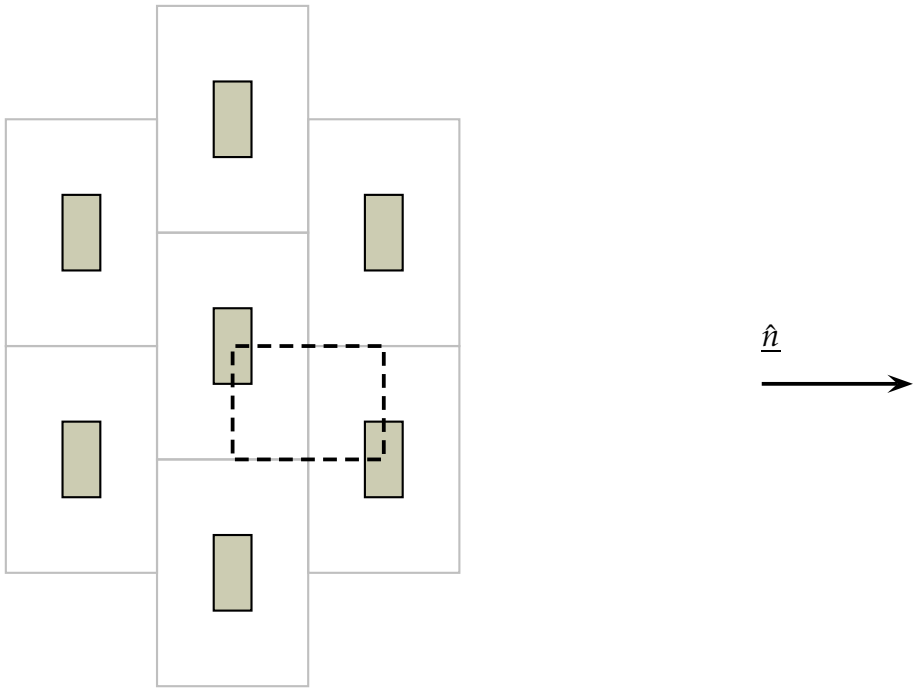

Figure A.22: Non-overlapping, streamwise staggered array with unit cell indicated by the dashed line.

Through substitution of this equation into the parallel formula, equation (5.7), the diffusion coefficient of the array, according to the PS model, is found to be

$$\frac{D_{PS}}{D} = 0. \tag{A.61}$$

A.3.2 $d_\perp > d_\parallel$

An example of a non-overlapping, transversally staggered array is given in Figure A.22. In this array the transverse cell length, $d_\perp$, is greater than the streamwise cell length, $d_\parallel$.

Non-overlapping SP model

The SP model is obtained through application of the parallel formula on the unit cell in Figure A.23, followed by the series formula.

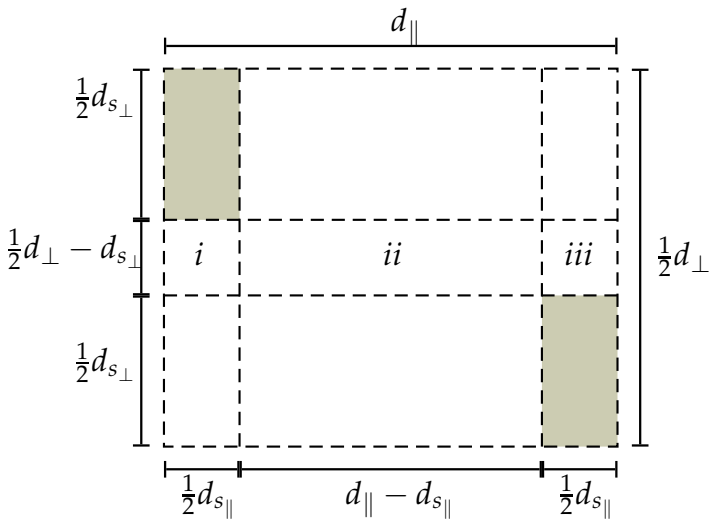

Figure A.23: Unit cell of non-overlapping, transversally staggered array using the SP model.

Application of the parallel formula, equation (5.7), on column i of Figure A.23 yields

$$\frac{1}{2}d_\perp D_i = \frac{1}{2}(d_\perp - d_{s_\perp})D,$$

thus

$$D_i = \left(\frac{d_\perp - d_{s_\perp}}{d_\perp}\right) D. \tag{A.62}$$

Similarly, for column ii

$$\frac{1}{2}d_\perp D_{ii} = \frac{1}{2}d_\perp D,$$

thus

$$D_{ii} = D \tag{A.63}$$

and column iii

$$\frac{1}{2}d_\perp D_{iii} = \frac{1}{2}(d_\perp - d_{s_\perp})D,$$

which yields

$$D_{iii} = \left(\frac{d_\perp - d_{s_\perp}}{d_\perp}\right) D. \tag{A.64}$$

Substitution of equations (A.62), (A.63) and (A.64) into equation (5.6), the series formula, yields

$$\frac{d_\parallel}{D_{SP}} = \frac{\frac{1}{2}d_{s_\parallel}}{D_i} + \frac{d_\parallel - d_{s_\parallel}}{D_{ii}} + \frac{\frac{1}{2}d_{s_\parallel}}{D_{iii}},$$

thus

$$\frac{D}{D_{SP}} = \frac{d_\perp d_{s_\parallel}}{d_\parallel(d_\perp - d_{s_\perp})} + \frac{d_\parallel - d_{s_\parallel}}{d_\parallel}. \tag{A.65}$$

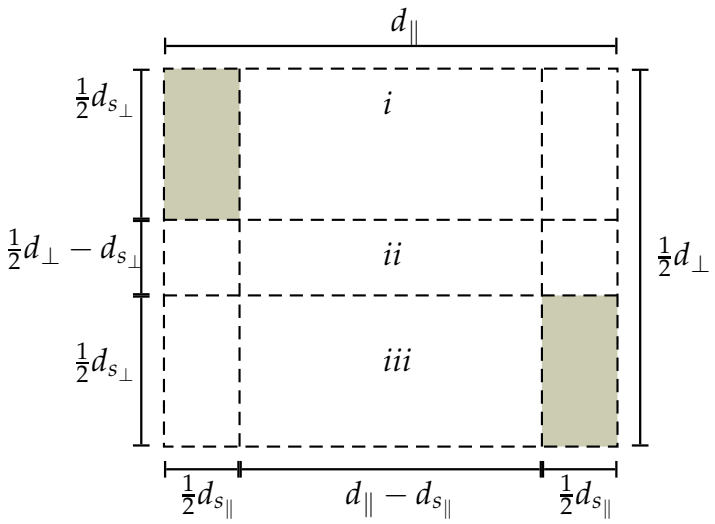

Figure A.24: Unit cell of non-overlapping, transversally staggered array using the PS model.

Through further simplification of equation (A.65), the diffusion coefficient of this array, according to the SP model, is found to be

$$\frac{D_{SP}}{D} = \left[1 + \frac{d_{s_\parallel} d_{s_\perp}}{d_\parallel (d_\perp - d_{s_\perp})}\right]^{-1}. \tag{A.66}$$

Non-overlapping PS model

The PS model is obtained through application of the series formula on the unit cell in Figure A.24, followed by the parallel formula.

Application of the series formula on columns *i* and *iii* of Figure A.24 yields diffusion coefficients of zero, i.e.

$$D_i = D_{iii} = 0, \tag{A.67}$$

while for column *ii*

$$D_{ii} = D. \tag{A.68}$$

Substitution of equations (A.67) and (A.68) into the parallel formula, equation (5.7), yields

$$\frac{1}{2} d_\perp D_{PS} = (\frac{1}{2} d_\perp - d_{s_\perp}) D. \tag{A.69}$$

Through simplification of equation (A.69), the diffusion coefficient of this array, according to the PS model, is found to be

$$\frac{D_{PS}}{D} = 1 - \frac{2 d_{s_\perp}}{d_\perp}. \tag{A.70}$$

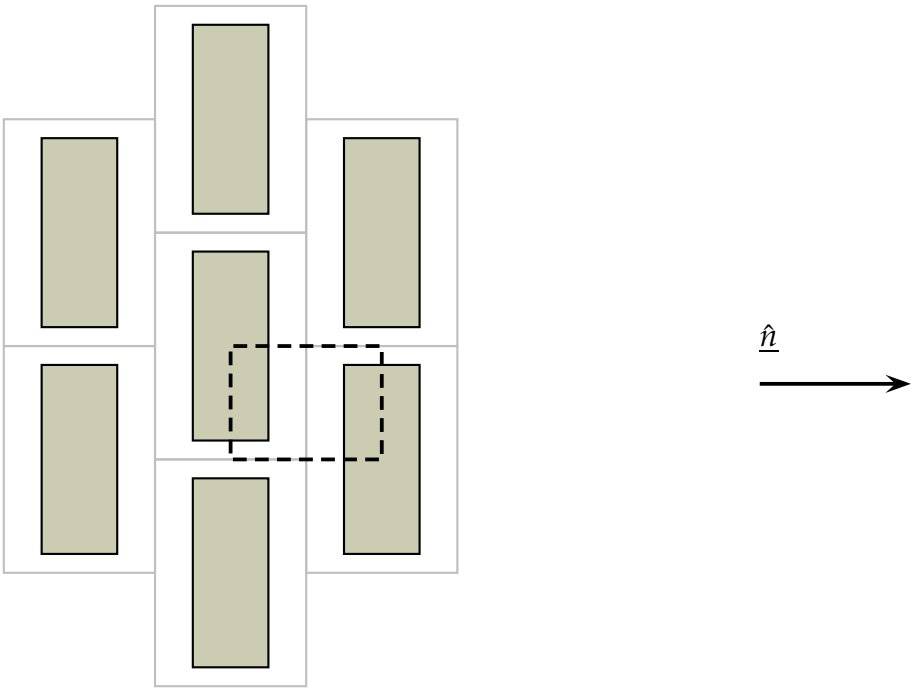

Figure A.25: Overlapping, fully transversally staggered array with unit cell indicated by the bold dashed frame.

Overlapping SP model

Figure A.25 shows an example of an overlapping, transversally staggered array.

The SP model is obtained through application of the parallel formula on the unit cell in Figure A.26, followed by the series formula.

Application of the parallel formula, equation (5.7), on column i of Figure A.26 yields

$$\frac{1}{2}d_{\perp}D_i = \frac{1}{2}(d_{\perp} - d_{s_{\perp}})D,$$

thus

$$D_i = \left(\frac{d_{\perp} - d_{s_{\perp}}}{d_{\perp}}\right) D. \tag{A.71}$$

Similarly, for column ii

$$\frac{1}{2}d_{\perp}D_{ii} = \frac{1}{2}d_{\perp}D,$$

thus

$$D_{ii} = D \tag{A.72}$$

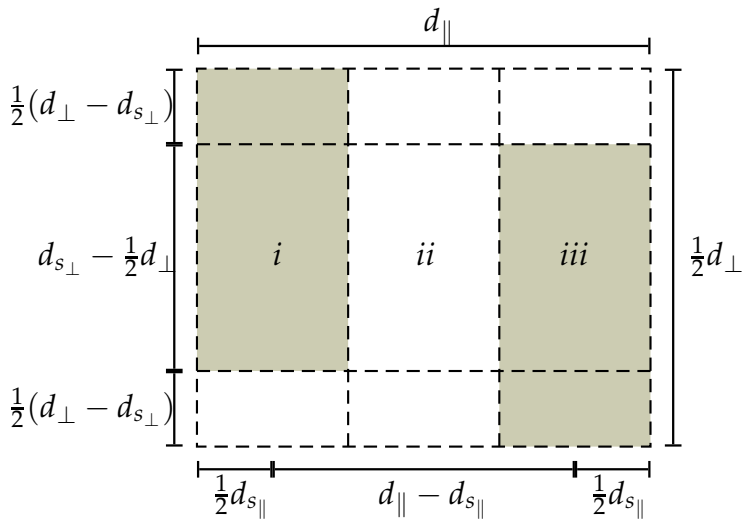

Figure A.26: Unit cell of overlapping, transversally staggered array using the SP model.

and column *iii*

$$\frac{1}{2}d_{\perp}D_{iii} = \frac{1}{2}(d_{\perp} - d_{s_{\perp}})D,$$

which yields

$$D_{iii} = \left(\frac{d_{\perp} - d_{s_{\perp}}}{d_{\perp}}\right)D. \tag{A.73}$$

Substitution of equations (A.71), (A.72) and (A.73) into equation (5.6), the series formula, yields

$$\frac{d_{\parallel}}{D_{SP}} = \frac{\frac{1}{2}d_{s_{\parallel}}}{D_i} + \frac{d_{\parallel} - d_{s_{\parallel}}}{D_{ii}} + \frac{\frac{1}{2}d_{s_{\parallel}}}{D_{iii}},$$

thus

$$\frac{D}{D_{SP}} = \frac{d_{\perp}d_{s_{\parallel}}}{d_{\parallel}(d_{\perp} - d_{s_{\perp}})} + \frac{d_{\parallel} - d_{s_{\parallel}}}{d_{\parallel}}. \tag{A.74}$$

Through further simplification of equation (A.74), the diffusion coefficient of this array, according to the SP model, is found to be

$$\frac{D_{SP}}{D} = \left[1 + \frac{d_{s_{\parallel}}d_{s_{\perp}}}{d_{\parallel}(d_{\perp} - d_{s_{\perp}})}\right]^{-1}. \tag{A.75}$$

Overlapping PS model

The PS model is obtained through application of the series formula on the unit cell in Figure A.27, followed by the parallel formula.

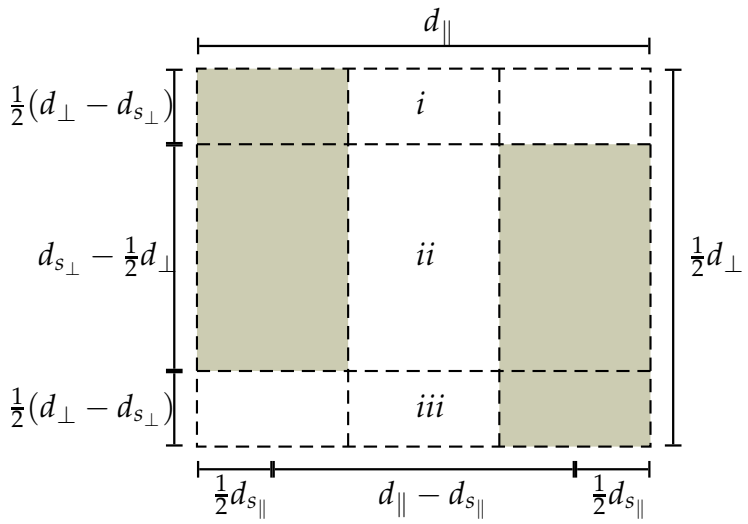

Figure A.27: Unit cell of overlapping, transversally staggered array using the PS model.

Application of the series formula on columns *i* and *iii* of Figure A.27 yields diffusion coefficients of zero, i.e.

$$D_i = D_{ii} = D_{iii} = 0. \tag{A.76}$$

Through substitution of this equation into the parallel formula, equation (5.7), the diffusion coefficient of the array, according to the PS model, is found to be

$$\frac{D_{PS}}{D} = 0. \tag{A.77}$$

Appendix B

Effective diffusion coefficients of arrays of squares

The effective diffusion coefficients of homogeneous arrays of squares are found through application of both the PS and SP models discussed earlier. The same array configurations are considered as in Appendix A.

B.1 Regular array

An example of a regular array of squares is given in Figure B.1.

B.1.1 SP model

The SP model is obtained through application of the parallel formula on the unit cell in Figure B.2, followed by the series formula.

Application of the parallel formula, equation (5.7), on column i of Figure B.2 yields

$$dD_i = dD - \frac{1}{2}d_s D - \frac{1}{2}d_s D,$$

thus

$$D_i = D\left(\frac{d - d_s}{d}\right). \tag{B.1}$$

Similarly, for column ii

$$dD_{ii} = dD,$$

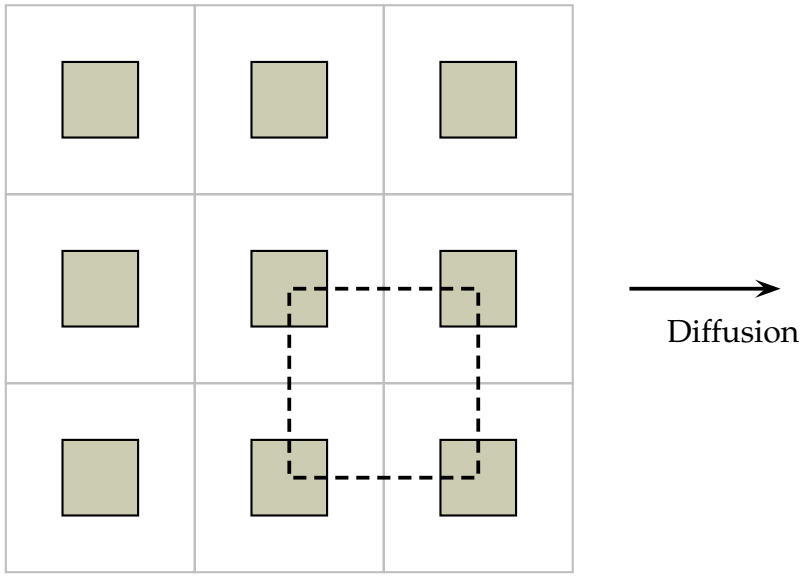

Figure B.1: homogeneous array of squares with a unit cell indicated by the dashed line.

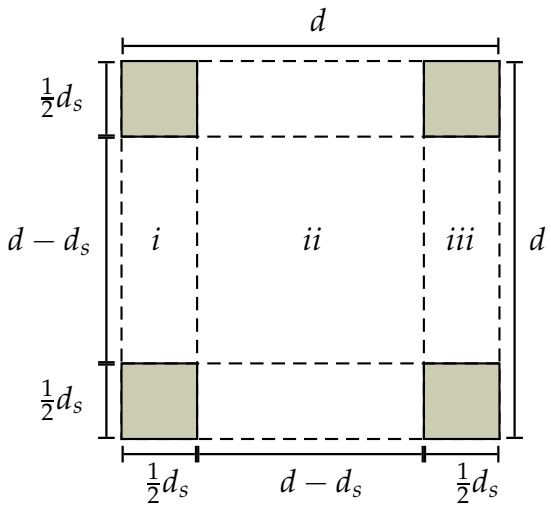

Figure B.2: Unit cell of regular array of squares using the SP model.

thus

$$D_{ii} = D \tag{B.2}$$

and column *iii*

$$dD_{iii} = dD - \frac{1}{2}d_sD - \frac{1}{2}d_sD,$$

which yields

$$D_{iii} = D\left(\frac{d - d_s}{d}\right). \tag{B.3}$$

Substitution of equations (B.1), (B.2) and (B.3) into equation (5.6), the series formula, yields

$$\frac{d}{D_{SP}} = \frac{\frac{1}{2}d_s}{D_i} + \frac{d - d_s}{D_{ii}} + \frac{\frac{1}{2}d_s}{D_{iii}},$$

thus

$$\frac{D}{D_{SP}} = \frac{d_s}{d - d_s} + \frac{d - d_s}{d}. \tag{B.4}$$

Through further simplification of equation (B.4), the diffusion coefficient of this array, according to the SP model, is found to be

$$\frac{D_{SP}}{D} = \left[1 + \frac{d_s^2}{d(d - d_s))}\right]^{-1}. \tag{B.5}$$

B.1.2 PS model

The PS model is obtained through application of the series formula on the unit cell in Figure B.3, followed by the parallel formula.

Application of the series formula on columns *i* and *iii* of Figure B.3 yields diffusion coefficients of zero, i.e.

$$D_i = D_{iii} = 0, \tag{B.6}$$

while for column *ii*

$$\frac{d}{D_{ii}} = \frac{\frac{1}{2}d_s}{D} + \frac{d - d_s}{D} + \frac{\frac{1}{2}d_s}{D},$$

thus

$$D_{ii} = D. \tag{B.7}$$

Substitution of equations (B.6) and (B.7) into the parallel formula, equation (5.7), yields

$$dD_{PS} = (d - d_s)D. \tag{B.8}$$

Through simplification of equation (B.8), the diffusion coefficient of this array, according to the PS model, is found to be

$$\frac{D_{PS}}{D} = \frac{d - d_s}{d}. \tag{B.9}$$

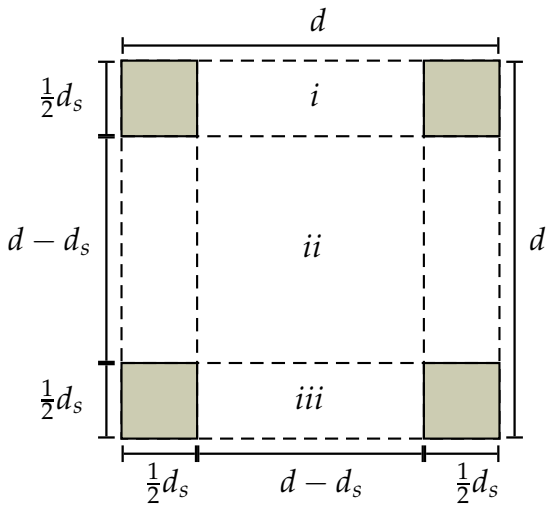

Figure B.3: Unit cell of array of squares using the PS model.

B.2 Streamwise staggered array

A schematic representation of a streamwise staggered array is shown in Figure B.4, where the solid frame indicates the representative unit cell chosen.

B.2.1 Non-overlapping SP model

The SP model is obtained through application of the parallel formula on the unit cell in Figure B.5, followed by the series formula.

Application of the parallel formula, equation (5.7), on column i of Figure B.5 yields

$$dD_i = dD - \frac{1}{2}d_s D,$$

thus

$$D_i = D\left(\frac{d - \frac{1}{2}d_s}{d}\right). \tag{B.10}$$

Similarly, for column ii

$$dD_{ii} = dD,$$

thus

$$D_{ii} = D \tag{B.11}$$

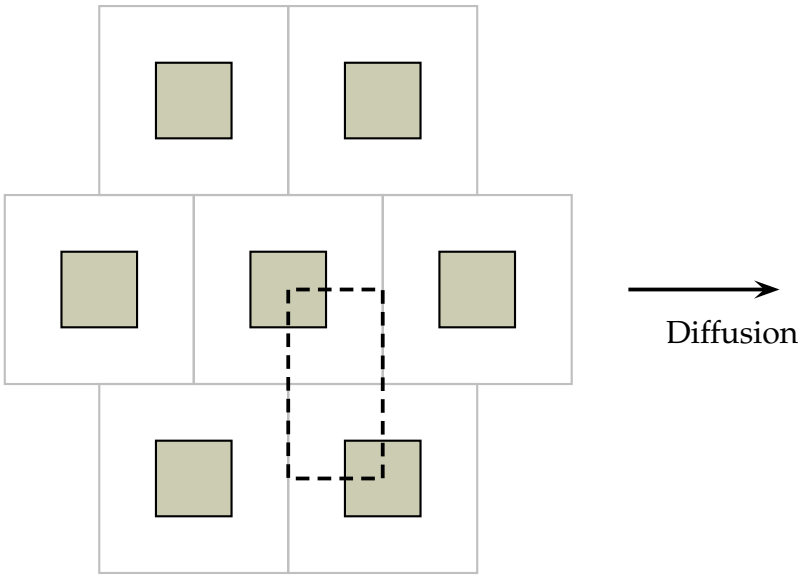

Figure B.4: Non-overlapping, streamwise staggered array of squares with a unit cell indicated by the dashed line.

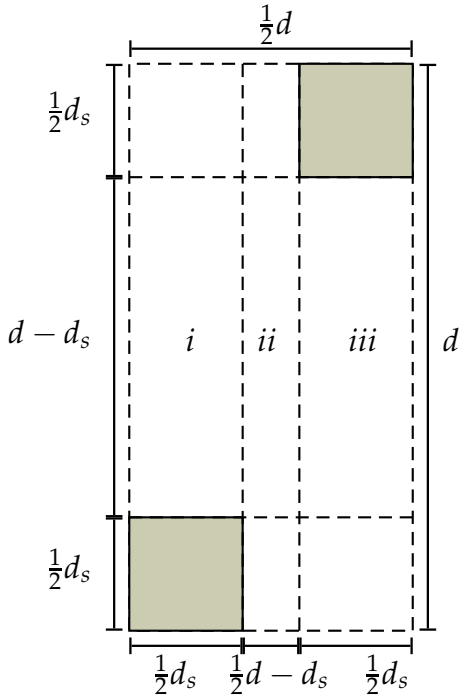

Figure B.5: Unit cell of non-overlapping, streamwise staggered array using the SP model.

and column *iii*

$$dD_{iii} = dD - \frac{1}{2}d_s D,$$

which yields

$$D_{iii} = D\left(\frac{d - \frac{1}{2}d_s}{d}\right). \tag{B.12}$$

Substitution of equations (B.10), (B.11) and (B.12) into equation (5.6), the series formula, yields

$$\frac{d}{D_{SP}} = \frac{\frac{1}{2}d_s}{D_i} + \frac{\frac{1}{2}d - d_s}{D_{ii}} + \frac{\frac{1}{2}d_s}{D_{iii}},$$

thus

$$\frac{D}{D_{SP}} = \frac{d_s}{d - \frac{1}{2}d_s} + \frac{\frac{1}{2}d - d_s}{d}. \tag{B.13}$$

Through further simplification of equation (B.13), the diffusion coefficient of this array, according to the SP model, is found to be

$$\frac{D_{SP}}{D} = \left[1 + \frac{d_s^2}{d(2d - d_s))}\right]^{-1}. \tag{B.14}$$

B.2.2 Non-overlapping PS model

The PS model is obtained through application of the series formula on the unit cell in Figure B.6, followed by the parallel formula.

Application of the series formula on columns *i* and *iii* of Figure B.6 yields diffusion coefficients of zero, i.e.

$$D_i = D_{iii} = 0, \tag{B.15}$$

while for column *ii*

$$D_{ii} = D. \tag{B.16}$$

Substitution of equations (B.33) and (B.34) into the parallel formula, equation (5.7), yields

$$dD_{PS} = D(d - d_s). \tag{B.17}$$

Through simplification of equation (B.35), the diffusion coefficient of this array, according to the PS model, is found to be

$$\frac{D_{PS}}{D} = \frac{d - d_s}{d}. \tag{B.18}$$

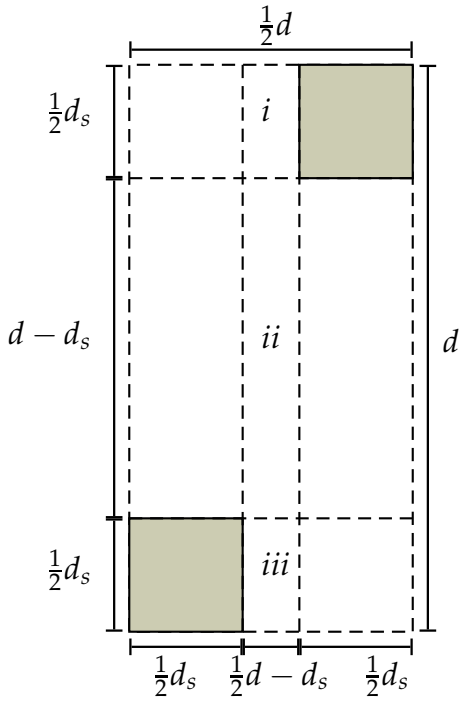

Figure B.6: Unit cell of non-overlapping, streamwise staggered array using the PS model.

B.2.3 Overlapping SP model

Figure B.7 depicts an example of an overlapping streamwise staggered array of squares.

The SP model is obtained through application of the parallel formula on the unit cell in Figure B.8, followed by the series formula.

Application of the parallel formula, equation (5.7), on column i of Figure B.8 yields

$$dD_i = (d - \frac{1}{2}d_s)D,$$

thus

$$D_i = D\left(\frac{d - \frac{1}{2}d_s}{d}\right). \tag{B.19}$$

Similarly, for column ii

$$dD_{ii} = (d - d_s)D,$$

thus

$$D_{ii} = \frac{d - d_s}{d}D \tag{B.20}$$

and column iii

$$dD_{iii} = (d - \frac{1}{2}d_s)D,$$

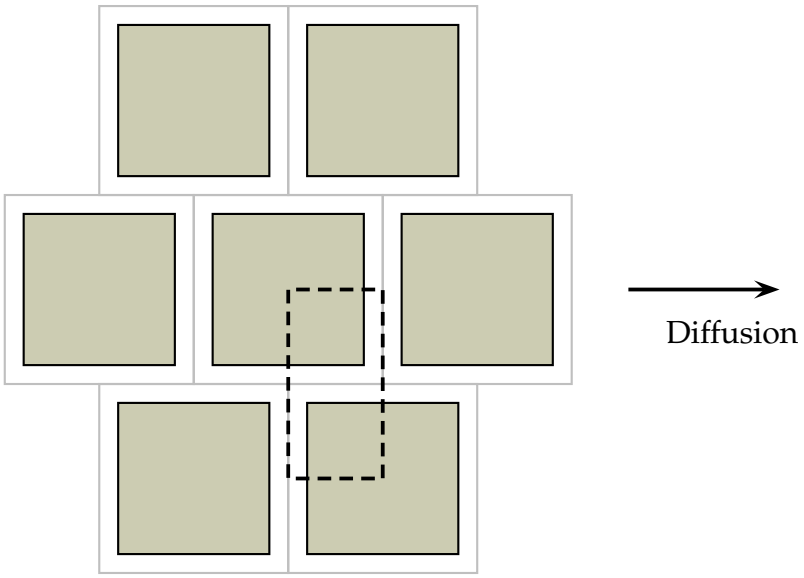

Figure B.7: Overlapping, streamwise staggered array of squares with a unit cell indicated by the dashed line.

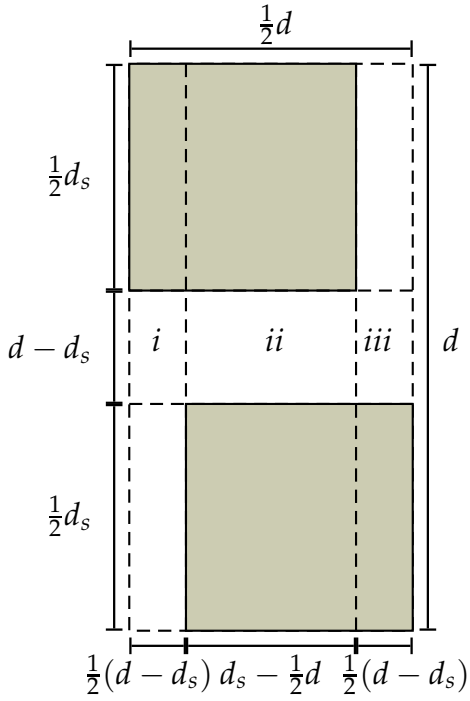

Figure B.8: Unit cell of non-overlapping, streamwise staggered array using the SP model.

which yields

$$D_{iii} = D\left(\frac{d - \frac{1}{2}d_s}{d}\right). \tag{B.21}$$

Substitution of equations (B.19), (B.20) and (B.21) into equation (5.6), the series formula, yields

$$\frac{\frac{1}{2}d}{D_{SP}} = \frac{\frac{1}{2}d - d_s}{D_i} + \frac{d_s - \frac{1}{2}d}{D_{ii}} + \frac{\frac{1}{2}d - d_s}{D_{iii}},$$

thus

$$\frac{D}{D_{SP}} = \frac{2(d - d_s)}{d - \frac{1}{2}d_s} + \frac{2d_s - d}{d - d_s}. \tag{B.22}$$

Through further simplification of equation (B.22), the diffusion coefficient of this array, according to the SP model, is found to be

$$\frac{D_{SP}}{D} = \left[\frac{d}{d - d_s} - \frac{d_s}{d - \frac{1}{2}d_s}\right]^{-1}. \tag{B.23}$$

B.2.4 Overlapping PS model

The PS model is obtained through application of the series formula on the unit cell in Figure B.9, followed by the parallel formula.

Application of the series formula on columns *i* and *iii* of Figure B.9 yields diffusion coefficients of zero, i.e.

$$D_i = D_{iii} = 0, \tag{B.24}$$

while for column *ii*

$$D_{ii} = D. \tag{B.25}$$

Substitution of equations (B.24) and (B.25) into the parallel formula, equation (5.7), yields

$$dD_{PS} = D(d - d_s). \tag{B.26}$$

Through simplification of equation (B.26), the diffusion coefficient of this array, according to the PS model, is found to be

$$\frac{D_{PS}}{D} = \frac{d - d_s}{d}. \tag{B.27}$$

B.3 Transversally staggered array

A schematic representation of a transversally staggered array is shown in Figure B.10, where the solid frame indicates the representative unit cell chosen.

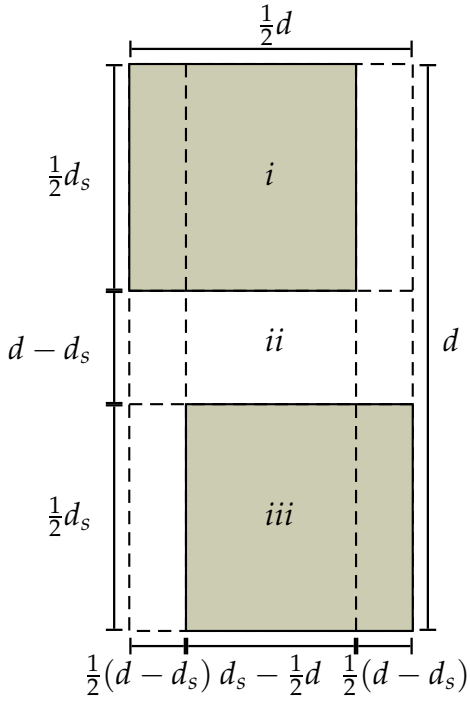

Figure B.9: Unit cell of non-overlapping, streamwise staggered array using the PS model.

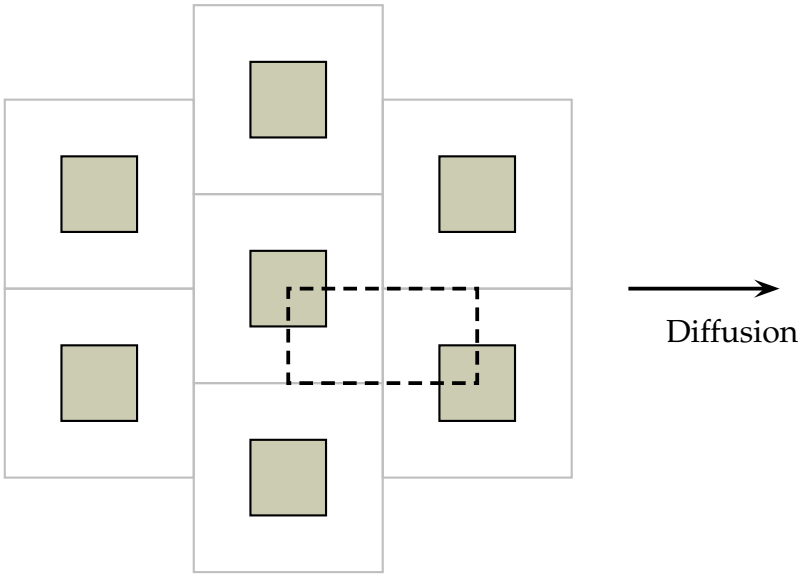

Figure B.10: Non-overlapping, transversally staggered array of squares with a unit cell indicated by the dashed line.

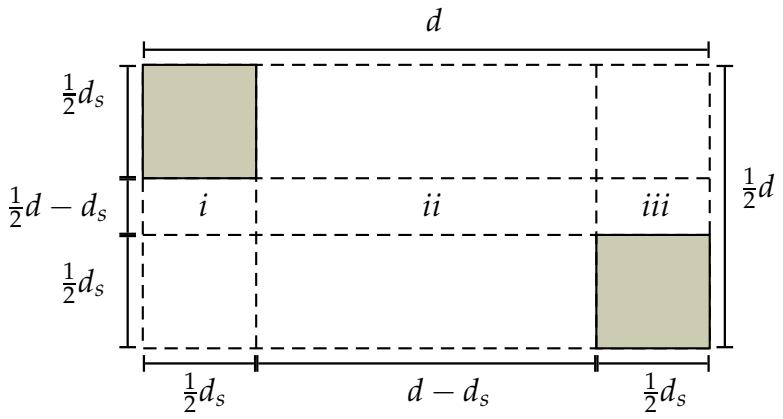

Figure B.11: Unit cell of non-overlapping, transversally staggered array of squares using the SP model.

B.3.1 Non-overlapping SP model

The SP model is obtained through application of the parallel formula on the unit cell in Figure B.11, followed by the series formula.

Application of the parallel formula, equation (5.7), on column i of Figure B.11 yields

$$\frac{1}{2}dD_i = \frac{1}{2}dD - \frac{1}{2}d_sD,$$

thus

$$D_i = D\left(\frac{d - d_s}{d}\right). \tag{B.28}$$

Similarly, for column ii

$$\frac{1}{2}dD_{ii} = \frac{1}{2}dD,$$

thus

$$D_{ii} = D \tag{B.29}$$

and column iii

$$\frac{1}{2}dD_{iii} = \frac{1}{2}dD - \frac{1}{2}d_sD,$$

which yields

$$D_{iii} = D\left(\frac{d - d_s}{d}\right). \tag{B.30}$$

Substitution of equations (B.28), (B.29) and (B.30) into equation (5.6), the series formula, yields

$$\frac{d}{D_{SP}} = \frac{\frac{1}{2}d_s}{D_i} + \frac{d - d_s}{D_{ii}} + \frac{\frac{1}{2}d_s}{D_{iii}},$$

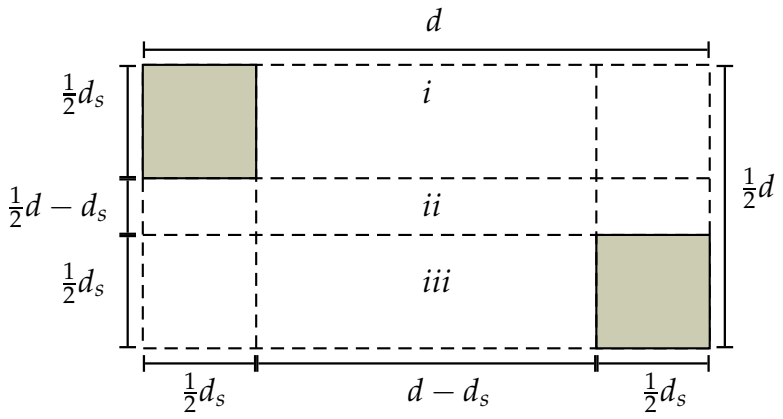

Figure B.12: Unit cell of non-overlapping, transversally staggered array of squares using the PS model.

thus

$$\frac{D}{D_{SP}} = \frac{d_s}{d - d_s} + \frac{d - d_s}{d}. \tag{B.31}$$

Through further simplification of equation (B.31), the diffusion coefficient of this array, according to the SP model, is found to be

$$\frac{D_{SP}}{D} = \left[1 + \frac{d_s^2}{d(d - d_s))}\right]^{-1}. \tag{B.32}$$

B.3.2 Non-overlapping PS model

The PS model is obtained through application of the series formula on the unit cell in Figure B.12, followed by the parallel formula.

Application of the series formula on columns *i* and *iii* of Figure B.12 yields diffusion coefficients of zero, i.e.

$$D_i = D_{iii} = 0, \tag{B.33}$$

while for column *ii*

$$D_{ii} = D. \tag{B.34}$$

Substitution of equations (B.33) and (B.34) into the parallel formula, equation (5.7), yields

$$\frac{1}{2}dD_{PS} = D(\frac{1}{2}d - d_s). \tag{B.35}$$

Through simplification of equation (B.35), the diffusion coefficient of this array, according to the PS model, is found to be

$$\frac{D_{PS}}{D} = \frac{d - 2d_s}{d}. \tag{B.36}$$

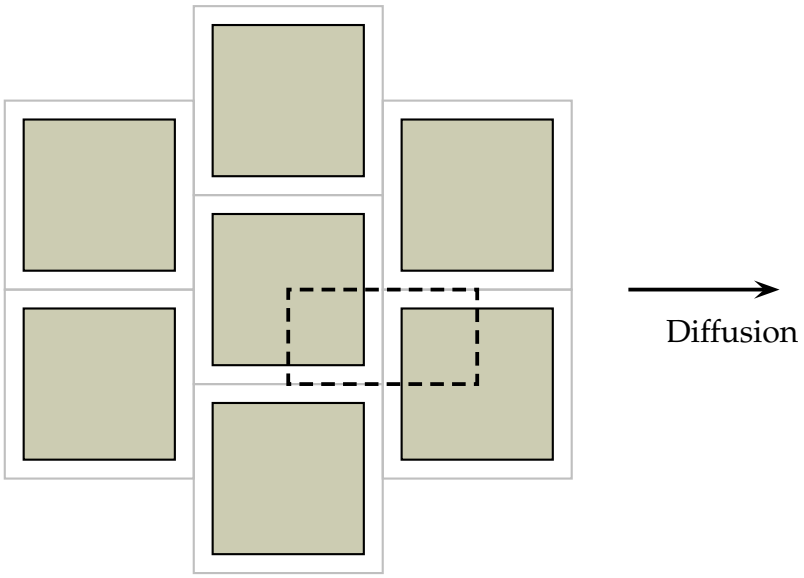

Figure B.13: Overlapping, transversally staggered array of squares with a unit cell indicated by the dashed line.

B.3.3 Overlapping SP model

Figure B.13 depicts an example of an overlapping transversally staggered array of squares.

The SP model is obtained through application of the parallel formula on the unit cell in Figure B.14, followed by the series formula.

Application of the parallel formula, equation (5.7), on column i of Figure B.14 yields

$$\frac{1}{2}dD_i = \frac{1}{2}(d - d_s)D,$$

thus

$$D_i = D\left(\frac{d - d_s}{d}\right). \tag{B.37}$$

Similarly, for column ii

$$\frac{1}{2}dD_{ii} = \frac{1}{2}dD,$$

thus

$$D_{ii} = D \tag{B.38}$$

and column iii

$$\frac{1}{2}dD_{iii} = \frac{1}{2}(d - d_s)D,$$

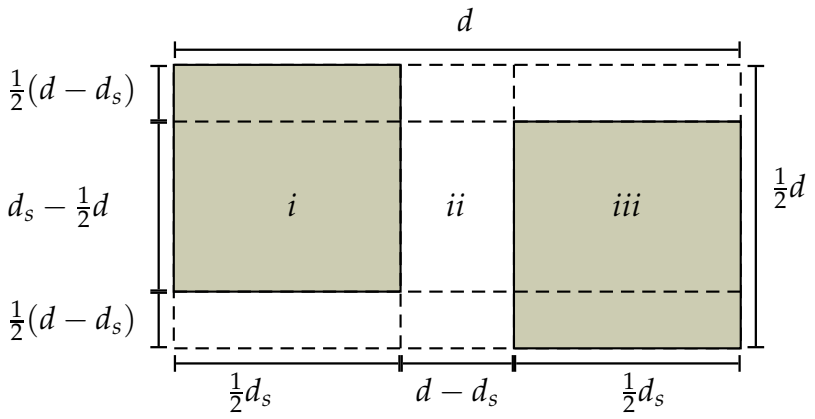

Figure B.14: Unit cell of non-overlapping, transversally staggered array using the SP model.

which yields

$$D_{iii} = D\left(\frac{d-d_s}{d}\right). \tag{B.39}$$

Substitution of equations (B.37), (B.38) and (B.39) into equation (5.6), the series formula, yields

$$\frac{d}{D_{SP}} = \frac{\frac{1}{2}d_s}{D_i} + \frac{d-d_s}{D_{ii}} + \frac{\frac{1}{2}d_s}{D_{iii}},$$

thus

$$\frac{D}{D_{SP}} = \frac{d_s}{d-d_s} + \frac{d-d_s}{d}. \tag{B.40}$$

Through further simplification of equation (B.40), the diffusion coefficient of this array, according to the SP model, is found to be

$$\frac{D_{SP}}{D} = \left[1 + \frac{d_s^2}{d(d-d_s))}\right]^{-1}. \tag{B.41}$$

B.3.4 Overlapping PS model

The PS model is obtained through application of the series formula on the unit cell in Figure B.15, followed by the parallel formula.

Application of the series formula on columns *i* and *iii* of Figure B.15 yields diffusion coefficients of zero, i.e.

$$D_i = D_{ii} = D_{iii} = 0. \tag{B.42}$$

Substitution of this result into the parallel formula, equation (5.7), yields a diffusivity ratio

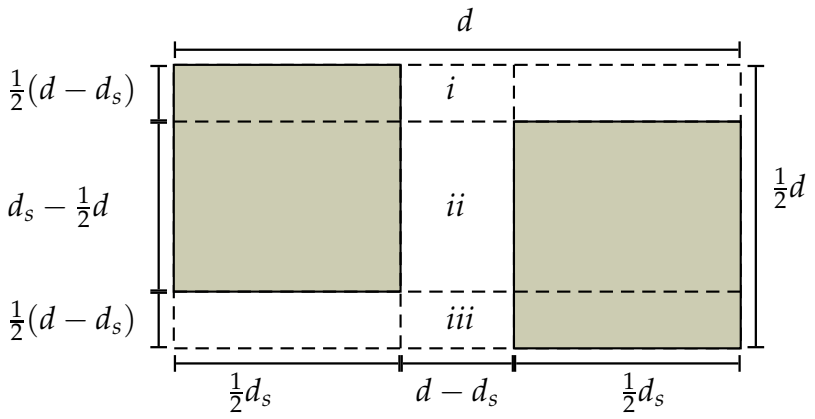

Figure B.15: Unit cell of non-overlapping, transversally staggered array using the PS model.

of

$$\frac{D_{PS}}{D} = 0. \tag{B.43}$$

Bibliography

Amaral Souto, H. P. (1993). *Diffusion-Dispersion en Milieu Poreux: Étude Numérique du Tenseur de Dispersion pour Quelques Arrangements Périodiques Bidimensionnels "Ordonnés"et "Désordonnés"*. PhD thesis, Institut National Polytechnique de Lorraine.

Bear, J. & Bachmat, Y. (1991). *Introduction to modeling of transport phenomena in porous media*. Dordrecht, Netherlands: Kluwer Academic Publishers.

Bell, G. E. & Crank, J. (1973). Influence of imbedded particles on steady-state diffusion. *Journal of the Chemical Society, Faraday Transactions 2: Molecular and Chemical Physics*, *70*, 1259–1273.

Bergman, T. L., D P. DeWitt, F. P. I., & Levine, A. S. (2007). *Fundamentals of Heat and Mass Transfer*. New York, USA: Jonh Wiley & Sons, Inc.

Beyenal, H. & Lewandowski, Z. (2000). Combined effect of substrate concentration and flow velocity on effective diffusivity in biofilms. *Water Research*, *34*(2), 528–538.

Bird, R. B., Lightfoot, E. M., & Stewart, W. E. (2007). *Transport Phenomena*. New York, USA: John Wiley & Sons.

Crank, J. (1975). *The Mathematics of Diffusion*. Oxford, UK: Clarendon Press.

Currie, J. A. (1960). Gaseous diffusion in porous media. part 2.- dry granular materials. *British Journal of Applied Physics*, *11*, 318–324.

Diedericks, G. P. J. & Du Plessis, J. P. (1995). On tortuosity and areosity tensors for porous media. *Transport in Porous Media*, *20*, 265–279.

Du Plessis, E. & Woudberg, S. (June 2009). Modelling of diffusion in porous structures. In Mammoli, A. A. & Brebbia, C. A. (Eds.), *Computational Methods in Multiphase Flow V*, (pp. 399–408)., Southampton. WIT Press.

Du Plessis, J. P. (Ed.). (1997). *Fluid Transport In Porous Media*, volume 13. Wessex, UK: Computational Mechanics Publications.

Du Plessis, J. P. & Masliyah, J. H. (1991). Flow through isotropic granular porous media. *Transport in Porous Media*, *6*, 207–221.

Gavalas, G. R. & Kim, S. (1981). Periodic capillary models of diffusion in porous solids. *Chemical Engineering Science*, *36*, 1111–1122.

Hoogschagen, J. (1955). Diffusion in porous catalysts and adsorbents. *Industrial Chemical Engineering*, *47*, 906–913.

Kim, I. C. & Torquato, S. (1992). Diffusion of finite-sized brownian particles in porous media. *Journal of Chemical Physics*, *96*(2), 1498–1503.

Kim, J., Ochoa, J. A., & Whitaker, S. (1987). Diffusion in anisotropic media. *Transport in Porous Media*, *2*, 327–356.

Lloyd, C. A., Du Plessis, J. P., & Halvorsen, B. M. (2004). On closure modelling of volume averaged equations for flow through two-dimensional arrays of squares. In Brebbia, C. A., Mendes, A., & Rahman, M. (Eds.), *Fifth International Conference on Advances in Fluid Mechanics*, (pp. 85–93). WIT Press.

Maxwell, J. C. *Treatise on Electricity and Magnetism* (2 ed.)., volume 1. USA: Clarendon Press.

Patankar, S. V. (1980). *Numerical Heat Transfer and Fluid Flow*. New York, USA: Hemisphere Publishing Corporation.

Rautenbach, C., Halvorsen, B. M., Du Plessis, E., Woudberg, S., & Du Plessis, J. P. (June 2009). Measurement and prediction for air flow drag in different packing materials. In Mammoli, A. A. & Brebbia, C. A. (Eds.), *Computational Methods in Multiphase Flow V*, (pp. 409–419)., Southampton. WIT Press.

Ryan, D., Carbonell, R. G., & Whitaker, S. (1981). A theory of diffusion and reaction in porous media. *AIChE Symposium Series*, *77*(202), 46–62.

Sáez, A. E., Perfetti, J. C., & Rusinek, I. (1991). Prediction of effective diffusivities in porous media using spatially periodic models. *Transport in Porous Media*, *6*, 143–157.

Shi, Y., Xiao, J., Quan, S., Puan, M., & Zhang, L. (2009). Fractal model for prediction of effective hydrogen diffusivity of gas diffusion layer in proton exchange membrane fuel cell. *International Journal of Hydrogen Energy*, *In Press*.

Singh, B. & Gupta, A. K. (2007). Mass transfer kinetics and determination of effective difusivity during convective dehydration of pre-osmosed carrot cubes. *Journal of Food Engineering*, *79*, 459–170.

Torquato, S. (1985). Electrical conductivity of two-phase disordered composite media. *Journal of Applied Physics*, *58*, 3790–3797.

Trinh, S., Arce, P., & Locke, B. R. (2000). Effective diffusivities of point-like molecules in isotropic porous media by monte-carlo simulation. *Transport in Porous Media*, *38*, 241–259.

Wakao, N. & Smith, J. M. (1962). Diffusion in catalyst pellets. *Chemical Engineering Science*, *17*, 825–834.

Weissberg, H. L. (1963). Effective diffusion coefficients in porous media. *Journal of Applied Physics*, *34*, 2636–2639.

Weissberg, H. L. (1987). Thermal conductivity of disordered heterogeneous media from the microstructure. *Reviews in Chemical Engineering*, *4*, 151–204.

Whitaker, S. (1999a). *Introduction to Fluid Mechanics*. The Physical and Chemical Engineering Sciences. Eaglewood Cliffs, New Jersey, USA: Prentice-Hall, Inc.

Whitaker, S. (1999b). *The Method of Volume Averaging*. Dordrecht, Netherlands: Kluwer Academic Publishers.

Woudberg, S., Du Plessis, J. P., & Smit, G. J. F. (2006). Non-newtonian purely viscous flow through isotropic granular porous media. *Chemical Engineering Science*, *61*, 4299–4308.